Modulation of PrP^C production and proteolysis for the attenuation of prion disease

by

Luis A Arce

A thesis submitted in partial fulfillment of the requirements for the degree of

Master of Science

Department of Biochemistry
University of Alberta

Abstract

Neurodegenerative diseases caused by prions afflict both humans and animals, and result from conformational conversion of the cellular prion protein, PrP^{C}, coded for by the *PRNP* gene, to an isoform called PrP^{Sc}. The infectious agent of PrP^{Sc} assembles into aggregate structures and can continue the conversion of PrP^{C} substrate into the disease-causing form. Aggregation of PrP^{Sc} causes neurodegeneration and neuronal death. However, to date effective therapeutics are lacking. We set out to attenuate prion disease by modulating expression and processing of PrP^{C} with the rationale that if the substrate for PrP^{Sc} is either absent, or is in a non-convertible form, then prion disease progress would be impeded.

In a first approach we utilised CRISPR/Cas9 technology to knock out *PRNP* gene expression through a "gene drive" strategy. Gene drives allow for CRISPR/Cas9-mediated edits to be passed on to offspring in an enhanced manner, essentially changing edited genes from a heterozygous state to a homozygous state in all progeny. We initially designed guide RNAs (gRNAs) to target the coding region of *PRNP* so that Cas9-induced edits would preclude the production of PrP^{C} and generated expression plasmids encoding these designed gRNAs and Cas9 endonuclease. We used the T7E1 mismatch assay but altogether were not able to detect editing events in the selected cell line. We infer that the complexity of targeting, low transfection efficiencies, and restricted sensitivity of editing assessment would have to be overcome for the development of a gene drive for animal prion diseases.

A second approach to attenuate prion disease is modify PrP^{C} proteolysis. Following posttranslational modification PrP^{C} can remain in full-length form (FL) or can undergo α-cleavage or β-cleavage, generating the C1 or C2 fragments, respectively. Unlike FL and C2 PrP,

C1 fragment cannot be converted to PrP^{Sc} so increasing α-cleavage or decreasing β-cleavage, could slow disease. We therefore performed a compound library screen to identify PrP^{C} proteolysis agonists/antagonists. Using RK13 cells expressing PrP^{C} we screened a Tocriscreen plus mini library and measured PrP^{C} fragment levels; we initially identified a total of nine compounds that modulated PrP^{C} cleavage, seven of which increased C1 fragmentation and two that decreased C2 fragmentation. However, upon retesting to derive dose-response curves, variability in fragmentation level confounded successful identification of a potential therapeutic modulator of PrP^{C} cleavage.

Lastly, *a third approach* used a candidate driven strategy to identify putative α-cleavage proteases (α-PrPases). Based upon the performance of Camostat mesylate, a general (non-class specific) serine protease inhibitor and gene expression profiles we identified six type II membrane proteases as candidates. Transfecting protease expression plasmids in the presence of PrP^{C} substrate, TMPRSS1 (Hepsin) and TMPRSS2 were notable in lowering the amount of both FL and C1 PrP. These two proteases exerted similar effects on other GPI anchored proteins such as Shadoo and Doppel (members of the PrP superfamily) and Thy-1; these data suggest a pathway affecting biogenesis of GPI-anchored proteins that warrants further exploration.

Dedications

Krystyna, this was all for you and impossible without you. You have given me unconditional love and care; I will never understand how I deserve it. You are undoubtedly my best friend, my partner in crime, my better half. We have done so much together already and will achieve so much more. Our journey through life is only just beginning, I am beyond excited to see where it will take us. Every day is a day I get to see you smile and fill me full of life and love. I'll never be the same I'll tell you for sure. I will never be able to describe in any language how I truly feel about you. I love you. Я люблю тебя. Te amo. ♥♥♥

Abuelo, I miss you. Your happiness and love still brightens my day. You are someone in every manner I strive to be like, a true role model. I know you are looking down and are proud and happy. Sigue riendo y sonriendo, te quiero. Bendición.

Acknowledgments

First of all, I would like to acknowledge my supervisor Dr. David Westaway for all of the help and support over the past few years. Thank you for all the suggestions and guidance over the projects we have completed and will complete. I have considered being a member of the Westaway lab as a great honour. I would also like to extend my gratitude to all members (past and present) of the Westaway lab. Thank you Dr. Serene Wohlgemuth and Dr. Andrew Castle for all of help, suggestions, and groundwork you have given to me for the projects, I would not have been able to complete this thesis without it. To Serene I would also like to thank you for all the support outside of the academic setting, you are truly a compassionate friend. I would also like to express gratitude to Dr. Ghazaleh Eskandari-Sedighi for all the walks and conversations about lab and life, I will always be down to get some bubble tea. To Klinton Shmeit, you are a truly consummate friend, I look forward to hanging out in retirement with you. Thank you, George Han, for all the discussions about science and life, you made me a better scientist without a doubt. I also want to acknowledge my committee members; Dr. Sue-Ann Mok, and Dr. Basil Hubbard for the direction and suggestions provided.

Krystyna Andrusiv, I will never be able to fully thank you for all the support in every single regard. You have been my motivator, my purpose, my shoulder to cry on, my love, my encouragement, you make me the person I am. To my parents Alvaro and Patricia Arce, and brother, Ryan Arce, thank you for all the love, understanding, encouragement, emotional support, and distraction when needed, I would not be where I am today without you. I also want to extend my sincerest gratitude to my other parents Alla and Viktor Andrusiv, you have taken me in as one of your own, heard every single presentation, fed me at every chance, thank you for all of the love and support, from the bottom of my heart спасибо, Дякую тобі. To the rest of my family, Alvaro Jose and Rebeca Arce, Herman and Pieta Borkent, Vitaliy and Laura Andrusiv, all my aunts, uncles, tías, tíos, cousins, primos, thank you for the love and encouragement, la familia es todo. To all my friends overseas and here in Canada thank you for the understanding, friendship, and keeping me sane, thank you Lewis, Daniel, Jonny, Jordan, James, Spencer, and anyone who I have forgotten.

Table of Contents

List of Tables

Page

List of Figures

Abbreviations

Abbreviation	Description
4RβS	Four-Rung β-Solenoid
AD	Alzheimer's Disease
ADAM	A Disintegrin and Metalloprotease
APP	Amyloid Precursor Protein
Aβ	Amyloid Beta
BBB	Blood-Brain Barrier
bp	base pair
BSE	Bovine Spongiform Encephalopathy
Cas	CRISPR Associated
CIB1	Calcium and Integrin Binding 1
CJD	Creutzfeldt-Jakob Disease
CNS	Central Nervous System
CR	Congo Red
CRISPR	Clustered Regularly Interspaced Short Palindromic Repeats
CRISPRa	CRISPR Activation
CRISPRi	CRISPR Interference
CRY2	Cryptochrome 2
cryo-EM	Cryo-Electron Microscopy
CWD	Chronic Wasting Disease
dCas9	dead Cas9

DMEM	Dulbecco’s Modified Eagle’s Medium
Dpl	Doppel
DSB	Double Strand Breaks
FBS	Fetal Bovine Serum
FFI	Fatal Familial Insomnia
GFP	Green Fluorescent Protein
GPI	Glycosylphosphatidylinositol
gRNA	guide RNA
GSS	Gerstmann-Sträussler-Scheinker Syndrome
HDR	Homology-Directed Repair
HEK293T	Human Embryonic Kidney 293 T
kDa	Kilodalton
MBM	Meat and Bone Meal
MDB	Mule Deer Brain
min	Minute
MW	Molecular Weight
NHEJ	Non-Homologous End Joining
ORF	Open Reading Frame
PAM	Protospacer Adjacent Motif
PD	Parkinson's Disease
PIRIBS	Parallel In-Register Intermolecular β-Sheet
PMCA	Protein Misfolding Cyclic Amplification
PNGase F	Peptide-N-Glycosidase F

PNS	Peripheral Nervous System
PrP	Prion Protein
PrP^{C}	Prion Protein Cellular
PrP^{Sc}	Prion Protein Scrapie
recPrP	Recombinant PrP
RK13	Rabbit Kidney Epithelial Cell line
ROS	Reactive Oxygen Series
RT-QuIC	Real-Time Quaking-Induced Conversion
Sho	Shadoo
SV40	Simian Virus 40
T7E1	T7 Endonuclease 1
TBS	Tris-Buffered Saline
VP16	Viral Protein 16

Chapter 1: Introduction

1.1: Prion disease: cause, pathogenesis, treatment

1.1.1: Discovery and initial characterisation of the prion protein and disease

Spongiform encephalopathies, transmissible dementias, and slow virus diseases are previous descriptors of prion diseases- a group of fatal diseases characterised by neurodegenerative conditions[1]. Proteinaceous infectious particles, the origin of the word prion, were initially elucidated as the causative agent of scrapie, a neurodegenerative disease afflicting sheep and goats[2]. Scrapie, in sheep, was known in European agriculture for centuries, but the agent of disease was thought to be virus related, hence the term 'slow virus disease'[3]. Prions were shown to be resistant to nucleic acid inactivation and sensitive to typical methods of protein deactivation, such as boiling with the detergent, sodium dodecyl sulphate (SDS)[2,4]. With the causative agent of scrapie determined to be proteinaceous in nature, further enrichment and purification resulted in identification of a protein between 27 and 30 kDa in size, subsequently designated PrP (*Pr*ion *P*rotein)[5,6]. A related cellular isoform of PrP (PrP^{C}) found in healthy tissue was shown to be non-infectious and distinct in molecular properties to the infectious PrP^{Sc} (scrapie prion protein)[7,8]. We now understand PrP^{Sc} to be the infectious agent causing a cohort of neurodegenerative conditions in both humans and animals. The first human prion diseases to be recognised include kuru, Gerstmann-Sträussler-Scheinker syndrome (GSS), and Creutzfeldt-Jakob disease (CJD), and are described in greater detail below[1]. The animals that demonstrate prion disease have extended beyond sheep scrapie to include cows with bovine spongiform encephalopathy (BSE), cervids with Chronic Wasting disease (CWD), and mink with transmissible mink encephalopathy[9]. Natural prion infections, which typically originate from a

food borne or environmental source, can be described as having three distinct phases: initial infection and peripheral replication, neuroinvasion (migration from periphery to the central nervous system (CNS)), and then neurodegeneration[10].

1.1.2: Human Prion disease presentation, progression, and phenotypic spectrum

Human prion diseases can be split into three etiological subtypes: inherited, acquired, and sporadic[1]. Clinical signs across the range of human prion diseases contain inherent heterogeneity with the consistent core feature of rapidly progressive cognitive decline leading to dementia[11]. In terms of histological tissue analysis, the common features are spongiform vacuolation/degeneration, neuronal loss, and astrocytic activation[12,13].

Acquired prion disease

Acquired prion diseases include kuru and iatrogenic CJD (iCJD), diseases which originate from the consumption or inoculation of human prion-contaminated material[1,12]. Kuru is a fatal neurodegenerative disease found solely in the Fore tribe in Papua New Guinea[14]. Clinical progression of disease can be categorized into three distinct stages: ambulant, sedentary, and recumbent (with an extended terminal state)[14]. A prodrome of headache and joint pain typically mark the subsequent onset of locomotor ataxia[15]. The progressive cerebellar ataxia that follows is ultimately fatal, albeit with some reported fluctuations in clinical onset[1,14,15]. The neuropathology of kuru has fundamental features that are congruent with all prion diseases- neuronal degeneration, vacuolation, astrocytic proliferation, and spongiform changes[14]. In addition, the subjects have "kuru plaques" which are striking amyloid deposits that stain with Congo Red dye to give green birefringence[16,17]. These histopathological changes are predominantly found in the cerebellum, with other brain structures and spinal cord still exhibiting features[15]. The infectious

agent of kuru was transmitted through the practice of transumption (cannibalistic consumption of deceased kinfolk) and, in turn, the intraspecies recycling of prions within the small, segregated community amplified both the disease and disease agent[1,14]. With the ending of endocannibalism in the mid-1950's, cases of kuru dropped over subsequent decades, with the last case occurring in 2005[14,18].

Iatrogenic CJD is the result of inoculation to prion agents through medical procedures or treatments[12]. The majority of iCJD sources are from human cadavers in which the pituitary hormones or dura matter were harvested and injected/implanted[19]. The method of inoculation dictates the clinical onset of disease with intracerebral having expected shorter incubation times than peripheral (months/years versus decades)[1,12]. Furthermore, the presentation of disease for intracerebral inoculation presents as 'classical CJD' (rapidly progressive dementia), and peripheral similar to kuru (progressive cerebral ataxia)[1,12]. Current practices, such as improved infection recognition and disinfection of surgical tools, have allowed for the practical elimination of iCJD[19].

Inherited prion disease

Inherited prion diseases can be categorized into three phenotypes: familial CJD (fCJD, but now often referred to as genetic CJD, gCJD), Gerstmann-Sträussler-Scheinker (GSS), and fatal familial insomnia (FFI)[20]. All of the above-mentioned phenotypes have the same causal root, autosomal dominant mutations in the open reading frame (ORF) of *PRNP* (coding region of PrP^{C}), resulting in the conversion of the cellar prion protein to PrP^{Sc} [20,21]. A wide variety of mutations have been linked to gCJD, such as point mutations (e.g., E200K), STOP codon mutations (e.g., Y145X), and insertion mutations (octarepeat insertion) [20]. It can be difficult to

clinically distinguish gCJD from sporadic CJD (sCJD) and thus, confirmation through genetic exploration of *PRNP* is needed[22]. GSS is characterised by a slow progressing ataxia, ending with dementia/cognitive decline[1,20]. Even though there are a variety of mutations found to produce the phenotype of GSS, the most common cause is the point mutation at codon 102 of a proline to a leucine (P102L)[12,20]. FFI presents as untreatable disturbances to the sleep-wake cycle, insomnia, hallucinations, and autonomic/motor dysfunction[12,20,21]. The genetic mutation that gives rise to FFI is D178N, when segregating with methionine at codon 129; if a valine is present at codon 129, the clinical diagnosis is typically gCJD[21,22].

Sporadic prion disease

Similar to inherited prion disease, sporadic disease also exhibits phenotypic heterogeneity[11]. Sporadic CJD (sCJD) is a rapidly progressive dementia, in which death occurs within 2-3 months of disease onset, and accounts for approximately 80% of CJD cases[1,11,23]. Initial symptoms include abnormalities in sleep and behaviour, cognitive deficits, eventually progressing to ataxia and myoclonus, then finally akinetic mutism and death[11,12]. The phenotypic range of sCJD is dependent on the genotype of the codon at position 129 (M/V), and the size of the PrP^{Sc} fragment[24,25]. Investigators based in Italy and the UK propose that all combinations have their own distinct pathogenesis and presentation, and with slightly different classification schemes[24,25].

1.1.3: Animal prion disease presentation, progression, and phenotypic spectrum

Scrapie

A wide range of animals present with prion disease; with the first identified being scrapie[2]. Scrapie is a naturally occurring disease that has been reported across the globe afflicting

sheep producing regions albeit originating from the UK and continental Europe[1,24]. Achieving consensus on worldwide incidence rates has proven to be difficult to calculate, as clinical diagnosis and knowledge of disease can be lacking outside of countries with sufficient diagnostic and teaching resources[24-26]. In 2019, within the EU, 821 cases of classical scrapie were found in 325,386 sheep tested (0.25%), and 517 reported cases of 138,128 goats tested (0.37%) [24-26]. The name derivation and primary clinical presentation of scrapie is itchiness (pruritis) of the animal, in which they compulsively scrape against the environment removing fleece in the process[27]. Other clinical signs include behavioural changes (e.g., removing themselves from the rest of the flock), tremors, motor abnormalities (e.g., change in gait), and ataxia[24,27]. Acquisition of scrapie disease in sheep appears to be through the oral route of exposure to the prion agent, where early propagation occurs in lymphoreticular tissues before the eventual spread to the central nervous system (CNS)[24]. Susceptibility to scrapie is dependent on missense polymorphisms within the PrP gene coding sequence, most notably at positions 136, 154, and 171[28,29]. The VRQ haplotype (i.e., V136, R154 and Q171) is considered to be the most susceptible, but ARQ (the most common genetic variant), can still develop scrapie[28,29]. In contrast, the ARR haplotype is resistant to classical scrapie, but is associated with another disease of sheep called Nor98[28,29].

Bovine spongiform encephalopathy

Bovine spongiform encephalopathy (BSE), commonly referred to as mad cow disease, was originally characterised in 1986 as a novel progressive spongiform encephalopathy afflicting cows[1,30]. By 1988, a major epidemic of over 195,000 cases was experienced in the UK, with cases also occurring in continental Europe; extrapolatory analysis estimate that the number of infected cattle totalled several million[31,32]. The disease origin is from cattle being exposed to the prion agent in supplementary feed containing contaminated meat and bone meal (MBM), and in

turn recycling of the agent into feed and the cattle population[33,34]. The clinical signs of BSE are like scrapie, minus the pruritus, initially presenting as behavioural abnormalities such as, difficulties in locomotion, and atypical sensations (increased sensitivity to sound and touch), before the onset of ataxia and death[31,35]. As per prion diseases in general, a wide variety of clinical symptoms can be encountered; some heterogeneities can be attributed to three varieties of BSE (classical, L-type and H-type) [31,34,36]. The only direct confirmation of BSE is through the neuropathologic signs of vacuolation and immunodetection of PrP^{Sc}, with the latter technique in western blot format distinguishing the C, L- and H-types[31,34,36].

Variant CJD

In 1996, a new form of CJD was reported in humans, variant CJD (vCJD)[37]. vCJD is an acquired zoonotic prion disease caused by the BSE agent present in contaminated beef and beef products[38,39]. vCJD diverges in the clinical pathology from sCJD; the onset is at an earlier age, florid plaques are seen in the brain, and there is a slower progression to death (14-month average versus 5 month)[12,37,38]. In nearly all confirmed cases of vCJD, where genetic testing was performed, methionine is homozygous at codon position 129 in *PRNP*, with valine at position 129 thought to attenuate the appearance of vCJD[38,40-42]. The disease incidence has decreased since the initial peak around 1999-2000 due to practices eliminating exposure of the beef food chain to the BSE agents (ban of MBM added to ruminant feed)[38,43,44].

Chronic wasting disease

Chronic wasting disease (CWD) is a prion disease afflicting cervids (family *Cervidae*), with the first reported case in the late 1970's occurring in captive mule deer (*Odocoileus hemionus*)[45,46]. The presentation of CWD in tissue distribution, horizontal spread, and

environmental contamination is similar to scrapie, although with enhanced horizontal transmission[45]. CWD has had a very rapid spread in North America with 24 states in the United States, and 2 provinces in Canada (including Alberta) having cases of CWD in free ranging and captive populations[47,48]. Outside of North America, there has been reported occurrence of CWD in South Korea which has been attributed to importation of deer[49]. Similarly, affected reindeer and moose have been described in Scandinavia[50,51]. The epidemiological origin of CWD, either in North America or in Scandinavia, has not been elucidated. One hypothesis suggests that spontaneous conversion of cervid PrP^{C} to PrP^{Sc} occurred (i.e., a sporadic origin), while another suggests that a scrapie strain variant arose in affected sheep and then spread to cervids[45]. In the early and median stages of disease pathogenesis, clinical symptoms can be challenging to decipher from cervid seasonal changes/behaviours[52]. Once in the observed clinical state of disease, cervids exhibit behavioural changes like isolation from the herd, depression, lowering of ears and head, and weight loss)[45,50,52]. Other symptoms include: teeth grinding (odontoprisis), excessive salivation (sialorrhea), ataxic head tremors, regurgitation, and polyuria/polydipsia (excessive urination/thirst)[45,50,52]. Progression to the terminal state of disease can last weeks to months, with the final clinical signs being lack of awareness, repetitive walking of enclosure perimeter, and a fixed stare[52]. The histopathology is generally undeviating from other animal prion diseases; lesions are seen in grey matter, along with dispersed spongiform vacuolation, neuronal degeneration, and presence of amyloid plaques[53].The differences observed between cervid species can be attributed to strain selection by missense polymorphisms at codon 226 of *PRNP*[54]. Glutamine is seen in deer at position 226, whereas elk have glutamate, which results in divergent time to death post inoculation and immunohistochemistry profiles[54,55]. The potent horizontal transmission of CWD in both captive and wild populations is a result of prion agent

shedding and environmental persistence[55-57]. Peripheral tissues of CWD infected cervids have substantial levels of infectious PrP^{Sc}; with the symptomatic shedding of the agent through polyuria, excessive salivation, regurgitation, and decomposition, the environment becomes contaminated which allows for the efficient horizontal transmission of disease[45,56,57]. Furthermore, the resilience of the prion agent to degradation by conventional methods (heat, proteases, and chemical disinfectants) holds true to inadequate environmental degradation and therefore, shed CWD prions can persist in the environment perpetuating infection within cervid populations[45,58]. To date, there has not been a reported zoonotic transmission of the CWD prion agent to humans, but some *in vitro* studies have shown that human PrP can be converted to a misfolded state by CWD prions, thus caution must be exercised with handling of CWD material and consumption of untested cervid material[59].

1.2: Structure and function of the cellular prion protein

1.2.1: Characteristics of the cellular prion protein

Genomic location of the PRNP gene

The cellular isoform of the prion protein is encoded for by the *PRNP* gene which is found on chromosome 20 in humans (chromosome 2 in mice) and is significantly conserved across mammals[60-62]. Paralogous genes to *PRNP*, *SPRN* and *PRND,* are the other members of the mammalian prion gene family and encode shadoo (Sho) and doppel (Dpl), respectively[63]. A scheme has been proposed linking the prion protein family to a common ancestor, a member of the ZIP (Zrt-Irt-like) metal ion transporter family[64]. *PRNP* consists of three exons in which the open reading frame (ORF) is in exon 3[63].

Primary to tertiary structure of PrP^C

PrP^C is synthesised as a 253 amino acid precursor protein (human numbering) with C- and N-terminal signal sequences (Figure 1A)[65]. The final, mature protein consists of amino acids 23-231 from the original precursor protein)[65-67]. The N-terminal signal peptide (residues 1-22) for processing in the secretory pathway is cleaved off during translocation across the endoplasmic reticulum (ER) membrane, and the 232-253 peptide is cleaved off commensurate with the ligation of a glycosyl-phosphatidylinositol (GPI) anchor (Figure 1B)[66,67]. The GPI anchor tethers PrP^C to the outer membrane of the plasma membrane cell surface, where PrP^C is typically localised[68]. In terms of posttranslational modifications, PrP^C exists in three forms within the cell: unglycosylated, mono-glycosylated, and di-glycosylated with the glycosyl groups

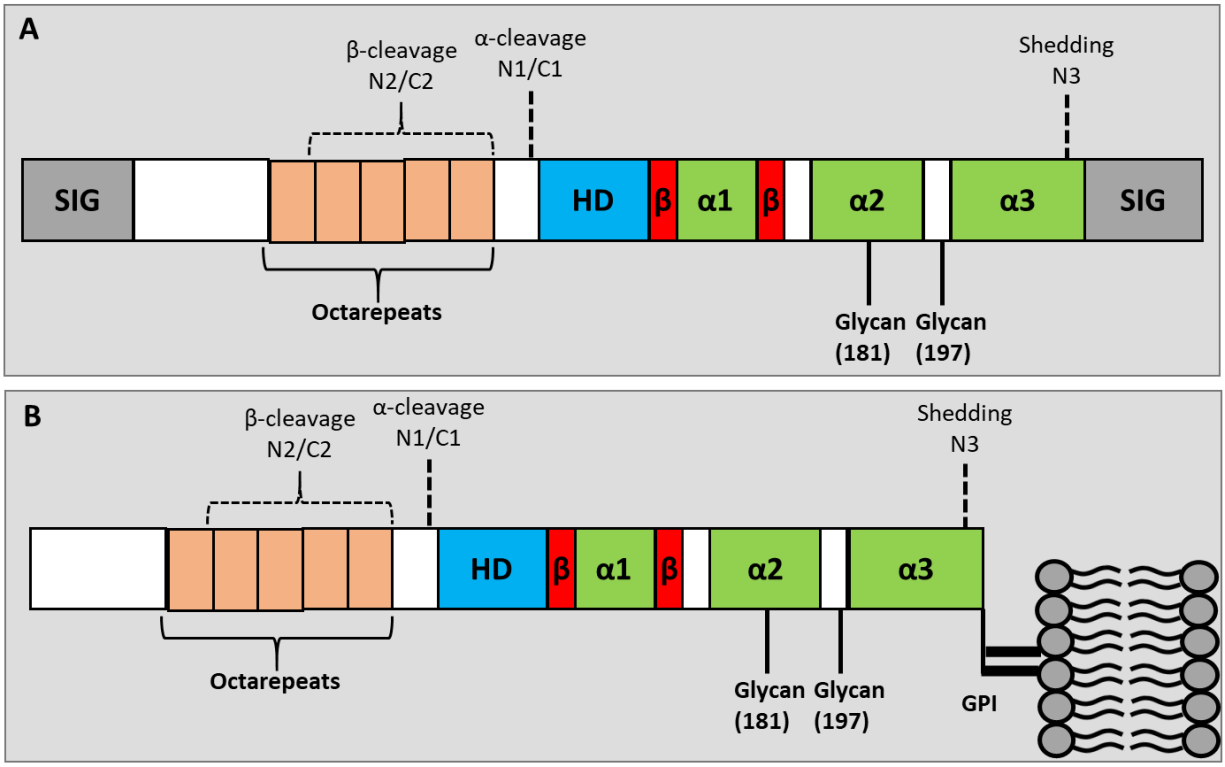

Figure 1. Schematic representation of PrP^C precursor and mature protein. Structural features (solid lines and coloured boxes) and cleavage sites (dashed lines) of PrP^C . SIG, N-/C-terminal signal peptides; HD, hydrophobic domain; GPI, glycosyl-phosphatidylinositol anchor. **A**, PrP^C precursor protein with attached signal peptides (Amino acids 1-254). **B**, mature PrP^C protein with signal peptide removed and GPI anchor attached to phospholipid bilayer.

attached to asparagine residues 181 and 197[67,69]. The domain structure of PrP^C remains remarkably conserved across mammalian species; the N-terminus is flexibly disordered, and the C-terminus has a globular structure consisting of three α-helices, two short β-strands, interconnecting loops, and a disulphide bond between residues 179 and 214[70-73]. Other features include an octarepeat region consisting of five sequential repeats of the sequence PHGGGWGQ (human PrP^C with the first repeat omitting the histidine), which can bind copper (through interactions with the histidine residues; see below), and a conserved hydrophobic domain involved in PrP^C dimerization[74-76]. The mature protein is summarised in Figure 1. Although expression of PrP^C is found in many tissues, the highest levels are found in the CNS[77]. The PrP^C levels increase over development and peak in early life, with a slight decline before adulthood[65,78,79].

Proteolytic cleavage of PrP^C

Following formation of the full-length mature protein, PrP^C can be proteolytically processed by PrPases; α-PrPase performs α-cleavage between residues 110 and 111 (human numbering) of PrP^C resulting in the designated C1 (membrane anchored) and N1 (soluble) fragments, β-PrPase cleaves between adjacent His and Gly residues within the octarepeat region resulting in C2 (membrane anchored) and N2 (soluble) fragments (Figure 1)[80-82]. Alternative cleavage sites within the hydrophobic domain have also been implicated for α-cleavage and β-cleavage in systems using recombinant proteins[82]. The exact proteases that perform α and β cleavage have not yet been fully elucidated. Studies first implicated A disintegrin and metalloprotease (ADAM), ADAM 10 as a primary candidate of the α-PrPase with the proteolytic cleavage being constitutive or regulated by protein kinase C[83,84]. However, other studies found that ADAM10 knockout did not lower the amount of N1/C1 present in cell culture or knockout

mice[76,85,86]. ADAM10 is most likely a sheddase, a protease that leads to the shedding of PrP^{C} following maturation; shedding occurs between residue 227 and 228 (mouse numbering) removing the GPI anchor and three adjacent residues which releases a fragment referred to as N3 into the extracellular medium[82,86,87]. The location of where α-cleavage occurs in the central region of the protein is also under debate and scrutiny; both a late compartment of the secretory pathway independent of lipid rafts, and an acidic endocytic compartment have been proposed[88,89]. The putative function of the C1 fragment has not been surmised, however it demonstrates a neuroprotective function against prion disease and when generated in excess, it is protective against accumulation of PrP^{Sc}, and can significantly increase time to disease onset[74,90,91]. The neuroprotective aspect of C1 cleavage can also be extended beyond PrP^{Sc} accumulation, as the corresponding N-terminal fragment, N1, has been shown to alleviate neurotoxicity of amyloid beta (Aβ) oligomers; furthermore, increased levels of C1 production are seen with neurological strenuous circumstances, such as morphine withdrawal[92,93]. The neuroprotective aspect of α-cleavage fragments in addition to the fact that C1 is the predominant form of PrP in cellular pools, suggest that elucidation of α-cleavage can allow for the production of therapeutics impacting not only prion diseases[94]. β-cleavage derived C2 is longer than C1 and in turn, does not demonstrate the same dominant, negative inhibition of PrP^{Sc} accumulation as it can be converted to the prion disease agent[95,96]. β-cleavage is dependent on the presence of Cu^{2+} and reactive oxygen series (ROS) and seems to react to oxidative stress[97,98]. Small amounts of C2 fragment are found physiologically in the brain[81,98].

1.2.2: Functions of the cellular prion protein

Knockout models of prion disease

PrP^C is implicated in several physiological functions rather than a signature, singular process. One of the key assessments of PrP^C function is when wildtype prion protein production is compared to that of a knockout mouse. The first established Zurich I and Npu PrP^C knockout mouse lines were derived using gene targeting strategies and had no developmental or behavioral abnormalities attributed to the loss of the cellular prion protein[99,100]. Several more lines of *Prnp*$^{0/0}$ mice have been established, however some of these subsequent lineages identified repercussions to ablating *PRNP* with the mice developing late-onset ataxia [101,102]. This effect was subsequently attributed to downstream activation of the neurotoxic protein Dpl by alternative splicing[101-103]. The issue has since been rectified using the Npu or Zurich III lines of *Prnp*$^{0/0}$ mice[104].

Stress protection and PrP^C

A common hypothesis for the function of PrP^C is to protect against oxidative stress. Cultured neuronal cells from *Prnp*$^{0/0}$ mice were more susceptible to agents inducing oxidative stress, and $PrP^{0/0}$ mice had increased levels of oxidative stress markers in the brain[105,106]. Furthermore, studies show that lesion damage is increased under ischemic and hypoxic conditions (conditions causing neuronal death through oxidative damage) in *Prnp*$^{0/0}$ mice compared to wildtype; this again suggests PrP^C plays a role in alleviating oxidative stress[107,108]. A proposed mechanism is that PrP^C acts to modulate enzymes that convert ROS into less toxic products, as levels of superoxide dismutase (SOD) and glutathione peroxidase are lower in $PrP^{0/0}$ mice and cell lines[109-112]. This hypothesis is not without its caveats, however as some studies

have shown that the copper-dependent SOD activity does not increase in $PrP^{0/0}$ tissues such as the spleen, heart, and brain[113,114].

PrP^C is a copper binding protein

It has been observed that another potential function of PrP^C is in the homeostasis of the metal ion Cu^{2+}, with the histidine-containing octapeptide repeat able to bind four copper ions with a high affinity[75,115]. Furthermore, copper is able to conformationally change the disordered N-terminal domain of PrP^C at the cell-surface allowing for three distinct coordination modes for binding[116,117]. It has been suggested that the binding interaction is physiologically relevant in cells, as copper is able to stimulate PrP^C endocytosis (via clathrin-coated pits) [118,119]. Moreover, PrP^C serves as a recycling receptor for Cu^{2+} reuptake, protecting cells from oxidative stress from excess Cu^{2+} [111,115]. However, there is contradictory evidence displaying the physiological relevance of Cu^{2+} and PrP^C binding interactions *in vivo* (as all studies demonstrate the interaction *in vitro*). Examinations into the metal ion content of wild-type, $PrP^{0/0}$, and Tga20 (10-fold PrP overexpression) mice were unable to find any differences in the whole brain or other subcellular fractions, and the PrP^C mediated Cu^{2+} internalization only occurs when levels of Cu^{2+} are significantly exceeding the physiological concentrations[111,114]. Studies looking at the influence of copper and zinc ions on the tertiary structure of PrP^C have found that the ions are able to drive interactions between the N-terminal to the C-terminal domains, which are weakened with disease state point mutations and strengthened in protective mutations[120,121].

PrP^C aids in neuronal function and maintenance

There have been reports of PrP^C aiding in synaptic function and myelin maintenance. In $PrP^{0/0}$ mice (Zurich I and Npu mice), demyelination occurs in the peripheral nervous system

(PNS) leading to a late-onset peripheral neuropathy with conduction velocity changes, however with no overt clinical symptoms[122-124]. With ablation of *PRNP,* a chronic demyelinating polyneuropathy (CDP) in neurons is observed and can be in turn rescued by neuron-specific PrP^C expression[124]. Research has shown that the N-terminal region of PrP^C interacts with a particular G protein-coupled receptor (GPCR), Gpr126, within Schwann cells promoting myelin homeostasis[125]. Furthermore, some patients suffering from multiple sclerosis (MS), an autoimmune disorder in which clinical demyelination occurs, have lower levels of PrP^C reiterating that neuronal expression of PrP^C is crucial for myelin homeostasis[126]. In addition, PrP^C is related to synaptic function, growth, structure, and maintenance. Studies show that within neurons, PrP^C is predominantly localised in the pre-synaptic terminals and axons[127-130]. During neonatal mouse brain development, higher levels of localised PrP^C are seen along the axonal fibre tracts, implying that PrP^C is contributing to axonal elongation, also with addition of recombinant PrP (recPrP) to cultured rat hippocampal neurons, a significant proliferation of dendrites, axons, and synaptic contact occurs[78,131]. Moreover, in $Prnp^{0/0}$ mice, hippocampal reorganisation transpires with mossy fibres taking a form resembling epileptic cases which corroborates the hypothesis that PrP^C is vital in typical neuronal organisation[132].

PrP^C and the pathogenesis of other neurodegenerative diseases

Another closely studied binding interaction of PrP^C is with Aβ, a peptide that accumulates during Alzheimer's disease (AD) through the action of β- and γ-secretases (endoproteases) on the amyloid precursor protein (APP)[133]. PrP^C is one of the several cell-surface proteins that have nanomolar binding constants for oligomeric forms of Aβ[134,135]. APP undergoes β-cleavage by β-secretase 1 to produce sAPPβ, a fragment subsequently processed by γ-secretase resulting in Aβ peptides[65]. Studies have shown that PrP^C is able to act as an inhibitor of β-

secretase 1; PrP^C overexpression inhibited the cleavage of APP and in turn, decreased the levels of Aβ peptides in cellular culture[136]. Furthermore, an inverse correlation exists between PrP^C levels and Aβ deposition[137]. Conclusions were initially made that increased PrP^C levels would in turn protect or reduce the amount of Aβ, and therefore could be looked at as a treatment for AD [136,137]. Having said that, more recent data has questioned this rationale, as genetic ablation of *PRNP* in transgenic mice expressing human wildtype APP did not change the amount of APP proteolysis and in turn the amount of Aβ deposition[138]. Other research exhibited that in transgenic mice encoding familial AD, cognitive impairments were only present when PrP^C was expressed; if PrP^C was not present, AD would progress, but no detectable impairment in spatial learning and memory was demonstrated[139]. Furthermore, it has been suggested that the binding interactions between Aβ and PrP^C activates Fyn kinase, which is able to hyperphosphorylate tau, accelerating AD[140]. A recent study has shown that soluble aggregates of tau and α-synuclein (protein misfolding monomer of Parkinson's disease) are able to bind plate-immobilised PrP and mouse cortical neurons in a fashion similar to Aβ (binding to the same N-terminal sites)[141]. Additionally, it was demonstrated that PrP^C is needed for the toxic function of Aβ, tau, and α-synuclein[141]. Altogether, the evidence of PrP^C interaction with the disease progression of AD is inconclusive, as studies have shown both alleviation and exaggeration of AD phenotypes. Regardless, the conclusion that PrP^C has some function and physiological relevance in AD can be made and substantiated, whether that be negatively or positively; also of note, the studies above rarely considered the properties of different metabolically stable fragments of PrP^C.

1.3: The disease state of the prion protein

1.3.1: Information transfer in prion disease does not follow the central dogma of molecular biology

The pathogenesis of prion disease stands out from every other transmissible disease, as the agent of infection does not carry a nucleic acid genome[2,142]. It is a protein structure (PrP^{Sc}) which embodies information for the pathogenic process and is able to convert the non-infectious protein (PrP^{C}) into the infectious agent forming an extended fibril of PrP^{Sc} monomers[143]. In other words, information transfer does not follow the central dogma of molecular biology (i.e., information flows from DNA to RNA to protein)[144]. DNA does not code for structural information in PrP^{Sc}, yet PrP^{Sc} is able to coerce PrP^{C} into a new secondary, tertiary, and quaternary structures[145]. To begin to understand this information transfer and disease pathogenesis, the proposed structures of PrP^{Sc} must first be considered.

1.3.2: Proposed structures of PrP^{Sc}

β-solenoid model of PrP^{Sc}

Initial studies using crystal electron crystallography, low-resolution fiber diffraction, and atomic force microscopy suggested that PrP^{Sc} exists in a left-handed β-helical structure[146,147]. Using cryo-electron microscopy (cryo-EM) and 3D reconstructions of anchorless PrP^{Sc} (deemed PrP 27-30, reflecting the protease resistant core and short connecting loops of PrP^{Sc}), a low-resolution structure has now been determined to be a four-rung β-solenoid (4RβS), with each molecule to have a predicted height of ~17.7Å[146,148,149]. X-ray fiber diffraction of PrP^{Sc} amyloid fibrils confirmed both the 4RβS structure and the 19.2Å beta sheet structure of individual PrP^{Sc} monomers within an amyloid fibril[148,150]. Corroboration of the 4RβS structure can be found

within studies exploring the biochemical and biophysical traits of PrP^{Sc}. Using mass spectroscopy analysis of hydrogen/deuterium exchange on brain-derived PrP^{Sc}, it was found that the C-terminal prion 'core' consisted of virtually no α-helices, only β-strands and short interconnecting loops/turns[151]. Fourier transform infrared spectroscopy (FTIR) and circular dichroism also confirm the overwhelming β-sheet and loop content of PrP^{Sc} demonstrating that PrP^{Sc} is 43-61% β-sheet, and the rest are loops/turns with little to no α-helical content[152-155]. Overall, its suggested that PrP 27-30 is a mixture (approximately 50/50) of β-sheets and loops/turns[145]. Moreover, the data presented from limited proteolysis of PrP^{Sc} reinforces the β-solenoid structure; PrP^{Sc} was shown to be proteinase K (PK) resistant, and this feature is explained by the compact nature of the β-solenoid core and the tight loop structure[4,143]. Research has proposed the concept that PrP^{Sc} retains some of the domain structure of the converted PrP^{C}; the C-terminus is the PK resistant region and corresponds to the β-solenoid core (the region allowing for amyloid fibril formation), whereas the natively disordered N-terminus is not altered in PrP^{Sc} formation and remains susceptible to broad-spectrum proteases[143,145].

Parallel in-register intermolecular β-sheet model

Another postulated theory of PrP^{Sc} structure is the parallel in-register intermolecular β-sheet model (PIRIBS) in which individual PrP^{Sc} monomers stack on each other in a perfectly in-register manner[156]. The PIRIBS model was initially thought to be incongruent with the x-ray fiber diffraction and cryo-EM data, specifically the height measurements established, and the stacking of individual monomers ignoring stereotaxic hindrances of the glycosylated side chains[146,148,157]. However, following *in silico* molecular dynamic (MD) simulations placing tri-antennary glycans on the N-linked glycosylation sites, the PIRIBS model does not have any steric hindrances which was further corroborated through modeling based on a newly resolved

PrP amyloid structure[158-160]. Moreover, a recent study has derived the structure of the core region of PrP^{Sc} from brain-derived PrP^{Sc} fibrils through cryo-EM to a resolution of 3.8Å[161]. The study demonstrates that PrP^{Sc} from the 263K prion strain with the full complement of sugars and GPI anchor forms a PIRIBS structure with proposed quintessential features such as the hydrophobic "Greek key" motif (as seen with α-synuclein), a middle β-arch (residues ~125-168 forming a major hairpin), and a disulphide β-arch (between residues C179 and C214)[161,162]. In this new structure, the disposition of the N-linked sugars is distinctly different from early models that suggested steric clashes.

1.3.3: Conversion of PrP^{C} to PrP^{Sc}

The way PrP^{Sc} converts PrP^{C} to the infectious agent remained a question until recently, where molecular dynamic work was performed utilising the X-ray fiber diffraction and cryo-EM data, and physiological/steric constraints. The previously proposed theory was that the β-solenoid core of PrP^{Sc} has at least one free and accessible rung which can act as a template; an unfolded or partially unfolded PrP^{C} molecule would be able to bind to this templating rung and in turn, undergo conversion into a new complete four rung β-solenoid complete with its own free templating rung[145]. The proposed theory has been found to be compatible with the MD simulations yielding a transition pathway in which the C-terminal rung of the β-solenoid starts as the initial conversion site of PrP^{C} [163]. The unstructured N-terminus of PrP^{C} is able to bind the C-terminal rung, followed by a cascade of conformational transitions resulting in templating rungs converting the next section of PrP^{C} to the eventual PrP^{Sc} in an amyloid fiber[163]. The MD simulation adhered to all steric hindrances, as well as establishing that the conversion happens in a head-to-tail manner, another question common to the conversion of PrP^{Sc} to PrP^{C} [145,163]. A recent study suggested that the method of replication within the PIRIBS model is through a

conformational change of the C-terminus, which becomes undistinguishable from the fourth rung of the β-solenoid model, and in turn the previously described β-solenoid templating/conversion occurs (it must be noted that the authors believe the *bona fide* structure of PrP^{Sc} to be that of the 4RβS)[159].

1.3.4: Transmission barriers to prion disease

Currently, the only transmission of prion disease to humans is through acquired means, as shown by iatrogenic CJD, kuru, and vCJD, with only BSE prion demonstrating a zoonotic origin. Even though PrP^{C} is generally well conserved between animalia, the spread of PrP^{Sc} between species is not easily facilitated. This has previously been called the 'transmission barrier phenomena', where transmission is dependent on the degree of similarity between the donor PrP^{Sc} and the host PrP^{C} [164,165]. As the pathogenesis of prion disease revolves around the structural change of PrP^{C} to PrP^{Sc}, the transmission barrier would almost certainly be due to structural differences in host prion protein to prion agent. Initial evidence using transgenic mice expressing both hamster and mouse PrP found that depending on the inoculum (hamster or mouse prions), the mice would synthesize the corresponding prions demonstrating that the specificity of conversion is dependant on the primary sequence of the host PrP^{C} [166]. In addition, the generation of rabbit-mouse PrP chimeras were able to confer infection of rabbits intracranially challenged to PrP^{Sc} (a process that rabbits are resistant to), reiterating that regions of PrP^{C} secondary structure are essential for PrP^{Sc} conversion[167,168]. Furthermore, general susceptibility of any animal to prion disease is linked to the secondary structure of PrP^{C}, be it VRQ/ARQ/ARR haplotypes in sheep scrapie, or codon 126 (E/Q) in cervids[28,55]. Bank voles show little to zero resistance to prion transmission being highly susceptible to human, sheep, mouse, and hamster prions; this is linked to the presence of isoleucine at the polymorphic codon 109 (M/I)[169]. The aforementioned

MD modelling demonstrating the viability of both the 4RβS and PIRIBS models of PrP^{Sc} structure could lead to clarification of the transmission barrier of prions between species; the model can be used to test the templating efficiency and tolerance of host PrP^{Sc} to the PrP^{C} substrate[159,163]. With the rise of CWD over the last few decades, the question of possible zoonotic transmission remains a concern. To date, there have been no reported cases of a human developing CWD, and several studies have shown no evidence of transmission capabilities[59].

1.3.5: Diagnosis and treatment methods for prion disease

Diagnostic tools for prion disease

Since prion disease progresses quickly and with most deaths occurring after only a few months of observable clinical onset, a diagnostic tool able to detect disease before symptomatic onset is crucial in treatment. Initial diagnostic tools applied *post-mortem* involved western blot detection, enzyme-linked immunosorbent assay (ELISA), and the conformation-dependent immunoassay[10,170]. These methods came with procedural caveats: proteolytic removal of PrP^{C} was needed, only denatured PrP^{Sc} was detected, and there was poor antibody discrimination between PrP^{C} and PrP^{Sc} [10,171]. Moreover, these diagnostic tools can fail to determine the presence of prion disease, as PrP^{Sc} levels are not always detectable in some stages/types of disease (i.e., false negatives)[172,173]. The limits of early prion disease diagnosis/detection have been rectified through the development of prion amplification techniques. The most widely used amplification techniques are protein misfolding cyclic amplification assay (PMCA), and real-time quaking-induced conversion (RT-QuIC)[174]. PMCA allows for the rapid conversion of PrP^{C} to PrP^{Sc} while utilising: an excess of PrP^{C}, minute amounts of PrP^{Sc}, sonication of aggregated units of PrP^{Sc}, and a cyclic pattern of growth, sonication, and amplification[175]. RT-QuIC is similar to PMCA

except it uses shaking instead of sonication, bacterial synthesised recPrP instead of brain homogenate, a multiwell format, and a real-time fluorescent readout with a generic amyloid dye, as opposed to a western blot[176,177]. Utilising these techniques, it is possible to detect prion seeding in a wide range of tissues/fluids such as: cerebrospinal fluid (CSF), nasal fluid, brain, blood, urine, spleen, milk, and liver, even if seeding levels are incredibly low[177]. These two techniques have also been adapted and utilised for the detection of CWD, with a recent study utilising RT-QuIC to detect prion infection from ear pinna punches of asymptomatic white-tailed and mule deer[178,179].

Anti-prion compounds

In terms of therapeutics for prion disease, there are three avenues to attenuate PrP^{Sc} production: PrP^{C} reduction, PrP^{Sc} disaggregation, and inhibition of PrP^{C} to PrP^{Sc} conversion[180]. Initial studies looking for prion therapeutics explored polyanionic compounds and amyloidogenic dyes, as they were able to stop *in vitro* conversion and thus, inhibit the accumulation of PrP^{Sc} [17,181]. Congo red (CR), is one of the originally identified dyes that was able to inhibit the accumulation of PrP^{Sc} however, as with other polyanionic compounds, was only effective in cell culture models; *in vivo*, CR proved toxic and had poor efficacy and pharmacokinetics (e.g., was unable to cross the blood-brain barrier (BBB))[182-184]. Due to the limitations of compound accessibility (crossing the BBB) and toxicity, endeavours moved to identifying a compound that had shown human efficacy and an appropriate safety profile, thus quinacrine was identified[185]. Quinacrine, an anti-malarial drug used since the 1930's, was shown to be a potent inhibitor of PrP^{Sc} formation in cell culture, and due to decades of previous use, clinical trials began quickly following compound identification[180,185]. However, no significant changes in survival rates between the control and experimental groups were found, and so

quinacrine was halted as a potential prion disease therapeutic[186-188]. An identical result occurred with doxycycline; the previously used tetracycline was effective in inhibiting the accumulation of PrP^{Sc} in cell culture, but in human clinical trials demonstrated no significant change to patient survival time[189,190]. Altogether, cell culture models have indicated compounds that are able to inhibit the accumulation of PrP^{Sc} (especially for rodent prion strains), but unfortunately are poor predictors of what might be effective *in vivo*, especially with the need to address human infections that are less well represented in cell culture models[191].

Immunotherapy of prion disease

Even though PrP^{C} and PrP^{Sc} share secondary structure and their epitopes are immunologically indistinguishable, some immunotherapies have been shown to be effective against protein misfolding diseases in general[192,193]. Previously established evidence that PrP^{Sc} infectivity could be lowered by the presence of a polyclonal antibody was confirmed with *in vitro* studies, where anti-PrP^{C} antibodies were able to prevent PrP^{Sc} accumulation in cell lines[194-196]. Furthermore, antibodies were able to reduce PrP^{Sc} accumulation in a persistently infected prion cell line, and a correlation between affinity of the antibody to PrP^{C} and the efficacy was established[197,198]. Immunization against prion disease is the next logical step, but thus far, the efficacy of developed antibodies has proven lackluster. In animal models, active immunization against prion disease has shown a delay to disease onset, but some animals in a cohort may still develop the disease or only achieve partial protection as evidenced by a longer incubation period[199-201]. In one instance, a disease specific epitope vaccine recognising only elk PrP^{Sc} unexpectedly accelerated the disease onset[202]. Active immunization to prion disease is difficult to achieve, as the body is unable to decipher PrP^{Sc} from PrP^{C} due to both being recognised as endogenous proteins and therefore, a self tolerance to the inoculation is developed[191,203]. Some

other caveats to immunotherapeutics are the access of the antibodies to the CNS (passage through the BBB remains a challenge), and neuronal apoptosis caused by a subset of antibodies[203,204]. There is potential that those with genetic prion diseases would find the prolongation to disease onset worthwhile with active immunization, however due to the aforementioned reasons, no human clinical trial is currently underway.

So far, the only effective mitigation of prion disease in human and animal populations is through limiting the transmission, be it through ending of cultural practices such as kuru, or mass culling strategies of cervids[205,206]. The search for an effective treatment of prion disease is of paramount importance, and the refinement of previous experimental models and utilisation of new technologies will be needed for new, viable therapeutics.

1.4: CRISPR/Cas9 technologies

1.4.1: New and emerging technologies such as CRISPR can allow for a fresh look at prion biology, function and treatment

With conventional technologies, there has not been an appropriate treatment design or therapeutic to tackle prion disease. Exploration of new technologies can serve to aid and elucidate new treatments, or to adapt pre-existing technologies to solve the caveats of prion disease treatment. In general, the application of CRISPR/Cas9 technologies for the attenuation of prion disease would be through modulation of the *PRNP* gene expression; knockouts would inhibit the production of PrP^{C} and thus, the propagation of disease and (temporally controlled) overexpression can allow for therapeutics to be deciphered whilst mitigating against features of the prion protein, such as its metabolic stability.

1.4.2: Discovery and development of CRISPR/Cas9 technologies

Function of CRISPR/Cas9 in bacteria

Newly developed CRISPR (clustered regularly interspaced short palindromic repeats) based technologies utilise a bacterial and archaeal defense mechanism against viral attack[207]. The CRISPR-Cas (CRISPR associated) system for defense against bacterial viruses (phage) can be split into three distinct stages with the first being viral spacer acquisition; Cas 1 and 2 allow for the integration of short sections of foreign DNA into the host genome between the CRISPR locus/array repeats[208,209]. The acquired DNA section is dependent on the presence of a protospacer adjacent motif (PAM), an AAG sequence that acts as a recognition site[210]. The second step is the CRISPR expression, where an RNA polymerase transcribes a pre-CRISPR RNA (pre-crRNA) which is processed into smaller CRISPR RNAs (crRNAs), acting as a guide and in turn, has been referred to as guide RNAs (gRNA)[211,212]. The final step is the formation of a CRISPR-associated complex for antiviral defense (CASCADE) consisting of the crRNA and a series of Cas proteins[211]. CASCADE recognises and binds with foreign DNA before cleavage occurs by a Cas endonuclease, which is able to induce a double stranded DNA cleavage[213]. The acquired DNA can be transcribed whenever there is detection of a complimentary foreign DNA sequence[208]. Three types of CRISPR-Cas systems have been characterised depending on phylogeny, sequence, content, and locus organization; each type consists of the universal Cas1/2, and type-dependent/signature Cas proteins[208]. Type II CRISPR-Cas systems differ from the other types in that they do not employ the entire CASCADE complex, but rather utilise crRNA and the endonuclease Cas9[214]. Moreover, type II systems utilise a trans-activating crRNA (tracrRNA) to help the maturation of pre-crRNA into the guide crRNA[215].

Use of CRISPR/Cas9 as a gene editing tool

The type II CRISPR/Cas system has been modified for use as a gene editing tool; connecting the tracrRNA and crRNA into a RNA chimera was shown to be effective in inducing sequence-specific DNA cleavage in bacterial cells[216]. The technology was then optimised for use within mammalian cells, where the targeting RNA chimera is a 20-nucleotide gRNA strand that contains a PAM recognition sequence (a NGG sequence), and a Cas9 can induce sequence specific double strand breaks (DSB)[217,218]. Following a CRISPR/Cas9 DSB, the DNA target undergoes one of two pathways for DNA repair in mammalian cells: non-homologous end joining (NHEJ) or homology-directed repair (HDR)[218-220]. The repair options differ in the componentry needed and the fidelity of repair; HDR requires a homologous DNA template but is accurate in repair, whereas NHEJ cannot insure accurate DSB repair and does not require a template[219,220]. Both repair pathways can serve a purpose in genetic editing. As NHEJ can leave base pair insertions and deletions, the opportunity for frameshift mutations and stop codon formation is present which in turn can be used to generate gene knockouts[221,222]. HDR can be used to generate precise modifications when in the presence of an exogenous repair template[223,224]. Previously generated gene editing tools such as zinc-finger nucleases (ZFNs) and transcription activator-like effector nucleases (TALENs) utilise the DNA cleavage domain of FokI endonuclease and a specific DNA binding domain for the editing of DNA (through NHEJ or HDR); importantly, CRISPR/Cas9 induced genomic editing has advantages over ZFNs and TALENs[225-227]. These advantages include multiplex genomic editing, improved targeting efficiency, significant time and cost savings, and ease of target locus customisation[218]. Limitations of the Cas9 system are the necessity of a PAM recognition site (albeit in the human

genome a PAM site occurs every 8-12 bp, on average) and off-target editing, as with a 20 bp gRNA more than one target can be cut[217,218].

1.4.3: Applications of CRISPR technologies

CRISPRi/a can allow for inducible regulation of select genes

Modifying Cas9 into a nuclease-deficient version, referred to as dCas9 ("dead Cas9"), allows for the system to be adapted for genomic targeting without cleavage, which enables specific genetic localization of a 'scaffold protein' where its attachments can perform a plethora of functions[228,229]. The initial studies demonstrating dCas9 CRISPR interference (CRISPRi) showed that binding of dCas9 was able to inhibit gene expression in bacterial cells through the blocking of RNA polymerase (RNAP) or transcription factor binding, when bound to promoter sequences[228,230,231]. Studies also showed that dCas9 can serve as a platform/scaffold in which transcriptional effectors can be recruited and modulate gene expression[228,230]. In mammalian cells, blocking of RNAP by dCas9 only achieved slight inhibition of gene expression, but when bound with a fusion protein, such as the Krüppel-associated box (KRAB), enhanced repression was achieved[228,232]. Disadvantages of CRISPRi include possible downstream effects of dCas9 binding (activation or repression of non-target genes), and for full repression or knockdown of endogenous genes, extremely select gRNA targeting is needed due to the possible presence of regulatory elements or the chromatin structure being inaccessible[229].

CRISPR activation (CRISPRa) also utilises dCas9 fusion proteins as a platform for a transcription effector. CRISPRa studies initially used viral protein 16 (VP16, transcriptional activator of Herpes simplex), or p65 (transactivator domain of nuclear factor kappa B), fused to dCas9 for targeted transcriptional activation[233]. Some caveats of the initial CRISPRa technology

were that multiple gRNA localisation sequences were needed for significant endogenous gene activation, and the activation by a single p65/VP16 did not cause a substantial increase of expression of some genes[234-236]. Developments in CRISPRa technology have allowed for mitigation of some of the above-mentioned issues. Fusion of dCas9 to a carboxy-terminal SunTag array allowed for the recruitment of multiple VP64 activators and significant gene activation using a single gRNA[237]. Another group developed a tripartite activator consisting of VP64, p65, and Rta (Epstein-Barr virus R transactivator) which improved CRISPRa of endogenous genes[234]. Looking to the gRNA design has also allowed for improved CRISPRa systems, such as the synergistic activation mediator (SAM) system which adds MS2 aptamers (short sequences of single-stranded nucleic molecules able to bind to target molecules) to gRNA[238]. The MS2 aptamers interact with the MS2 binding protein (MCP) which in turn is fused to the activator domain of p65 and heat shock factor 1 (HSF1), and by these means, significantly improve transcriptional activation of a single gRNA[238,239].

To allow for the spatial and temporal control of CRISPRi/a systems, coupling of the dCas9 and transcriptional effector domains to chemical and optical induced dimerization domains has been shown to produce inducible transcriptional activation and repression[233]. The dCas9 and transcriptional effector are separately bound to inducible dimerization domains, which under the correct conditions, will dimerize and cause transcriptional activation/inhibition; some examples include: the chemically inducible rapamycin FK506 binding protein 12 (FKBP12) and FKBP rapamycin binding (FRB) domain, the blue light-inducible cryptochrome 2 (CRY2) and calcium and integrin binding 1 (CIB1) protein, and the red light-inducible phytochrome B (PhyB) and phytochrome interaction factor 3 (PIF3)[240-242]. Being able to have a system for controllable expression of endogenous genes can allow for therapeutic applications.

Consequently, a therapeutic can be tested while modulating nascent levels of a gene/protein, perhaps previously found to be confounding.

Gene drive systems allow for a super-Mendelian inheritance of an edited gene

CRISPR/Cas9 technology has been utilised to generate gene drive systems converting typical Mendelian inheritance to super-Mendelian inheritance. In typical Mendelian inheritance, the probability a specific gene or allele is passed to offspring is 50%; with a gene drive, this probability is heavily driven to become 100% and thus, has been dubbed super-Mendelian inheritance (Figure 2). Gene drives seek to force a modified allele (for the biological trait of interest and containing the gene drive componentry) into a population over the wild type allele through one of two methods; one being that the gene drive element is able to copy itself into the opposite chromosome, changing zygosity from heterozygosity to homozygosity for the

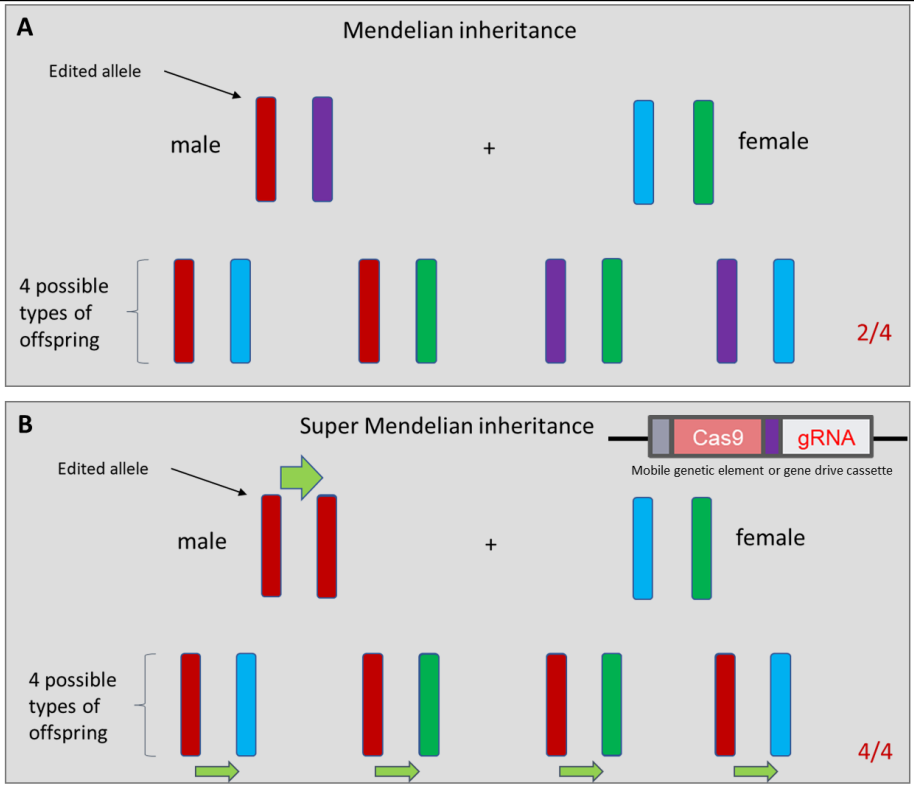

Figure 2. Schematic representation of Mendelian and super Mendelian inheritance. Bars indicate alleles with red representing edited allele, and green arrow indicating editing occurring via mobile genetic element. **A**, Mendelian inheritance schematic in which an edited allele only has a 50% chance of passing on to offspring. **B**, super Mendelian inheritance schematic in which an edited allele has a 100% chance of being present in progeny.

gene drive element (resulting in 100% gene drive element presence in offspring), and in the other method, the gene drive element will provide a fitness advantage over the wild type allele[243].

The initial application of CRISPR/Cas9 technologies to gene drive was the generation of the "mutagenic chain reaction" in which a plasmid contains a cassette of a Cas9 coding region immediately followed by the gRNA coding region, and either side of the Cas9/gRNA are homology arms (Figure 2B)[244]. The gRNA targeting a genomic locus of interest will guide the Cas9 to induce a DSB; following this, HDR will occur using the homology arms specific to the adjacent sequences of the cleavage site in order to insert the Cas9/gRNA cassette into the selected allele[244]. In turn, the cassette will be able to induce cleavage and HDR of the second allele resulting in homozygous edited alleles[244].

So far, the mutagenic chain reaction has been utilised to generate a highly efficient gene drive system in yeast (*Saccharomyces cerevisiae*), mosquitoes (*Anopheles stephensi* and *gambiae*), and fruit flies (*Drosophila melanogaster*)[244-248]. The progeny transmission rates in yeast, mosquitoes, and fruit flies are highly efficient with lowest being 91.4% effective (*Anopheles gambiae*), and the highest being 99% (yeast); yet the same cannot be stated for the mammalian gene drives[245,247,249]. Issues have occurred when attempting gene drives in mammalian models; the only published work achieved a transmission rate of 22.5%, where only female mice underwent HDR for the gene drive cassette[249]. The major complication of using a gene drive in mice is that the window for which Cas9 expression occurs (during meiosis) needs to be finely tuned to result in a DSB and HDR[249,250].

Gene drives have a potent capability to address global ecological issues surrounding health, agriculture, and conservation[251,252]. Issues such as insect borne disease and pest

management can be remedied using a gene drive; several studies have looked at targeting mosquitos to block the transmission of malaria. Antimalarial or infertility genes have been shown to be transmitted to approximately 90% of *Anopheles* mosquito progeny through a gene drive; enabling this population control/modification can result in the eradication of malaria within hotspot regions[246,247,253,254]. Even though there has not been a successful mammalian gene drive performed within a laboratory setting, the application of population control and/or disease management remains a future possibility for CRISPR/Cas9 mediated super-Mendelian inheritance.

1.5: Hypotheses

We wish to develop methods for the treatment and/or removal of prion disease through modulation of PrP^{C}. If there is not an appropriate conversion substrate for PrP^{Sc}, then prion disease would be unable to perpetuate. We believe that a multipronged approach looking at different features of PrP^{C} production/processing with a variety of technologies (CRISPR/Cas9, library screens, and candidate-based approaches) will provide us with an effective measure for the attenuation of prion disease.

Utilising CRISPR/Cas9 technologies, we wish to develop a system in which we can stop the spread of CWD within cervid populations. CWD is rapidly proliferating through North America and being identified in new countries. So far there are no effective therapeutics, and the only management is mass culling or pre-emptive harvest strategies[206,255]. Gene drive technologies are a potent method of forcing a null allele into a population, and we hypothesise that disruption of *PRNP* through super-Mendelian inheritance would stop the spread of CWD. Without the production of PrP^{C}, there can be no spread of PrP^{Sc}, and as there are no obvious

phenotypic abnormalities in *PRNP* knockout animals (e.g., mice, goats, and cows), we suggest that a gene drive knocking out PrP^{C} production in cervids would have no gross phenotypic perturbations whilst stopping the spread of the prion agent[256,257].

As CRISPR/Cas9 gene drives have yet to have been effective in mammals, we decided to simultaneously explore other avenues of prion disease treatment. Based upon a previously developed assay using a capillary-based western in the Westaway lab and successful hits within a small compound library screen (unpublished data), we hypothesise that by exploring a larger library, we will find compounds that are able to modulate the cleavage of PrP^{C}. Identifying a compound that can increase C1 fragmentation or decrease C2 fragmentation would be of therapeutic potential, as it would increase the pool of neuroprotective PrP fragments and lower those that can be converted to PrP^{Sc}. We expect five possible outcomes for a compound: C1 fragment increase, C1 fragment decrease, C2 fragment increase, C2 fragment decrease, and mixed outcomes (two of the previous outcomes occurring simultaneously). Through identification of compounds able to increase the fragmentation of both the C1 or C2 fragment, there is also potential for elucidation or identification of the α- and β-PrPase (proteases responsible for α- and β-cleavage of PrP^{C}).

As the C1 fragment of PrP^{C} is neuroprotective, deciphering the protease responsible would be an invaluable asset for prion disease therapeutic derivation[90]. We are performing a candidate driven approach for elucidation of the α-PrPase, and we hypothesize that the prospective α-PrPase is a type II membrane serine protease expressed within neurological tissues and is inhibited by the non-class specific protease inhibitor, Camostat mesylate. Through this approach, we may also identify proteases that are involved in the biosynthesis and functionality of PrP^{C}.

Chapter 2: Materials and Methods

2.1: Small molecule library screen methodology

2.1.1: Cell culture and compound addition

A S3-PrP stable cell line generated from the parental rabbit kidney epithelial (RK13) cell line, as per previously published methods, was used for the entirety of the compound library screen[74]. The cells were cultured in Dulbecco's modified Eagle's medium (DMEM) containing 1g/liter D-glucose, 4 mM L-glutamine, and 1 mM sodium pyruvate, supplemented with 10% (v/v) fetal bovine serum (FBS), 50 units/mL penicillin, and 50 µg/mL streptomycin (all manufactured by Gibco). The cells were grown in a T25 flask (Falcon) at 37 ºC in 5% CO_2 and 95% humidity, and passaged every 3 to 5 days depending on confluency.

To begin the cell-based screen, cells approaching confluency were trypsinized (1x Liquid 0.25% Trypsin/1 mM EDTA, Gibco) and used to seed a 96-well tissue culture plate (Falcon) at a concentration of 5000 cells/well, which was then incubated for 24 hours prior to the first compound addition. The tested compound library, #5841 Tocriscreen Plus Mini (TOCRIS, Bristol, UK), contained 1280 compounds pre-dissolved in DMSO at a concentration of 10 mM. The compounds were prepared as a working stock at a concentration of 2 mM (DMSO) for the addition to the gridded S3 RK13 cells within a 96 well V-bottom microplate (Greiner). The compounds were added to the cells by a Perkin Elmer JANUS^{TM} automated liquid handling system (Experiments were performed at the University of Alberta Faculty of Medicine & Dentistry High Content Analysis Core, RRID:SCR_019182), to a final compound concentration of 20 µM. Following the initial compound addition, the plates were incubated at 37 ºC, 5% CO_2, and 95% humidity for 72 hours. After 72 hours elapsed, the media was replaced, and a second

addition of compounds occurred. 24 hours after the second compound addition (or 96 hours of total compound exposure), the cells were lysed.

2.1.2: Cell lysis and PNGase F treatment

The cells were lysed in-plate using radioimmune precipitation assay (RIPA) lysis buffer (50 mM Tris, 150 mM NaCl (pH 7.4), 1% (v/v) NP-40, and 0.5% (w/v) sodium deoxycholate) supplemented with 1.3 mM EDTA, 0.32% (w/v) SDS, 26 mM DTT, Roche Complete Protease Inhibitor Cocktail, and placed on ice for 15 min. To pellet the cell debris, the plate was centrifuged at 1000 x *g* for 10 min at 4 ºC (Avanti J-E Centrifuge, Beckman Coulter). The supernatants were transferred to 96-well microplates (Greiner) for PNGase F (Peptide-N-Glycosidase F) digestion. All PNGase F digestion reagents were acquired from New England Biolabs (NEB). The in-plate deglycosylation occurred using a glycoprotein denaturing buffer consisting of GlycoBuffer 2, 1.25% (v/v) NP-40, and 5 units/µL of PNGase F, as described previously[258]. Following the addition of PNGase F, the plate was incubated for 1 hour at 37 ºC.

2.1.3: Capillary western analysis

Protein Simple Inc. (San Jose, CA, USA) supplied all of the reagents and equipment, with the exception of the lysates and primary antibodies. The cell lysates were mixed in a 4:1 ratio with the Fluorescent 5X Master Mix, which provides a denaturing and reducing buffer environment (1% (w/v) SDS and 40 mM DTT). The samples were then vortexed and denatured at 95 ºC for 5 min. 4 µL of the denatured samples were then loaded into the top row well of a 12-30 kDa microplate that is prefilled with electrophoresis buffers and has 24 lanes for sample electrophoresis. Following the manufacturer's instructions, the subsequent rows were filled with Antibody Diluent 2, primary antibodies, secondary antibodies, chemiluminescence reagents, and

wash buffer. The primary antibodies used were mouse mcAb Sha31 (Spi-Bio Inc., A03213, 1:500 dilution) and anti-β-tubulin (Novus Biologicals, NB600-936, 1:400 dilution) which were diluted in Antibody Diluent 2. The secondary antibodies used were anti-mouse secondary HRP conjugate and 20X anti-rabbit secondary HRP conjugate. Following a 5-minute centrifugation at 1000 x *g* at room temperature, the plate was loaded into the Wes machine; fresh capillaries were also loaded at this time. The assays were performed utilising the Compass software 12-230 kDa separation range protocol, with the separation time being adjusted from 25 min to 30 min. Compass outputs data in the form of apparent molecular weight (MW) versus chemiluminescence signal. The apparent MW is determined by Compass through establishing ladder peaks to capillary positions and using the signal output from fluorescently labeled protein standards present in the 5X Master Mix to adjust for capillary migration differences. Compass software was then used to perform peak area calculations utilising the default Gaussian fit method.

2.2: Experimental procedures for candidate-based protease studies

2.2.1: Plasmid preparation for protease candidates

The expression plasmids encoding proteases of interest are summarized in Table 1. Following resuspension of the plasmid in accordance with manufacturer's instructions, the DNA was transformed into DH5α Oneshot/MAX Efficiency cells (Invitrogen) and plated on LB plates (Difco) supplemented with ampicillin (100 µg/mL, Sigma). The DNA purification following amplification occurred using a maxiprep kit (Qiagen Inc., Toronto, Ontario) abiding by manufacturer's instructions. The DNA was diluted to a concentration of 1 mg/mL).

Protease expressed	GeneScript clone ID	Vector	ORF Accession Number	ORF size (bp)
TMPRSS1 (Hepsin)	OMu01663	pcDNA3.1+/C-(K)-DYK	NM_008281.4	1248
TMPRSS2	OMu20152	pcDNA3.1+/C-(K)-DYK	NM_015775.2	1470
TMPRSS4	OMu82772	pcDNA3.1+/C-(K)-DYK	NM_001364528.1	885
TMPRSS5	OMu08401	pcDNA3.1+/C-(K)-DYK	NM_030709.2	1335
TMPRSS11D	OMu20166	pcDNA3.1+/C-(K)-DYK	NM_145561.2	1251
HTRA1	OMu19003	pcDNA3.1+/C-(K)-DYK	NM_019564.3	1440

Table 1. Protease plasmids used for transfection experiments, and clone information. The plasmids were purchased from GenScript and subsequently transformed and maxiprepped prior to transfection. All plasmids used the vector backbone of pcDNA3.1+/C-(K)-DYK.

2.2.2: Cell culture methods

Two cell lines were used for the *in vivo* assay of candidate proteases: RK13 cells and a derivative encoding WT (*Prnp*^{a}) mouse PrP, RK13-WT10 cells. Cell culture was completed as per section ***2.1.1***.

2.2.3: Transfections and co-transfections

To initiate the transfections, cells approaching confluency were treated with 0.25% Trypsin-EDTA (1x Liquid 0.25% Trypsin/1 mM EDTA, Gibco) and used to seed a 96-well tissue plate (Falcon) at a concentration of 15,000 cells/well in an antibiotic free medium

(DMEM, 10% FBS), which was left for 24 hours in the incubator prior to the transfection. For the co-transfections, the expression vectors at a concentration of 1 mg/mL were thawed and prepared at 4X final concentration whilst limiting the total DNA to ~100 ng per well, using OptiMEM (Gibco) as the diluent. The vectors encoding GPI-anchored proteins were as follows: pCDNA3.PrP.wt, pBud.CE4.PrP.wt (EF1a), and pcDNA3.Thy1 (all generated within the Westaway lab). All of the transfections were performed using the Lipofectamine 3000 kit (Invitrogen). Following mixing of the DNA, Lipofectamine 3000, and P3000 reagent, the solution was left for 15 min before gentle pipetting into the appropriate well. The cells were left for 4-6 hours in a 37 ºC incubator (5% CO_2, and 95% humidity), before the media was replaced with growth media containing antibiotics. The cells were left for ~2 days before lysis and processing.

2.2.4: Lysis and capillary western

Both lysis and capillary westerns were performed as described above (***2.1.2*** and ***2.1.3***), with a few noted changes to the capillary western for the stable cell clone transfection. The primary antibody used was Sha31, but β-tubulin (as an internal control) was omitted for the use of the Total Protein Detection Module (purchased from Protein Simple). All samples ran with Sha31 primary antibody were also ran using the Total Protein Detection Module, as per the manufacturer's instructions.

2.2.5: Conventional western blot analysis

Following lysis and deglycosylation, the samples were reduced and denatured prior to loading into a 12% Tris-glycine gel. The samples were separated by SDS-PAGE using a Bio-Rad Mini-PROTEAN Tetra cell and transferred to a polyvinyl difluoride membrane (PVDF,

Immobilon) using a Bio-Rad SD semi-dry electrophoretic transfer cell[259]. The membrane was subsequently incubated overnight at 4 ºC with Sha31 primary antibody (diluted 1:30,000 in TBS/0.5% Tween 20). After 3 washes with TBS/0.1% Tween 20, the membrane was incubated at room temperature for 1 hour with goat anti-mouse IgG-HRP conjugate (Bio-Rad, 170-6516) diluted 1:10,000 in blocking buffer (5% skimmed milk in Tris-buffered saline (TBS) containing 0.1% (v/v) Tween 20). After three additional washes, the membrane was visualised using enhanced chemiluminescence reagents (Pierce, PI32106). After exposure of the membrane to X-ray film, the films were scanned utilising a Fluor Chem E Imager (ProteinSimple Inc.). When the primary antibodies of sPrPG228 (diluted 1:1000 in TBS/0.1% Tween 20, 5% milk) or α-Thy1 (diluted 1:2000 in TBS/0.1% Tween 20, 5% milk) were used, the membrane after transfer was blocked using blocking buffer (TBS/0.1% Tween 20, 5% milk). The secondary antibody used for sPrPG228 primary was goat anti-rabbit IgG-HRP conjugate (Bio-Rad, 172-1019) diluted 1:10000 (in TBS/0.1% Tween 20, 5% milk), and for α-Thy1 was goat anti-rat IgG-HRP conjugate (Bio-Rad, 5204-2504) diluted 1:10000 (in TBS/0.1% Tween 20, 5% milk).

2.2.6: Collection and processing of conditioned media

For the experiments that required analysis of the conditioned cell culture media, after the cells recovered in supplemented media following transfection, the media was changed for non-supplemented DMEM (Gibco). The cells were then left for approximately 48 hours at 37 ºC in 5% CO_2 and 95% humidity. Following this, the media was collected and centrifuged at 300 x *g* for 5 min at 4 ºC to pellet any detached cells. The media was then transferred to a pre-washed Amicon Ultra-4 Centrifugal Filter Unit with a molecular cut-off of 3 kDa (MilliporeSigma) and centrifuged at 4000 x *g* for 40 min at 4 ºC.

2.3: Inducible PrP/CRISPRa

Previously published methods for blue light CRISPRa were adapted for use as an inducible PrP system[241].

2.3.1: Cell culture

The cell line utilised for the inducible PrP/CRISPRa system was the human embryonic kidney 293 T (HEK293T). The cells were cultured as per ***2.1.1***.

2.3.2: Plasmid preparation

All plasmids used for the blue light CRIPSRa PrP induction were purchased from Addgene and provided as an agar stab. The plasmids were as follows: NLSx3-CRY2PHR-p65 (catalogue number 64124), NLS-dCas9-trCIB1 (catalogue number 64119), and pgRNA-Humanized (catalogue number 44248). The plasmids were purified following amplification utilising a maxiprep kit (Qiagen) and prepared to a concentration of 1 mg/mL. Following purification of the pgRNA-Humanized plasmid, DNA was linearized using *Bst*XI and *Not*I restriction enzymes (NEB). gRNA inserts were subsequently ligated into the linearized plasmid to create the gRNA expression vectors using T4 ligase (NEB) summarised in Table 2. gRNA inserts were prepared through

Plasmid Name	gRNA target sequence	PRNP locus
pgRNA-Humanized.gRNA1	TTAAATTTTGAGGCGTAGAA	-143 to -124
pgRNA-Humanized.gRNA2	GGAAGCAATTTCTGGAACTT	-36 to -17
pgRNA-Humanized.gRNA3	GCAAAAAATTTTGCTTAACC	-84 to -65
pgRNA-Humanized.gRNA4	ATAAATATTAATCTCAATCC	-105 to -86
pgRNA-Humanized.gRNA5	AGGAATGAGGAAGCAATTTC	-28 to -9

Table 2. gRNA vectors for the targeting of dCas9 to the human *PRNP* promoter. The backbone vector of pgRNA-Humanized was purchased from Addgene (44248) and the gRNA sequence was ligated into the linearized plasmid.

the annealing of complimentary DNA oligomers (with sticky ends) designed to target a specific region of interest of the human *PRNP* promoter (Table 2). The oligomers were purchased from Integrated DNA Technologies (IDT) and prepared to 100 µM concentration with buffer (50 mM Tris pH 8.8, 100 mM NaCl, and 1 mM EDTA). To anneal the DNA oligos resulting in sticky-end overhangs, a linker protocol was used (95 ºC for 2 min, 52 ºC for 10 min, and a 4 ºC hold).

Following insertion of DNA coding for the gRNA into the expression vector, the plasmids were transformed into DH5α Oneshot/MAX Efficiency (Invitrogen) cells, and plated on LB plates (Difco) supplemented with ampicillin at a final concentration of 100 µg/mL (Sigma). The plasmid DNA was purified using a QIAcube (classic) automated machine (Qiagen) and for initial confirmation of gRNA insertion, we initially performed a digest with *Eco*RI and *Bam*HI restriction enzymes. The reaction products were ran on a 1-2% agarose gel at 50 V utilising 0.5X Tris-Borate-EDTA (TBE; 89 mM Tris, 89 mM Borate, 2 mM EDTA) buffer and visualised with SYBR™ Safe DNA gel stain (Invitrogen) within an agarose electrophoresis apparatus[260]. The plasmids were subsequently sent for Sanger sequencing with the Molecular Biology Facility (MBSU, Department of Biological Sciences, University of Alberta). After sequence confirmation, plasmid purification occurred using a maxiprep kit (Qiagen) following manufacturer's instructions. The DNA was diluted to a concentration of 1 mg/mL.

2.3.3: Transfection and blue light induction

Cells approaching confluency were used to seed 6 well plates (Falcon) and kept in a 37 °C incubator (with 5% CO_2 and 95% humidity) until cell confluency was ~80%. Prior to transfection, the media in the wells was replaced with OptiMEM media (Gibco). All transfections utilised the Lipofectamine 3000 kit (Invitrogen). The DNA for transfection was

prepared in a 1:1:1 ratio of NLSx3-CRY2PHR-p65, NLS-dCas9-trCIB1, and pgRNA-Humanized (1-5) which was in a 1:1:1:1:1 ratio itself. Following mixing of the DNA, Lipofectamine 3000, and P3000 reagent, the solution was left for 15 min before dropwise addition into the appropriate well. The cells were left for 4-6 hours in a 37 ºC incubator (with 5% CO_2 and 95% humidity) before the media was replaced with the typical growth media containing antibiotics. The cells were left for ~2 days under blue light irradiation (470±20 nm) before lysis and processing.

2.3.4 Lysis and capillary western

Lysis and capillary western analysis were performed as per above (***2.1.2*** and ***2.1.3***)

2.4: Targeting of PRNP for NHEJ knockout by CRISPR/Cas9

2.4.1: Culture of the MDB cell line

Mule deer brain (MDB) cells generated from mule deer brain tissue, transfected with a plasmid containing the simian virus 40 (SV40) genome were housed in a dedicated incubator and propagated as per previously published[261]. The cells were cultured in OptiMEM media, supplemented with 10% (v/v) FBS, 50 units/mL penicillin, 50 µg/mL streptomycin, and 1X Glutamine (all manufactured by Gibco). Cells were grown in a T25 flask (Falcon) at 37 ºC in 5% CO_2 and 95% humidity and passaged when at ~80% confluency.

2.4.2: Plasmid preparation for PRNP gene knockout

Plasmids expressing the Cas9 endonuclease were modified to include the gRNA encoding region, the unmodified vector was px330.U6-eSpCas9-1.1 purchased from Addgene

(catalogue number 71814). The plasmid was initially linearized with the *Bbs*I restriction enzyme. gRNA-encoding inserts were prepared and inserted as above (***2.3.2***).

2.4.3: Transfection of CRISPR/Cas9 plasmids into the MDB cell line

Cells approaching 80% confluency were used to seed 6 well plates (Falcon) and then kept in a 37 °C incubator (with 5% CO_2 and 95% humidity) until cell confluency was ~60%. Before transfection, the media in the wells was replaced with OptiMEM media (Gibco). All transfections were performed as above (***2.2.3***).

2.4.4: DNA collection and T7E1 CRISPR cleavage test

To isolate the DNA for the T7E1 mismatch assay, cells were detached from the wells using trypsin (1x Liquid 0.25% Trypsin/1 mM EDTA, Gibco), and then neutralised using the serum containing media. The cells were then pelleted at 300 x *g* for 5 min at room temperature and resuspended in PBS. Genomic DNA from the cells was purified using a Qiagen DNeasy Blood and Tissue kit. To detect genome editing by the CRISPR/Cas9 system, the Alt-R Genome Editing Detection Kit (IDT) was used which utilised the T7 endonuclease 1 (T7E1) resolvase. Primers for amplification of the DNA target region by PCR were designed following manufacturer's recommendations of attaining an amplicon of approximately 1000 bp with the Cas9 cut site off centre of amplicon for fragment resolution by gel analysis.

Following PCR amplification using AccuPrime Taq DNA Polymerase, High Fidelity (Invitrogen) of the 'edited' DNA (and the Alt-R Genome Editing Kit Control DNA samples A and B), the protocol for forming DNA heteroduplexes was followed as per the instruction with the deviation of a 30 min digest at 37 °C rather than 60 min. To stop enzyme activity, the reactions were placed on ice, and 0.5 M EDTA (pH 8.0) was added to a final concentration of 20

mM. For visualisation of the T7E1 mismatch detection results, the reaction products were ran on a 1-2% agarose gel at 50 V utilising 0.5X Tris-Borate-EDTA (TBE, 89 mM Tris, 89 mM Borate, 2 mM EDTA) buffer and SYBR^{TM} Safe DNA gel stain (Invitrogen) within an agarose electrophoresis apparatus[260].

Chapter 3: Results

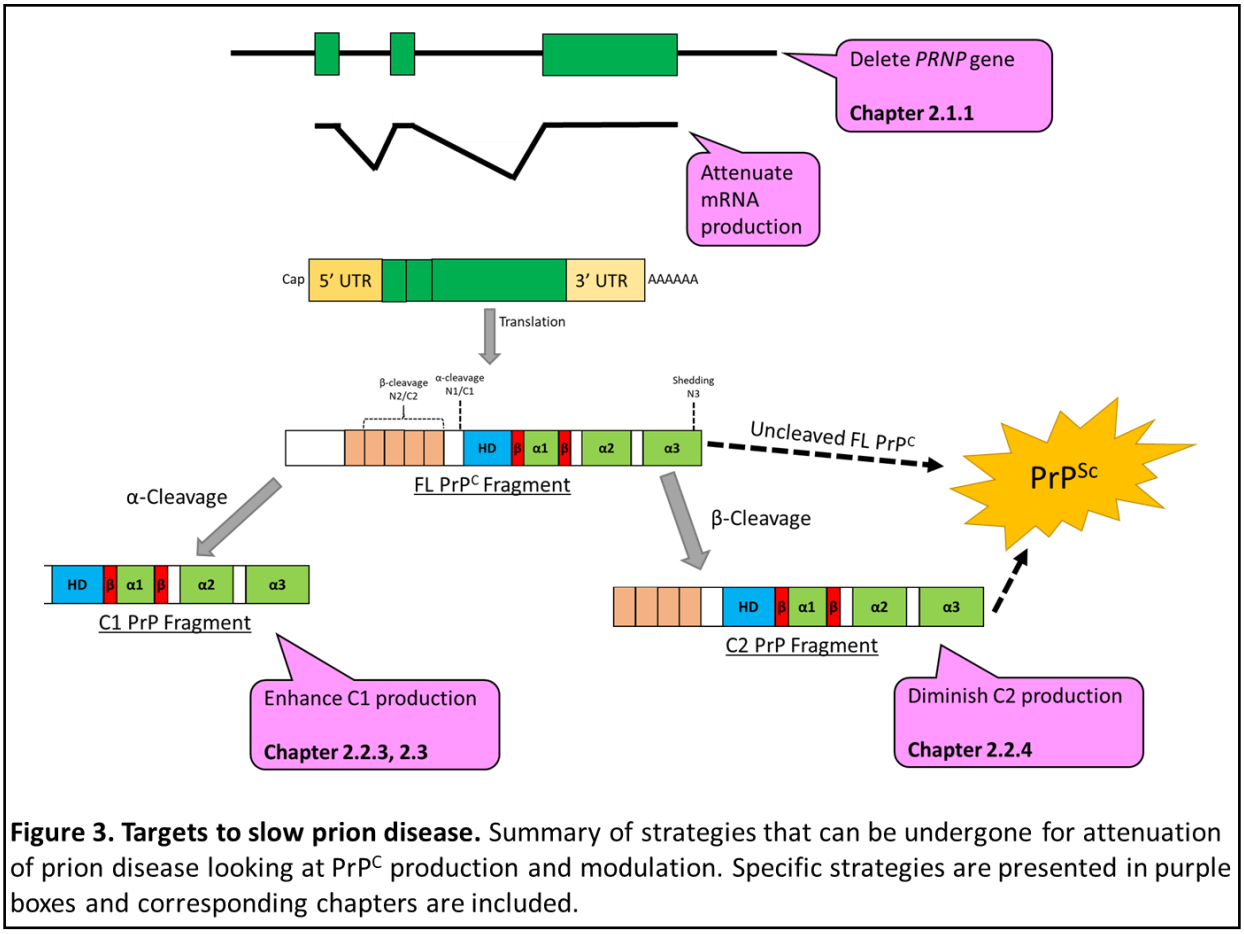

Figure 3. Targets to slow prion disease. Summary of strategies that can be undergone for attenuation of prion disease looking at PrP^C production and modulation. Specific strategies are presented in purple boxes and corresponding chapters are included.

3.1: CRISPR/Cas9 based modulation of PrP^C production

3.1.1: gRNA design for the PRNP target locus

We wished to utilise CRISPR/Cas9-derived editing and non-homologous end joining (NHEJ) to create a loss of function mutation in deer *PRNP*. If there is no production of PrP^C, then there can be no presence of PrP^{Sc} (Figure 3). The implication is that if the gRNA and Cas9 combination are successful in our target region, the machinery can be adjusted for the design of a mobile genetic element or gene drive cassette to apply in a gene drive strategy against CWD.

The gene region we targeted for editing was between the region coding for residue 23 and 50, with a consideration for three possible confounds (Figure 4A). If an edit were to occur close to the 5' splice acceptor of exon 3 of *PRNP,* the possibility of downstream *PRND* gene activation through alternative splicing could occur, generating the neurotoxic Dpl protein (Figure 4B, as seen in several knockout mice models)[101-103]. Furthermore, if the edit occurs too far 3' within the exon 3 ORF, a truncated PrP protein could be morbific in nature based upon the behavior of pathogenic stop codon alleles Y145X, Q160X, and Y163X (Figure 4A)[262-264]. Attempted editing in the octarepeat region of PrP would present a technical problem because the DNA sequences are not unique, but instead are arranged in five tandem degenerate blocks. For these reasons, we focused our gene editing upon the region encoding amino acids 23-50 of mule deer *PRNP* ORF. As for design of the gRNA, we took the genome region corresponding to peptide range 23-50 of mule deer *PRNP,* uploaded it to the MIT gRNA design tool (crispr.mit.edu), and selected two gRNA target sequences:

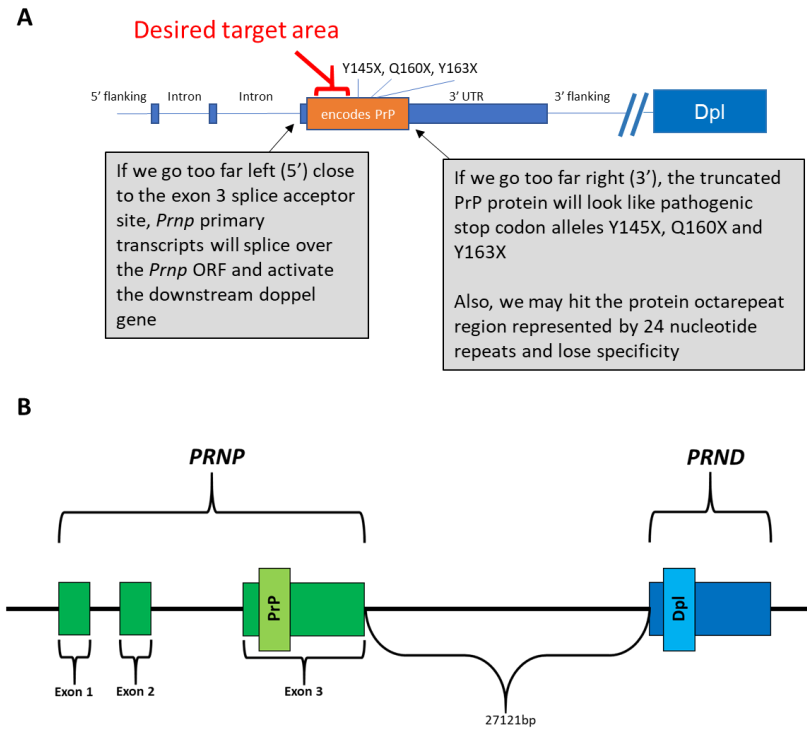

Figure 4. *PRNP* gene target area for CRISPR/Cas9 editing. A, target region for CRISPR/Cas9 edit to negate possible side effects. Corresponds to residue 23-50 of PrP. **B**, distance of *PRNP* to *PRND* (27121 bp). Distances between exon 1, exon 2, and exon 3 are 2409 bp and 13836 bp (respectively).

GGGAGCCGATACCCGGGACA, and GGAGGAGGATGGAACACTGG. These sequences were also cross referenced to another gRNA design tool recommended by the Zhang lab (developers of crispr.mit.edu) under the url of e-crisp.org. The sequences were labelled as gRNA1 and gRNA2 (respectively) and correspond to the regions of the *PRNP* gene that encode amino acids 38-44 and 31-37 (respectively).

3.1.2: CRISPR/Cas9 editing plasmid construction

Following the design of gRNA1 and gRNA2, we ligated the inserts into px330 (a Cas9/gRNA expressing vector originally designed and developed in the Zhang lab, Figure 5B) by engineering sticky ends complimentary to the *Bbs*I cut site (Figure 5A). After ligation into the *Bbs*I site, the site is no longer present allowing for confirmation through digestion with *Bbs*I and

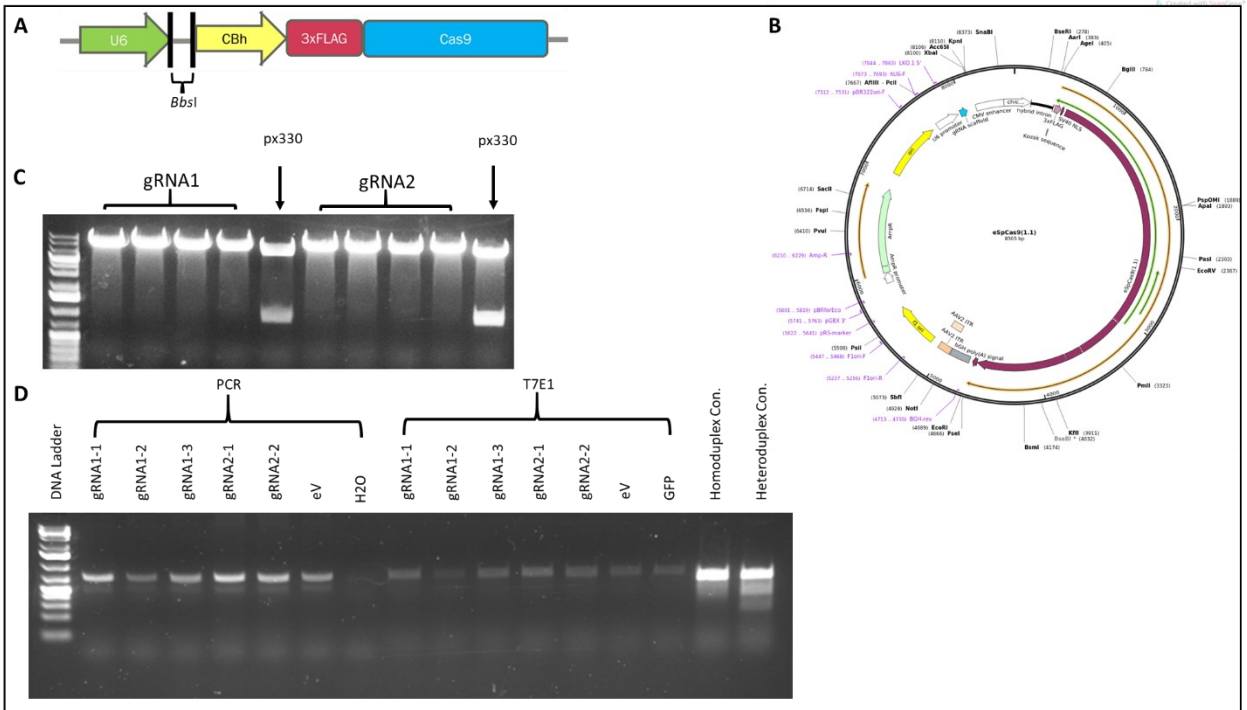

Figure 5. CRISPR/Cas9 px330 vector preparation and T7E1 gene editing assay. A, schematic showing the ligation region for gRNA inserts into px330. **B**, sequence map of px330 (https://www.addgene.org/71814/) **C**, 1% agarose gel demonstrating a double digestion with *Bbs*I and *Age*I of ligated gRNA inserts into px330 and px330 (empty). Successful ligation is demonstrated by a single band, *Bbs*I cut site is no longer present. **D**, 1 % agarose gel analysis of potential gene editing by px330.gRNA1/2 clones, PCR amplicon shown on the left and T7E1 assay results on the right. eV, empty vector (px330). The homoduplex and heteroduplex controls were provided with the T7E1 assay kit. The CRISPR/Cas9 plasmids were unable to generate editing of the *PRNP* gene.

*Age*I. We found that four clones for both gRNA1 and gRNA2 had successful ligation, as there was a single band present at ~8500 bp in a 1% agarose gel (Figure 5C). This process was also repeated for another Cas9/gRNA vector, px458, which is identical to px330 except for an EGFP expression region (Figure 6B); the ligation was successful as we saw a band at ~9300 bp (Figure 6A). The above-mentioned successful ligations were confirmed through Sanger sequencing with MBSU at the University of Alberta.

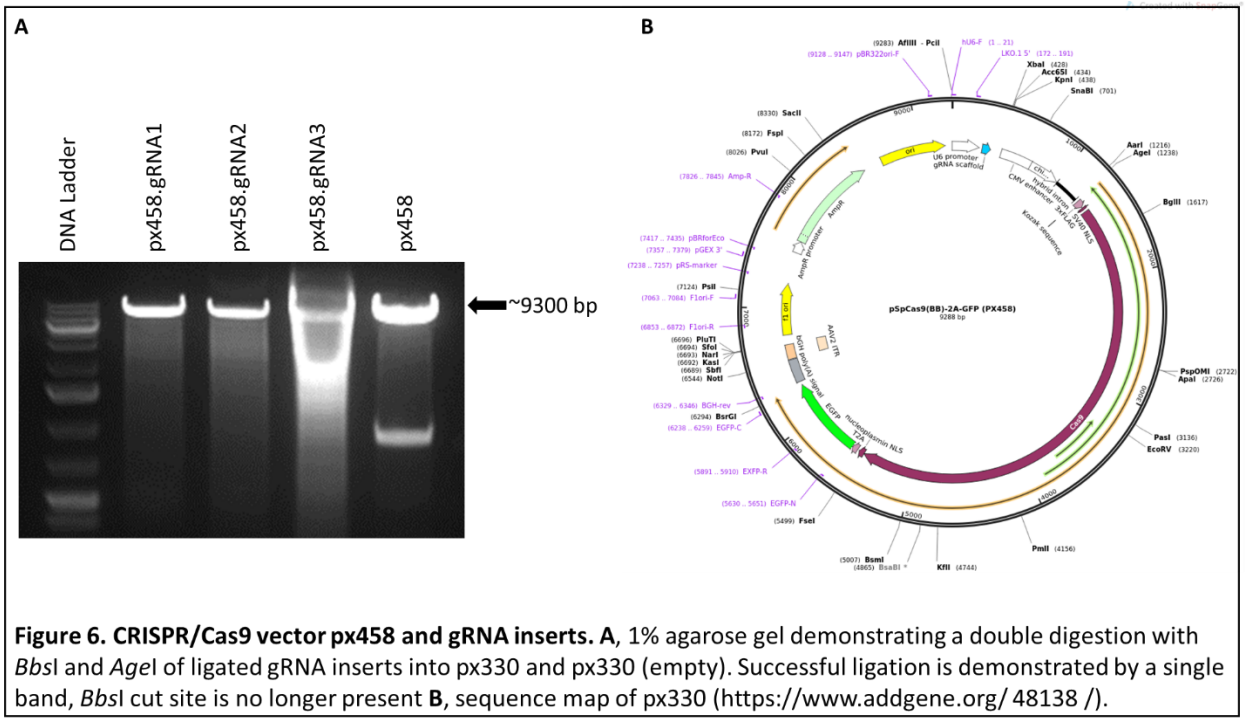

Figure 6. CRISPR/Cas9 vector px458 and gRNA inserts. A, 1% agarose gel demonstrating a double digestion with *Bbs*I and *Age*I of ligated gRNA inserts into px330 and px330 (empty). Successful ligation is demonstrated by a single band, *Bbs*I cut site is no longer present **B**, sequence map of px330 (https://www.addgene.org/ 48138 /).

3.1.3: Assessment of editing success through the T7E1 mismatch assay and primer design for pseudogene exclusion

As we are interested in the capability of CRISPR/Cas9-directed editing on the *PRNP* gene for attenuation of CWD in deer through a gene drive system, we utilised the MDB cell line (from Dr. Gregory Raymond of RML) for initial experiments[261]. For editing assessment, we used the previously published T7E1 mismatch assay (Figure 7, adapted from Zischewski *et al*.

(2017))[265]. The assay detects mismatches in DNA sequences generated by NHEJ through use of the T7E1 resolvase that cleaves heteroduplex DNA at the mismatch site (situated off center so that the two resulting fragments will be dissimilar in size when resolved)[265].

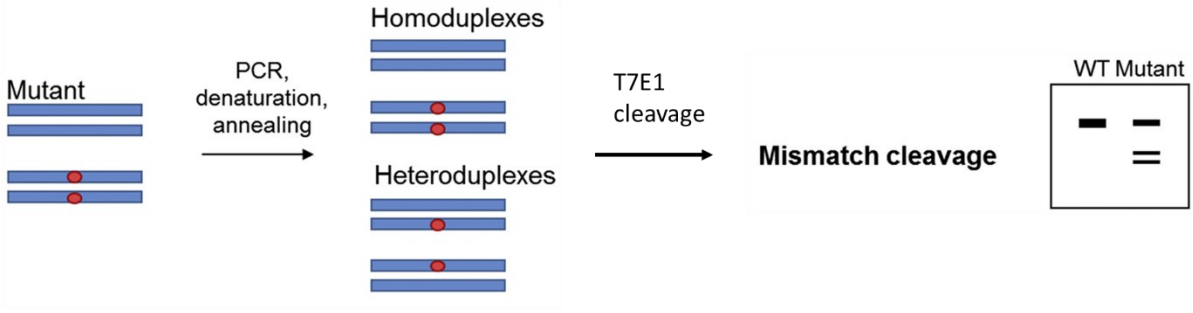

Figure 7. On target mutation detection with the T7E1 mismatch assay. Prior to performing the mismatch assay the target DNA region is amplified, denatured, and then reannealed to form homoduplexes and heteroduplexes. The T7E1 endonuclease recognises heteroduplex DNA bulges and digests the mismatch, the resultant fragments can be resolved in an agarose gel. Figure adapted from Zischewski *et al*. (2017)[265].

Mule deer have a *PRNP* pseudogene which would give rise to a two amino acid difference, if expressed (Figure 8A). The pseudogene does not have a promoter nor an intron indicating it presumably arose from the integration of a *PRNP* mRNA reverse transcript[266]. To exclude the pseudogene from being amplified prior to sequence analysis of edited *PRNP* coding sequences, we placed the forward primer for PCR amplification (prior to T7E1 enzyme incubation) within intron 2 of *PRNP*, as the pseudogene does not have this intron (Figure 8B)[266]. The primer set (LA18) would generate a 985 bp PCR fragment and after T7E1 enzymatic cleavage of edited DNA, would generate two fragments of ~630 bp and ~350 bp (Figure 8B and C).

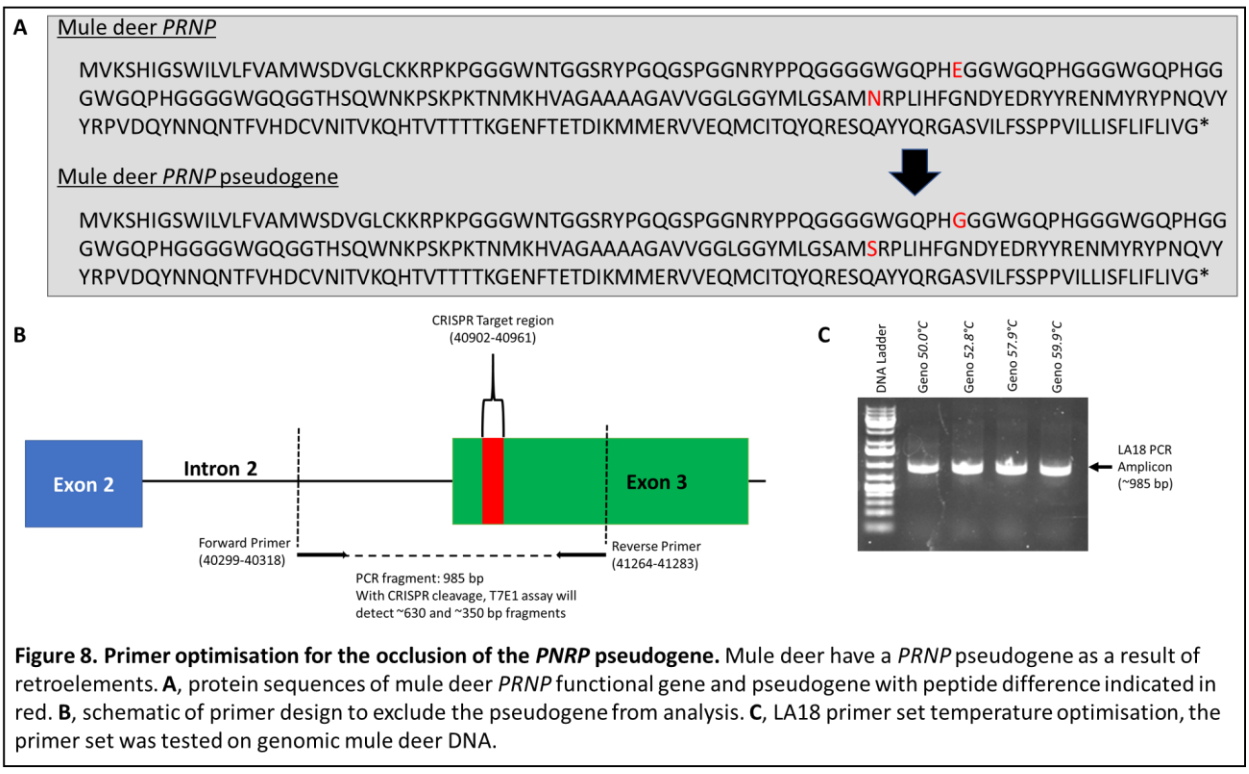

Figure 8. Primer optimisation for the occlusion of the *PNRP* pseudogene. Mule deer have a *PRNP* pseudogene as a result of retroelements. **A**, protein sequences of mule deer *PRNP* functional gene and pseudogene with peptide difference indicated in red. **B**, schematic of primer design to exclude the pseudogene from analysis. **C**, LA18 primer set temperature optimisation, the primer set was tested on genomic mule deer DNA.

Following transfection into MDB cells with our px330.gRNA1 and px330.gRNA2 plasmids and 48 hours of incubation, genomic DNA was collected, amplified, and subjected to the T7E1 mismatch assay. A positive result would be a total of three bands visible on the agarose gel (as seen with the heteroduplex control), one being the entire amplicon and the other two being fragments generated by the T7E1 resolvase (Figure 5D). We tested several replicates of both plasmids and were not able to detect any editing taking place, as seen in Figure 5D.

3.1.4: Blue light CRISPRa inducible PrP system

Another way to control PrP^C substrate for prion replication is pharmacologically, by modifying its pattern of proteolysis. As a tool to help these types of investigations, we wanted to have a system for inducible production of PrP^C; *de novo* induction of wild type PrP^C can allow for exploration of nascent protein whilst avoiding the confounding effects of pre-existing PrP

fragments, two of which are metabolically stable (see also below, Chapter **3.2**)[267,268]. We decided to adapt an optogenetic system in which inducible expression of endogenous protein is possible through CRISPRa for the use of PrP^C expression[241]. The system involves two fusion proteins: the 'anchor' (dCas9/CIB1), and the 'activator' (CRY2/p65)[241]. Targeting of dCas9 is achieved by the gRNA (based on complementarity to the consensus DNA sequence), and then blue light irradiation allows for heterodimerization of CRY2 and CIB1[241]. Finally, the p65 transcriptional activator allows for the expression of the *PRNP* gene (Figure 9A)[241]. We designed five gRNA sequences, utilising the MIT gRNA design tool (crispr.mit.edu), to target the CRISPRa apparatus to the promoter region of *PRNP* (in this case human *PRNP*; Figure 9C). The designed gRNA sequences were inserted into the pgRNA.Humanized expression vector and confirmed via a restriction digestion using *Bam*HI and *Eco*RI (Figure 9B), and Sanger sequencing (MBSU, University of Alberta). The plasmids encoding the CRISPRa machinery were transfected into HEK293T cells, which were then irradiated with blue light over a 48-hour period. The cell lysates were tested on a conventional western system as well as a capillary western (Figure 10A

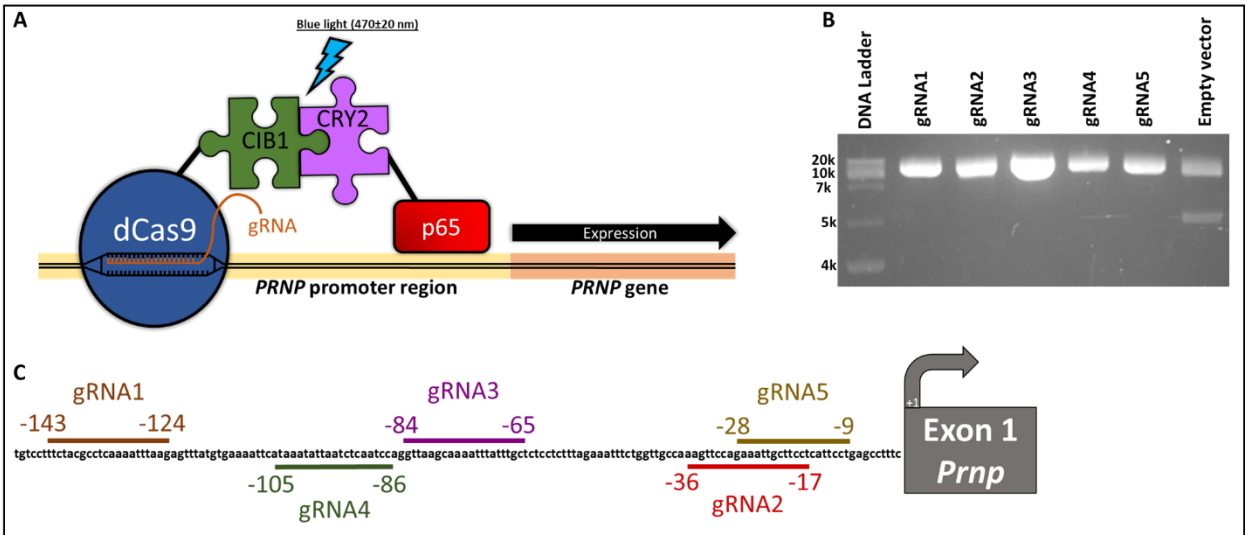

Figure 9. A blue light CRISPRa inducible PrP system. A, schematic representation of the blue light inducible CRIPSRa system for the induction of PrP. **B**, 1% agarose gel showing a double digest (*Eco*RI and *Bam*HI) of pgRNA.Humanized vector with gRNA1/2/3/4/5 inserted. **C**, schematic of gRNA targeting loci on *PRNP* for dCas9.

and B). Unfortunately, the gRNA and optogenetically activated system were unable to induce PrP^C expression clearly above the level of control samples, a result that may relate to the intrinsic complexity of this gene regulation system (as discussed further below, chapter ***4.1.4***).

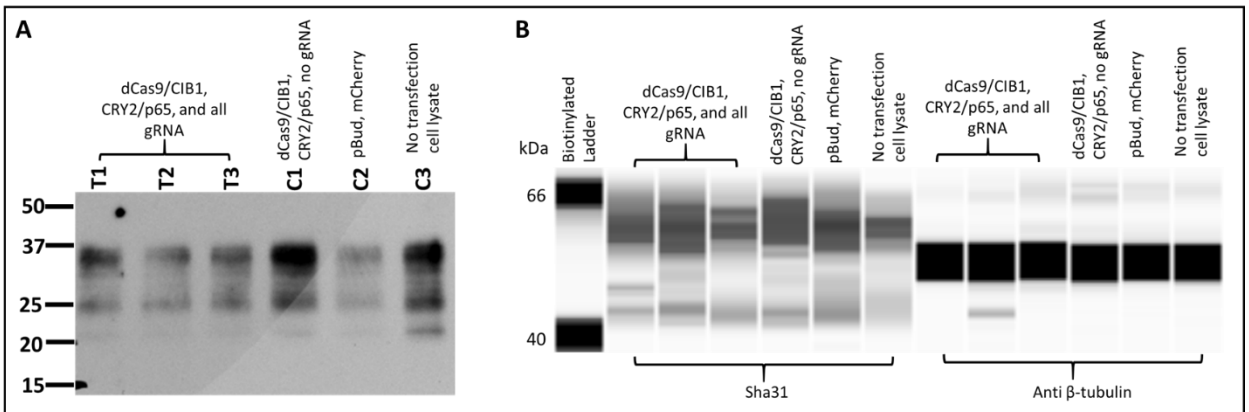

Figure 10. Western analyses of lysates from HEK293T cells transiently co-transfected with blue light inducible CRISPRa machinery. Plasmids expressing dCas9/CIB1, CRY2/p65 fusion proteins, and gRNAs were transfected into HEK293T cells. **A**, western blot of lysates probed with Sha31 1° antibody (1:30000, 10 minute exposure). **B**, capillary western lane view of lysates, with loading control β-tubulin on the right most lanes. The CRISPRa machinery was unable to induce an increase in PrP^C production.

3.2: Using a compound library screen for elucidation of PrP^C cleavage

The CRISPR/Cas9 technologies we explored for modulation of PrP^C synthesis were of a genetic manner and looked specifically at diminishing the production of PrP^C for the purpose of limiting substrate levels for conversion to PrP^{Sc} (Figure 3). Another way of inhibiting the conversion of PrP^C to PrP^{Sc} is through pharmacological approaches that modulate the pattern of PrP^C proteolysis; enhancing α-cleavage would result in increased neuroprotective C1 fragment levels and diminished C2 fragment levels which would lower the amount of cellular PrP^{Sc}-convertible substrate (Figure 3). Wanting to test an expansive set of potential pharmacological modulators of PrP^C proteolysis, we decided to explore commercial compound libraries. Dr. Andrew Castle of the Westaway lab has previously explored a protease inhibitor library (Apex Bio Discovery set, Apex Bio Houston Texas; unpublished data) providing the initial framework

for exploration of a larger library screen. We expected that a library of compounds tested on S3 RK13 cells, which express significantly increased levels of C2 fragmentation (compared to wildtype RK13), will provide five possible outcomes: increase in C1 fragmentation, decrease in C1 fragmentation, increase in C2 fragmentation, decrease in C2 fragmentation, and mixed outcomes.

3.2.1: Compound screen selection

Prior to performing a compound library screen, careful consideration is needed in the development of the assay in which the compounds will be tested; the assay must be robust, replicable, relevant, and reliable[269]. Utilising previously published methods for testing compounds on PrP^C cleavage in 96 well plates and elucidation with capillary-based western technology, we arranged our assay with four steps: initial compound addition at a concentration of 20 μM (in well) by a Janus (Perkin-Elmer) liquid handling robot designed for accurate delivery of small sample volumes, a 72-hour incubation to limit the effects of pre-existing metabolically stable C1 fragment, in plate lysis and PNGase F digestion, followed by determination of fragment abundance using a capillary western system (Figure 11A)[258,270]. After defining the assay for compound exploration, we asked questions essential for prospective screens such as: the cost of the screen, who will be managing the library, sophistication and range of compounds provided, and relevancy to the assay[271]. Upon consideration of these factors, we purchased the #5841 Tocriscreen Plus Mini screening library, which contains 1280 compounds pre-dissolved in DMSO at a concentration of 10 mM, several of which are neuroactive compounds (relevant to the assay and active at a range of pharmacological targets). The library was donated to and managed by the High Content Analysis (HCA) Core at the University of Alberta. The breakdown of how plates were separated and tested is summarised in

Figure 11B, with the capillary western breakdown summarised in Figure 11C. Each Tocris compound plate contains 80 compounds which were tested alongside DMSO (vehicle), positive (Linagliptin), and negative (nothing added) controls. The Linagliptin positive control is a DPP-4 inhibitor, identified by Dr. Andrew Castle (Westaway lab), that consistently lowers the production of the C2 fragment of PrP^C (unpublished data).

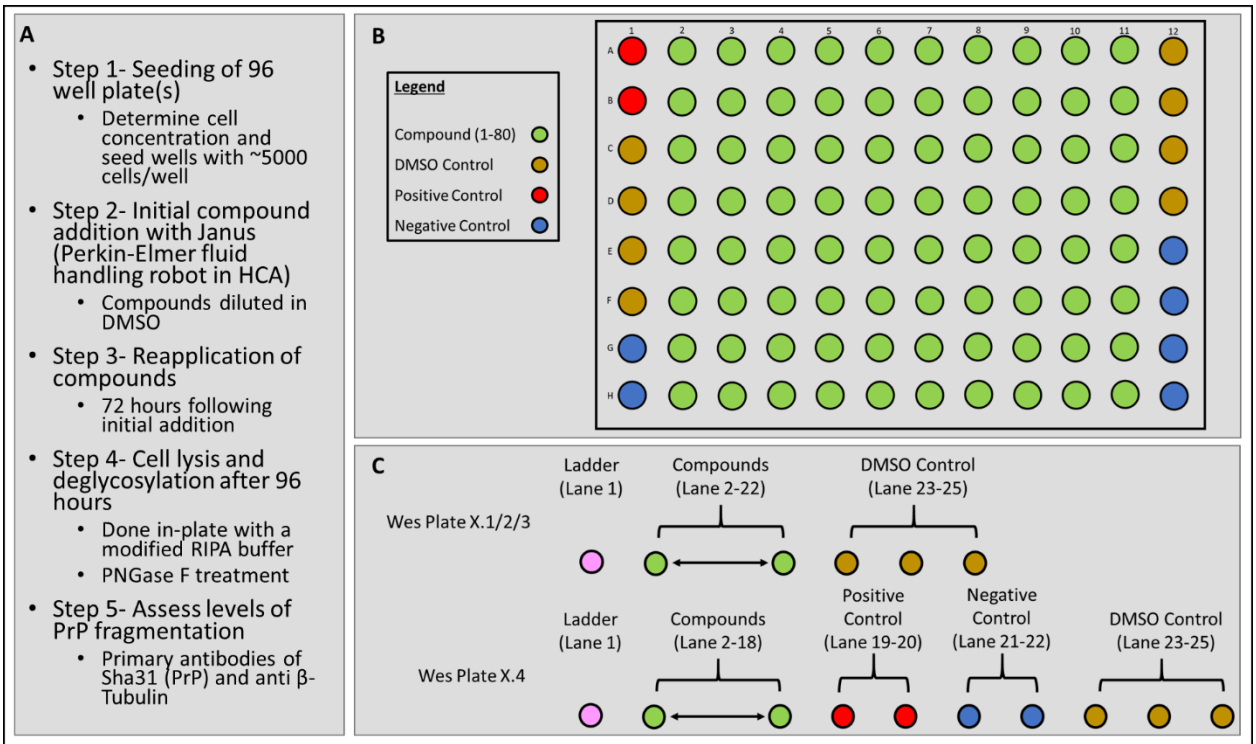

Figure 11. Compound library screen workflow and plate layout. A, workflow of TOCRIScreen plus mini library compound screen. **B**, layout of 96 well plate seeded with S3 RK13 cells for compound addition. There is a total of 16 TOCRIS plates with 80 compounds per plate. The center 80 wells have the compounds added and the outer columns have the controls (DMSO (vehicle), positive (Linagliptin), and negative (nothing added)) **C**, layout of Wes plates for lysate analysis, each 96 well compound addition plate gets separated over 4 Wes plates with the first 3 containing 21 compound lysates, 3 DMSO (vehicle) control lysates, and the final plate containing the remaining 17 compound lysates, 3 DMSO controls, 2 positive controls, and 2 negative controls. X denotes TOCRIS compound plate, 1-16.

3.2.2: Defining target compound hits

Within the Tocriscreen library, compounds that are defined as a "hit", that is to say compounds that impact levels of PrP fragments, pre-set parameters must be met that control for problematic functionalities, possible toxicity effects, and set baseline changes for compound effectiveness[271]. To ascertain compounds that were not toxic, we compared the peak area of β-tubulin (within the capillary Wes spectra data) in DMSO controls to the compounds of interest, and initially assigned a ratio of 0.5 or more (of compound β-tubulin to DMSO control) as healthy. β-tubulin is a microtubule subunit involved in many cellular functions and thus, can be used as an indicator of cell health[272]. Furthermore, the detection of PrP^C and β-tubulin can be multiplexed without band interference on Wes capillary analysis[258]. Following elimination of toxic compound data, we compared the area under the peak of the C1 and C2 fragments to the corresponding full length (FL) PrP^C peak and determined the percentage change of fragmentation compared to the DMSO controls. Initially, we set a change ad hoc of ±25% as a threshold for defining a compound of interest. We then separated the compounds of interest into four categories: C1 increase, C1 decrease, C2 increase, and C2 decrease. Following further data filtering based on increasing the lower limits for β-tubulin ratio to 0.75 and percentage change values in which changes were only seen in one category (percentage change in other category is within ±7.5%, essentially removing mixed outcomes), we established a preliminary set of compounds for each category. Subsequently, these sets underwent spectra scrutiny with removal of compounds, in which the spectra were poor or abnormal in comparison to the DMSO control spectra. The filtering process is summarised in Figure 12A.

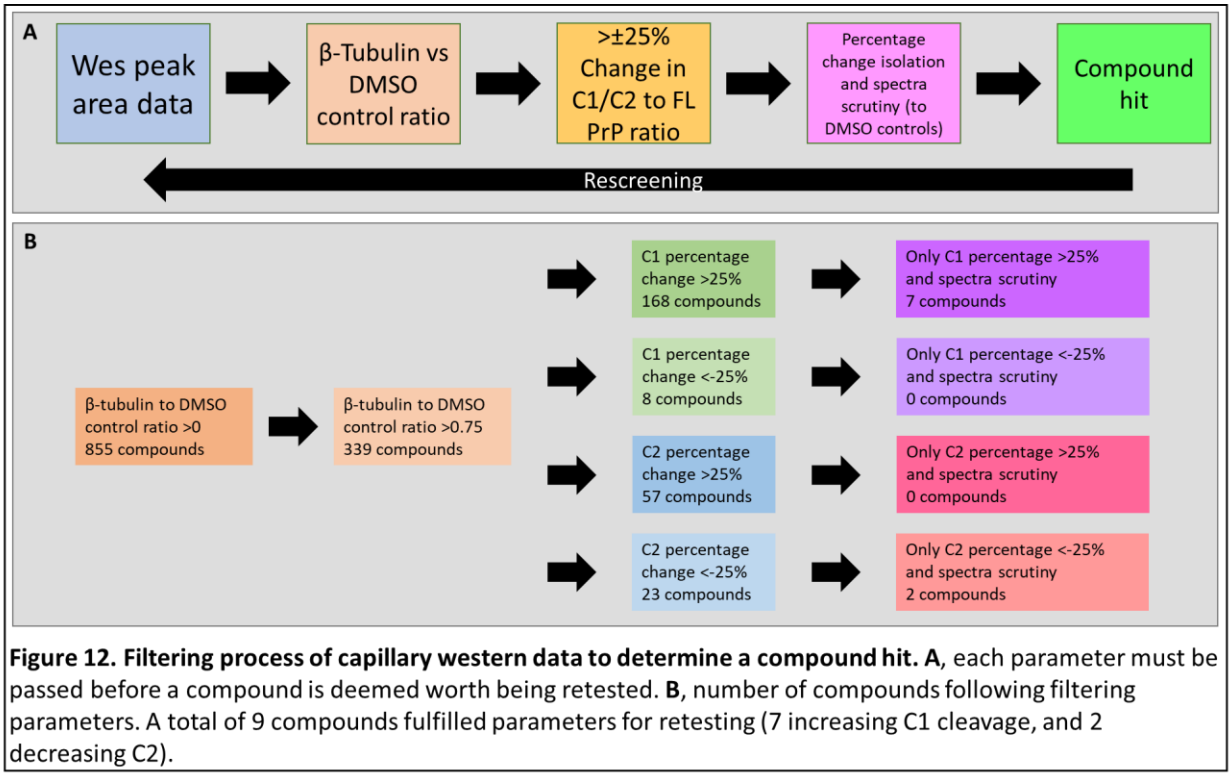

Figure 12. Filtering process of capillary western data to determine a compound hit. A, each parameter must be passed before a compound is deemed worth being retested. **B**, number of compounds following filtering parameters. A total of 9 compounds fulfilled parameters for retesting (7 increasing C1 cleavage, and 2 decreasing C2).

3.2.3: Compounds that modulate C1

Following β-tubulin ratio filtering (0.75), 168 compounds increased the C1 to FL PrP^C ratio over 25% and 8 less than -25%, for a total of 176 compounds that modulate C1 fragmentation (Figure 12B). After filtering for compounds that only increased or decreased C1 levels (with C2 levels changing within ±7.5%) and removing poor and abnormal spectra in comparison to their corresponding DMSO control spectra (spectra in which the peaks were poorly resolved or had low signal across all PrP peaks), we found a total of 6 compounds that increased C1 production and none that decreased C1. It must be noted that we added the compound, C-1, based on the spectra (Figure 13K) even though C2 production was above a 7.5% increase (13%) for a final total of 7 compounds (Figure 13, Table 3). In Figure 13, the compound spectra are presented on the left (with a visible increase in C1 peak), and their corresponding DMSO control spectra overlap on the right. The percentage change in fragmentation compared to DMSO controls is

presented in Table 3, with a range of 34% (S 18886) to 109% (C-1) increase in C1 production across the 7 compounds. To establish if there is any significant variation between controls and to ascertain precision of the assay, we calculated the coefficient of variation of the area under the curve of the DMSO control peaks (Table 4); we arbitrarily set a level of <10% as an indication of limited variation.

		Percentage change vs DMSO controls				
Compound Name	**Basic information**	**C1/FL**	**C2/FL**	**FL PrP/β-tubulin**	**Total PrP/β-tubulin**	**β-tubulin vs DMSO control**
Felbamate	NMDA antagonist, acts on glycine site	62.2	2.5	9.8	18.2	0.81
Repaglinide	Kir6 (KATP) channel blocker	53.2	7.0	-12.5	-5.5	0.84
Carbamazepine	Inhibitor of neuronal voltage-gated Na+ channels; anticonvulsant	39.1	4.4	0.5	6.0	0.75
GANT 58	GLI1 antagonist; inhibits Hedgehog (Hh) signaling	55.3	-1.6	2.1	6.2	0.89
NK 252	Nrf2 activator	72.4	7.5	1.5	13.8	0.95
C-1	Protein kinase C inhibitor	109	13	-17	1	0.87
S 18886	Potent thromboxane A2 (TP) antagonist	34.0	-2.5	8.9	12.2	0.78

Table 3. Percentage change of fragmentation compared to DMSO controls. Table showing the percentage change of PrP fragments, and β-tubulin ratio versus the DMSO controls. The basic information of compound action is also included.

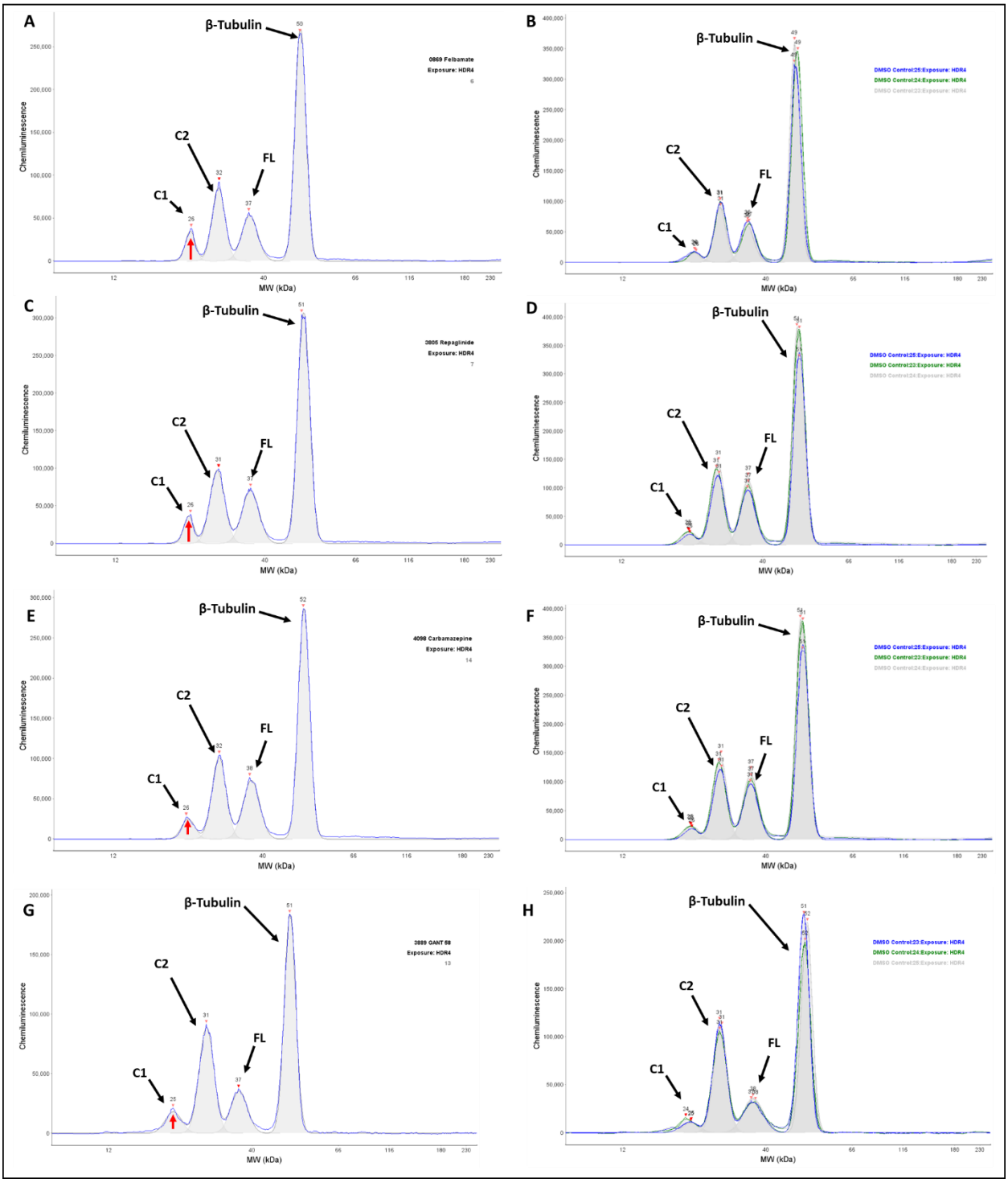
A
β-Tubulin
C2
FL
C1
0869 Felbamate
Exposure: HDR4
Chemiluminescence
MW (kDa)
B
β-Tubulin
C2
FL
C1
DMSO Control:25:Exposure: HDR4
DMSO Control:24:Exposure: HDR4
DMSO Control:23:Exposure: HDR4
Chemiluminescence
MW (kDa)
C
β-Tubulin
C2
FL
C1
3805 Repaglinide
Exposure: HDR4
Chemiluminescence
MW (kDa)
D
β-Tubulin
C2
FL
C1
DMSO Control:25:Exposure: HDR4
DMSO Control:23:Exposure: HDR4
DMSO Control:24:Exposure: HDR4
Chemiluminescence
MW (kDa)
E
β-Tubulin
C2
FL
C1
4098 Carbamazepine
Exposure: HDR4
Chemiluminescence
MW (kDa)
F
β-Tubulin
C2
FL
C1
DMSO Control:25:Exposure: HDR4
DMSO Control:23:Exposure: HDR4
DMSO Control:24:Exposure: HDR4
Chemiluminescence
MW (kDa)
G
β-Tubulin
C2
FL
C1
3889 GANT 58
Exposure: HDR4
Chemiluminescence
MW (kDa)
H
β-Tubulin
C2
FL
C1
DMSO Control:23:Exposure: HDR4
DMSO Control:24:Exposure: HDR4
DMSO Control:25:Exposure: HDR4
Chemiluminescence
MW (kDa)

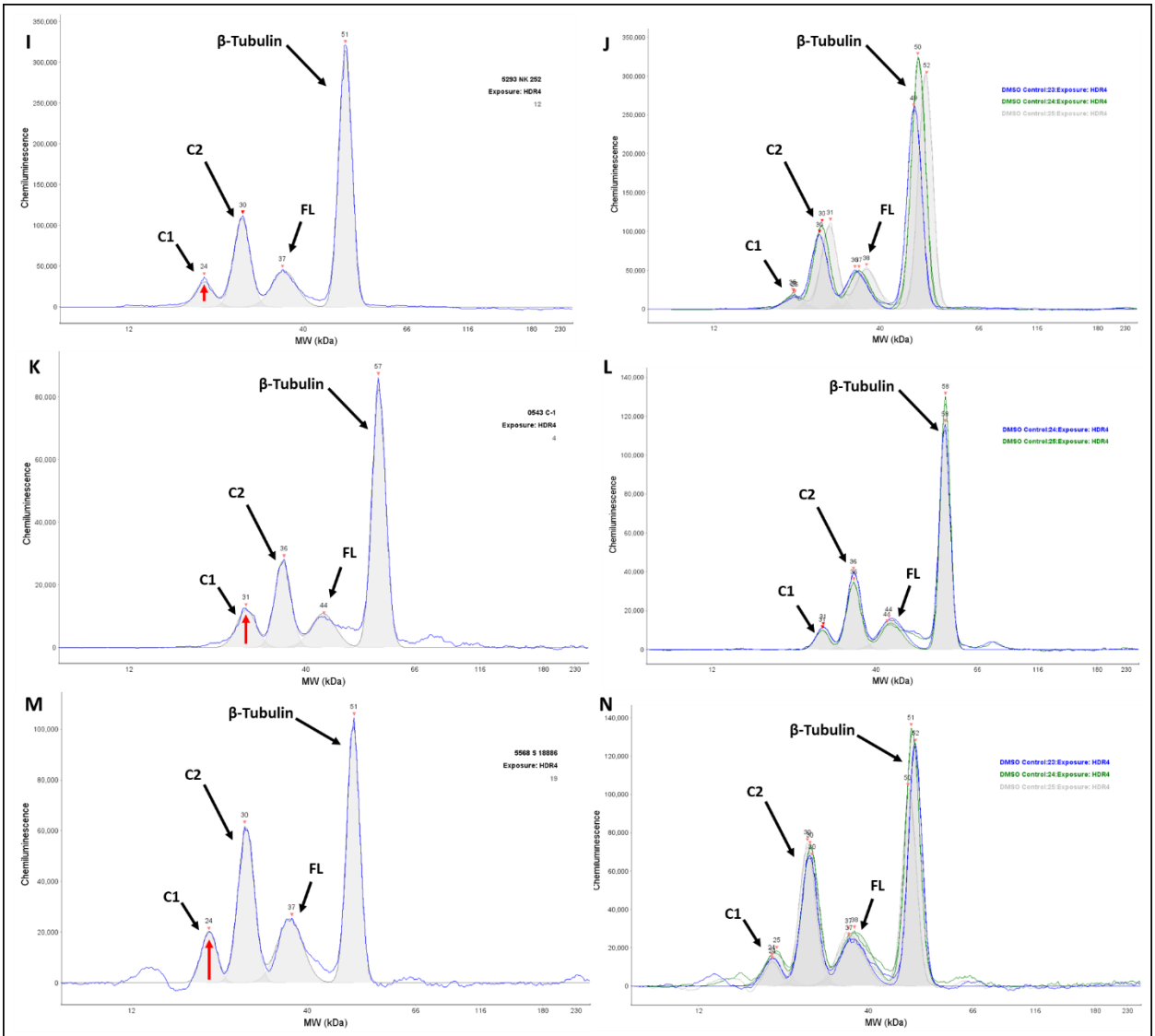

Figure 13. Capillary western spectra and analysis of S3 RK13 cell lysates following 96 hours compound addition in which C1 fragmentation increased. A-N, Wes spectra using Sha31 (PrP detection) and α-β Tubulin of S3 RK13 lysates with PrP fragments and β- tubulin indicated. **A, C, E, G, I, K, M**, spectra of Felbamate/Repaglinide/Carbamazepine/GANT 58/NK 252/C-1/S 18886 (respectively) treated S3 RK13 cell lysate. **B, D, F, H, J, L, N**, overlapping spectra of DMSO treated control S3 RK13 lysates corresponding to Felbamate/Repaglinide/Carbamazepine/GANT 58/NK 252/C-1/S 18886 (respectively) compound addition plate.

	Coefficient of variation of DMSO controls			
Compound Name	**C1/FL**	**C2/FL**	**FL PrP/β-tubulin**	**Total PrP/β-tubulin**
Felbamate	5.5	3.0	12.0	11.0
Repaglinide	6.7	2.2	4.2	3.7
Carbamazepine	6.7	2.2	4.2	3.7
GANT 58	14.0	3.8	7.1	5.9
NK 252	9.7	7.5	11.4	7.1
C-1	1.4	5.0	18.4	16.1
S 18886	26.6	7.7	12.5	10.8

Table 4. DMSO controls coefficient of variation. Table showing variation within DMSO controls of respective plate in which compound was tested.

3.2.4: Compounds that modulate C2

Following β-tubulin ratio filtering (0.75), 57 compounds increased the C2:FL PrP^C ratio over 25% and 23 less than -25%, for a total of 80 compounds that modulate C2 fragmentation (Figure 12B). After filtering for compounds that only increased or decreased C2 levels (with C1 levels changing within ±7.5%) and removing poor and abnormal spectra in comparison to their corresponding DMSO control spectra, we found 2 compounds that decreased C2 production, but failed to find compounds that increased C2 production (Figure 14). The compound spectra are

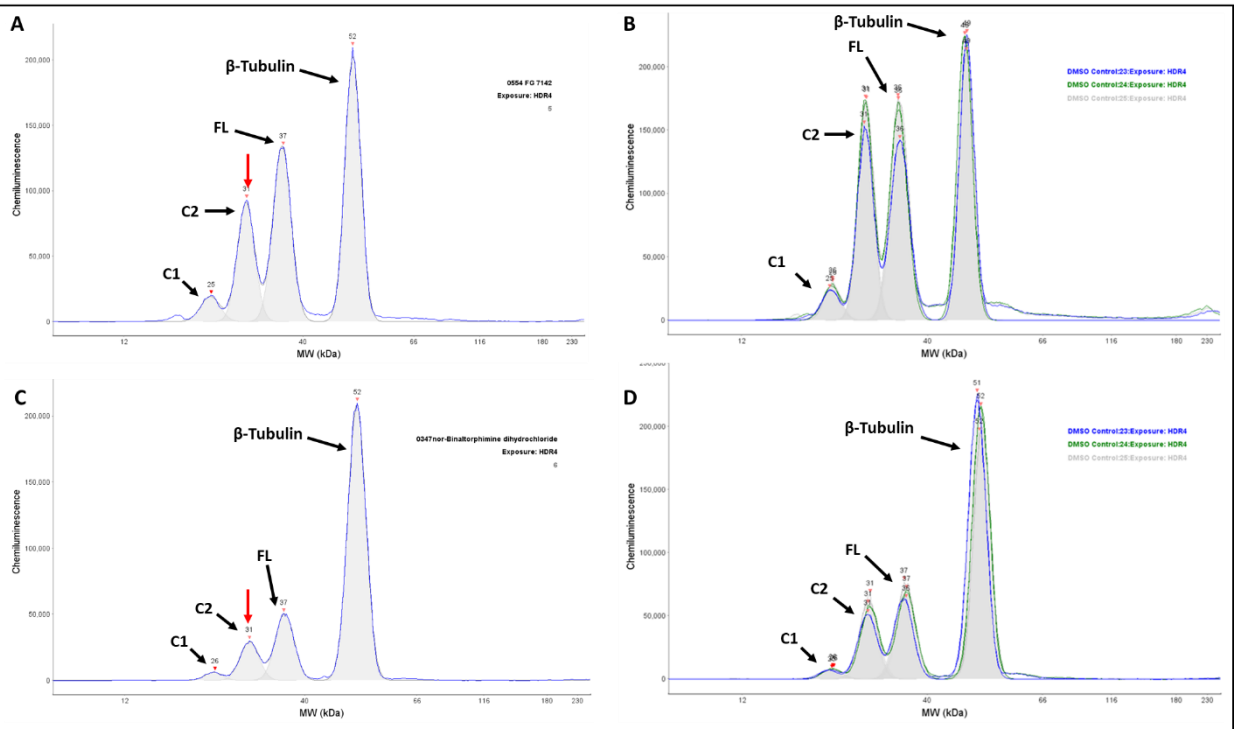

E

Compound Name	Info	Percentage change vs DMSO controls: C1/FL	C2/FL	FL PrP/β-tubulin	Total PrP/β-tubulin	β-tubulin vs DMSO control
FG 7142	Benzodiazepine inverse agonist	-2.8	-27.3	-15.3	-25.4	0.92
nor-Binaltorphimine dihydrochloride	Standard kappa selective antagonist	0.8	-28.0	-30.2	-38.3	1.06

F

Compound Name	Coefficient of variation of DMSO controls: C1/FL	C2/FL	FL PrP/β-tubulin	Total PrP/β-tubulin
FG 7142	5.9	2.8	10.5	8.8
nor-Binaltorphimine dihydrochloride	5.8	3.0	15.7	14.2

Figure 14. Capillary western spectra and analysis of S3 RK13 cell lysates following 96 hours compound addition in which C2 fragmentation decreased. A-D, Wes spectra using Sha31 (PrP detection) and α-β Tubulin of S3 RK13 lysates with PrP fragments and β- tubulin indicated. **A, C**, spectra of FG 7142/nor-Binaltorphimine dihydrochloride (respectively) treated S3 RK13 cell lysate. **B, D**, overlapping spectra of DMSO treated control S3 RK13 lysates corresponding to FG 7142/nor-Binaltorphimine dihydrochloride (respectively) compound addition plate. **E**, table showing the percentage change of PrP fragments, and β-tubulin ratio versus the DMSO controls. **F**, table showing coefficient of variation of DMSO controls.

presented in Figure 14 (A and C) on the left (with a visible decrease in C2 peak) and their corresponding DMSO control spectra overlap on the right (B and D). The percentage change in fragmentation compared to DMSO controls is presented in Figure 14E, with a 27% decrease in C2 fragmentation for FG 7142 and a 28% decrease for nor-Binaltormphimine hydrochloride. The coefficient of variation of the DMSO control peaks are summarised in Figure 14F to establish if there is any significant variation between controls.

3.2.5: Serial dilution of potential target compounds

Following the identification of 9 compounds which fulfilled our parameters of modulating PrP^C α- or β-cleavage (changing the levels of detected C1 or C2 cleavage), we tested these compounds in a serial dilution over five concentrations (30 µM, 10 µM, 3 µM, 1 µM, and 0.3 µM) (Table 5). The workflow and experiments were performed as per Figure 11A. In only one condition did the compound/concentration pass our parameters, and that was for a 30 µM concentration of nor-Binaltorphimine dihydrochloride, which produced a 26% change in C2 production compared to DMSO controls (with a -8% change in C1 production). For all other compounds and concentrations, we see a drift from the previous results or mixed outcomes (Table 5). For example, both C-1 and Carbamazepine have a dose response correlation in which we see increased C1 production across concentrations, but also have a mixed outcome where C2 production levels are changed (Figure 15).

Concentration	30 µM		10 µM		3 µM		1 µM		0.3 µM		Previous Results (20 µM)	
Percentage change in ratio (vs DMSO Control)	C1/FL	C2/FL	C1/FL	C2/FL	C1/FL	C2/FL	C1/FL	C2/FL	C1/FL	C2/FL	C1/FL	C2/FL
Compound												
FG 7142	-28	-1	23	30	-17	-24	53	51	5	-5	-3	-27
nor-Binaltorphimine dihydrochloride	-8	-26	24	13	23	14	-4	-12	12	6	1	-28
Felbamate	54	45	-6	-10	26	31	-7	6	61	77	62	3
Repaglinide	47	69	118	143	127	152	71	109	30	37	53	7
Carbamazepine	330	446	173	157	30	48	15	32	14	12	39	4
GANT 58	NA	NA	-14	-24	-14	-23	NA	NA	55	20	55	-2
NK 252	19	15	33	12	-10	-28	31	36	3	-21	72	8
C-1	89	72	76	82	11	5	-2	-1	-1	10	109	13
S 18886	13	-34	17	-32	NA	NA	-10	-11	-14	-36	34	-3

Table 5. Percentage change in fragmentation of target compounds retested at a range of concentrations. Results represent change versus DMSO (vehicle) controls. Table of the 9 target compounds tested in a serial dilution on S3 RK13 cells showing the percentage change in ratio of C1/FL and C2/FL. Blue indicates compounds expected to have decreased percentage change (C2/FL). Green indicates compounds expected to have increased percentage change (C1/FL). Red/NA indicates where tested lysate gave no result on capillary western. Previous results from the initial screen are presented in last two columns.

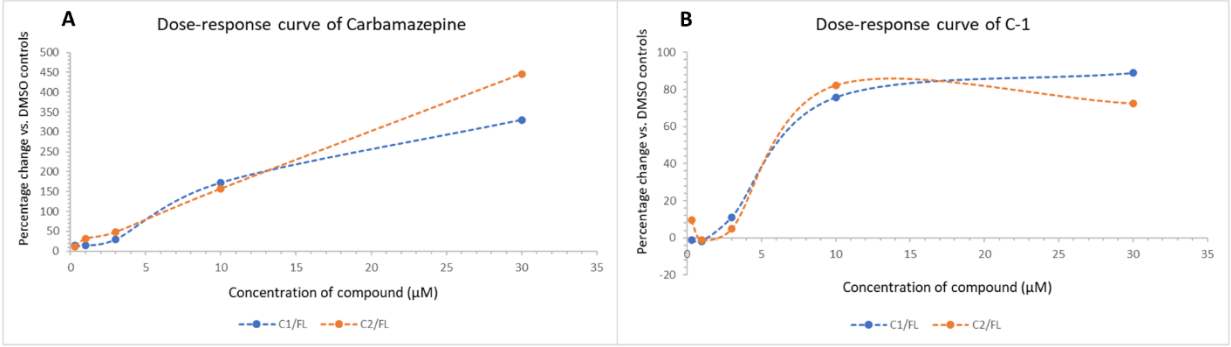

Figure 15. Dose-response curves of Carbamazepine and C-1. Compounds were retested at concentrations of 30, 10, 3, 1, and 0.3 µM. Blue curve indicates percentage change in C1 fragmentation levels. Orange curve indicates percentage change in C2 fragmentation levels.

3.3: A candidate-based response for C1 protease elucidation

Due to the variability of results in the library screen and inability to identify a modulator of PrP^C cleavage, we still wished to probe the capabilities of α- and β-cleavage as therapeutic targets and decided to pursue a candidate-based approach. Based on preliminary data completed by Dr. Andrew Castle, we identified a general (non-class specific) serine protease inhibitor, Camostat mesylate, which was able to induce a dose response change in α-cleavage of PrP^C (unpublished data). Looking to the literature regarding type II membrane proteases present in the

brain that Camostat mesylate inhibits or has the potential to inhibit, we identified six proteases as potential α-PrPases: TMPRSS1 (Hepsin), TMPRSS2, TMPRSS4, TMPRSS5, TMPRSS11D, and HTRA1.

3.3.1: Testing candidate proteases on PrP^C α-cleavage

Next, we tested the cleavage capabilities of the aforementioned proteases on a PrP^C substrate. We initially performed transient co-transfections of protease expression plasmids and a plasmid expressing PrP^C (pcDNA3.PrP.wt). Through probing cell lysates for full-length PrP^C and its fragments (after a glycosylation step), we found that Hepsin and TMPRSS2 behaved differently from the other proteases; Hepsin caused little to no FL PrP signal with a significant loss of C1 signal (compared to controls), and TMPRSS2 caused an overall significant loss of FL and C1 signal (Figure 16). Next, we performed a transient transfection of the proteases into a stable cell line that expresses PrP (RK13-WT10). When testing the lysates, we found that neither Hepsin nor TMPRSS2 elicited the same loss of signal as seen in the co-transfection, both in conventional western analysis (Figure 17A), and capillary western analysis (Figure 17B). The

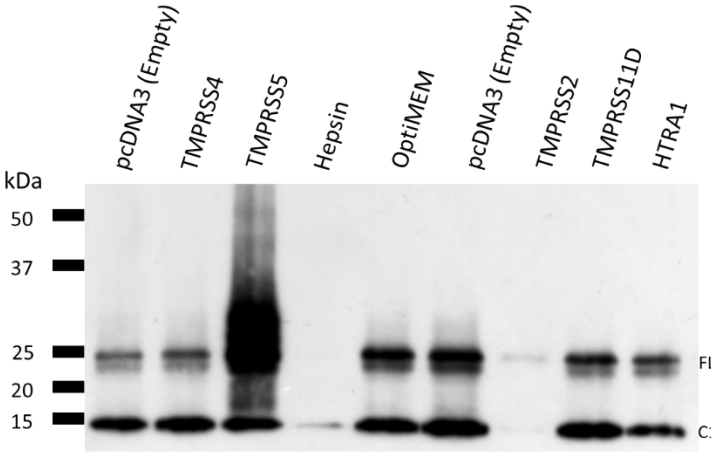

Figure 16. Western blot analysis of lysate from RK13 cells transiently co-transfected with a PrP expressing plasmid and plasmids expressing serine proteases. A plasmid using the pcDNA3 backbone expressing PrP was co-transfected with plasmids expressing TMPRSS1 (Hepsin), TMPRSS2, TMPRSS4, TMPRSS5, TMPRSS11D, HTRA1, and a control pcDNA3 (Empty) vector. Lysates were PNGaseF treated. Blot was probed with Sha31 1° antibody (1:30000, 15 minute exposure), FL and C1 PrP species are indicated. Hepsin and TMPRSS2 behaved differently from the other proteases studied here. Figure is representative of 3 repeat experiments.

western analyses demonstrated little to no change across the proteases (and controls) tested for the amount of FL and C1 PrP produced (Figure 17).

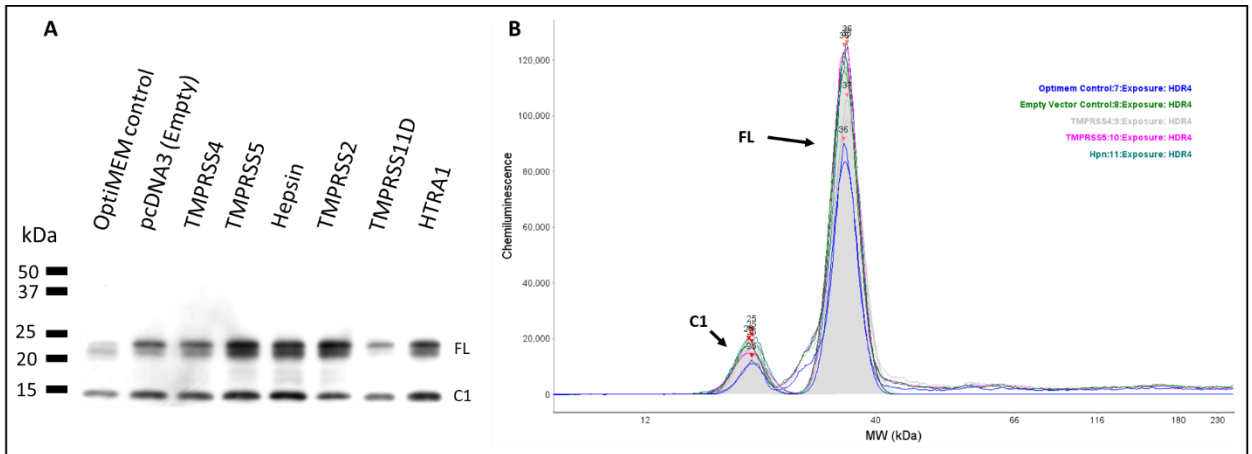

Figure 17. Western analyses of lysates from RK13-WT10 cells transiently transfected with plasmids expressing serine proteases. Plasmids expressing TMPRSS1 (Hepsin), TMPRSS2, TMPRSS4, TMPRSS5, TMPRSS11D, HTRA1, and a control pcDNA3 (Empty) vector were transiently transfected into RK13-WT10 cells. Lysates were PNGaseF treated. **A**, western blot of lysates probed with Sha31 1° antibody (1:30000, 5 minute exposure). **B**, capillary western of TMPRSS1, TMPRSS4, and TMPRSS5 lysates. C1 and FL peak are indicated with arrows. Stable transfection does not give a similar result to the acute transfection.

Due to published data describing Hepsin as an activator of pro-matrix metalloproteinases, we wanted to test whether both Hepsin and TMPRSS2 were causing activation of ADAM10, a metalloprotease that results in shedding of PrP^{273}. To explore this hypothesis, we collected the media from transiently co-transfected cells and probed for both PrP (Sha31) and PrP that has been shed (using a 1° antibody sPrPG228, which can specifically detect the Gly at position 228 resulting from ADAM 10 shedding (Figure 1A)). The results in Figure 18 show that once again Hepsin and TMPRSS2 are providing signals that are different to the other proteases and controls. Figure 18A demonstrates that the amount of PrP (as probed by Sha31) in the media is lower in Hepsin and TMPRSS2 co-transfections. Moreover, the patterning is more reminiscent of PNGase F-treated lysate, as there are discrete PrP species rather than the smears seen in other experimental conditions that leave N-linked antennary sugar structures intact. Figure 18B shows there is no signal in the Hepsin and TMPRSS2 lanes for shed PrP.

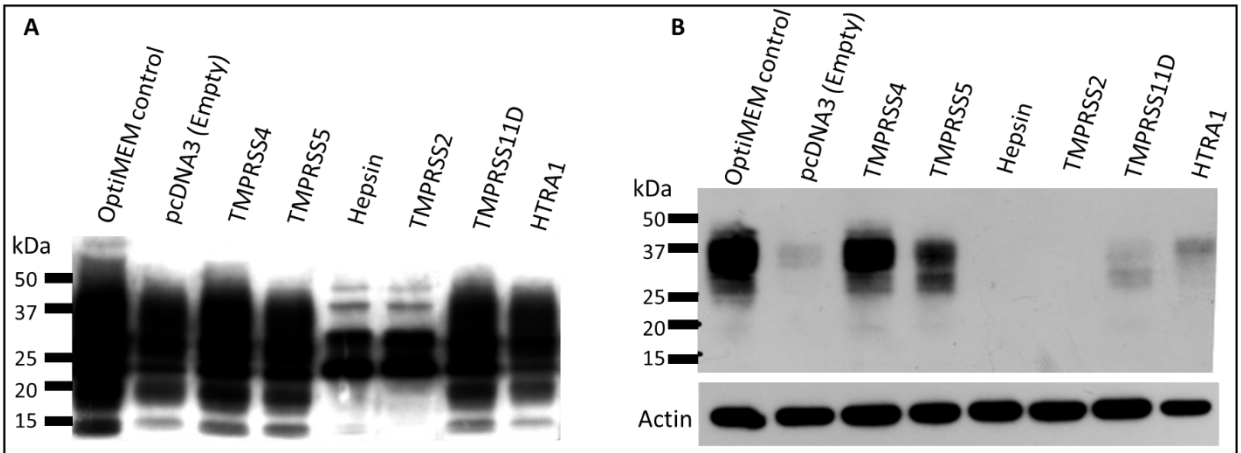

Figure 18. Western blot analyses of concentrated media from RK13 cells transiently co-transfected with a PrP expressing plasmid and plasmids expressing serine proteases. A plasmid using the pcDNA3 backbone expressing PrP was co-transfected with plasmids expressing TMPRSS1 (Hepsin), TMPRSS2, TMPRSS4, TMPRSS5, TMPRSS11D, HTRA1, and a control pcDNA3 (Empty) vector. The media was collected and concentrated. **A**, western blot of concentrated media probed with Sha31 1° antibody (1:30000, 2 minute exposure). **B**, western blot of concentrated media probed with sPrP 1° antibody (1:1000, 60 minute exposure). Hepsin and TMPRSS2 again behaved differently from the other proteases studied.

3.3.2: Hepsin and TMPRSS2 exert their effect on other GPI-anchored proteins

As PrP^{C} shares two paralogous proteins in the form of Sho and Dpl, we wished to see if Hepsin and TMPRSS2 have similar effects on these protein "cousins" of PrP. We performed a transient co-transfection with the protease expressing plasmids and a plasmid expressing Dpl or Sho. We found that there is a loss of signal (for Hepsin and TMPRSS2) when lysates are analysed on a western blot (Figure 19A and B, experiment performed by Dr. Serene Wohlgemuth). Next, we wanted to decipher if Hepsin and TMPRSS2 act more broadly to affect the production of other GPI-anchored proteins outside of the PrP superfamily, so we performed a transient co-transfection with our protease expressing plasmids and a plasmid expressing Thy1, a diglycosylated and GPI-anchored protein (Figure 20A). Again, we found that Hepsin and TMPRSS2 are lowering the signal within protein lysates when probed on a western blot (in comparison to other tested proteases and controls) for Thy1 (Figure 20B).

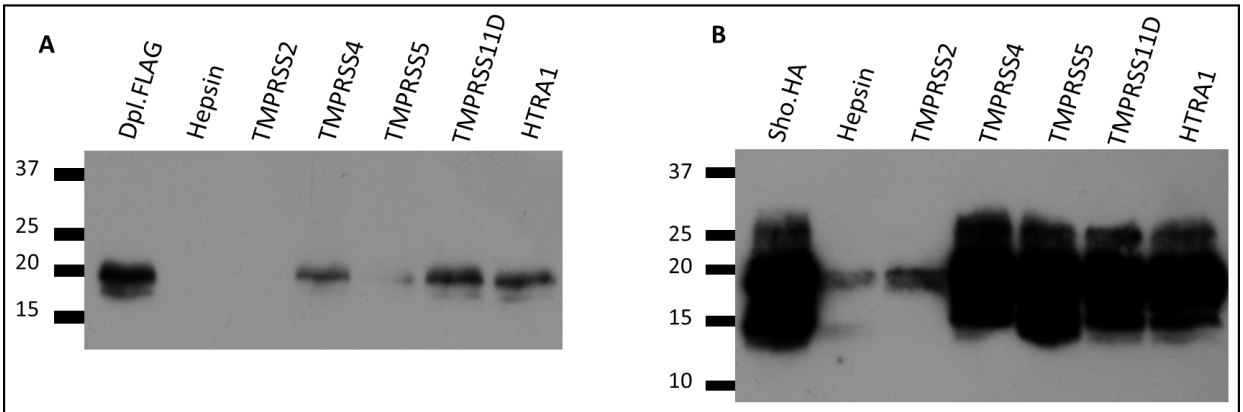

Figure 19. Western blot analyses of lysate from RK13 cells transiently co-transfected with Dpl or Sho expressing plasmids and plasmids expressing serine proteases. Plasmids expressing Dpl (FLAG tagged) or Sho (HA tagged) were co-transfected with plasmids expressing TMPRSS1 (Hepsin), TMPRSS2, TMPRSS4, TMPRSS5, TMPRSS11D, and HTRA1. **A**, western blot of lysates with α-FLAG 1° antibody (1:1000, 60 minute exposure). **B**, western blot of lysates probed with α-HA 1° antibody (1:2500, 60 minute exposure). Blot analysis performed by Dr. Serene Wohlgemuth. Sho blot was over exposed to reveal signals within Hepsin and TMPRSS2 lanes.

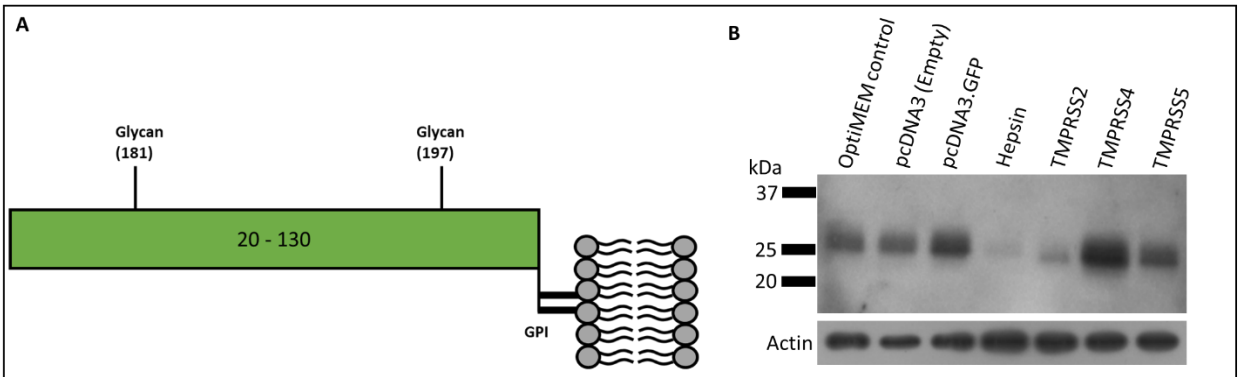

Figure 20. Thy1 is a di-glycosylated GPI anchored protein. A, schematic of Thy1 protein following GPI linkage. Signal peptides 1-19 and 131-161 are replaced by the GPI anchor. **B**, western blot analysis of lysatse from RK13 cells transiently co-transfected with a Thy1 expressing plasmid and plasmids expressing serine proteases**.** A plasmid using the pcDNA3 backbone expressing Thy1 was co-transfected with plasmids expressing TMPRSS1 (Hepsin), TMPRSS2, TMPRSS4, TMPRSS5, and a control empty pcDNA3 and pcDNA3.GFP vector. Blot was probed with α-Thy1 1° antibody (1:1000, 30 minute exposure). Blot was stripped and reblotted with α-Beta actin. Hepsin and TMPRSS2 again behaved differently from the other proteases studied in interaction with Thy1.

3.3.3: Hepsin and TMPRSS2 exert their effect independent from the protein promoter

As all the tested plasmids expressing GPI-anchored proteins contained the CMV promoter, and since competition for shared transcription factors may affect net protein levels, we tested the protease plasmids in a co-transfection on a plasmid expressing PrP under the EF1a promoter, considered to have housekeeping gene properties (pBud.CE4.PrP.wt (EF1a)). Yet again, we found that Hepsin and TMPRSS2 behave differently to other proteases and controls with the C1 signal being greatly reduced or absent both in conventional western (Figure 21A) and capillary western analyses (Figure 21B and C).

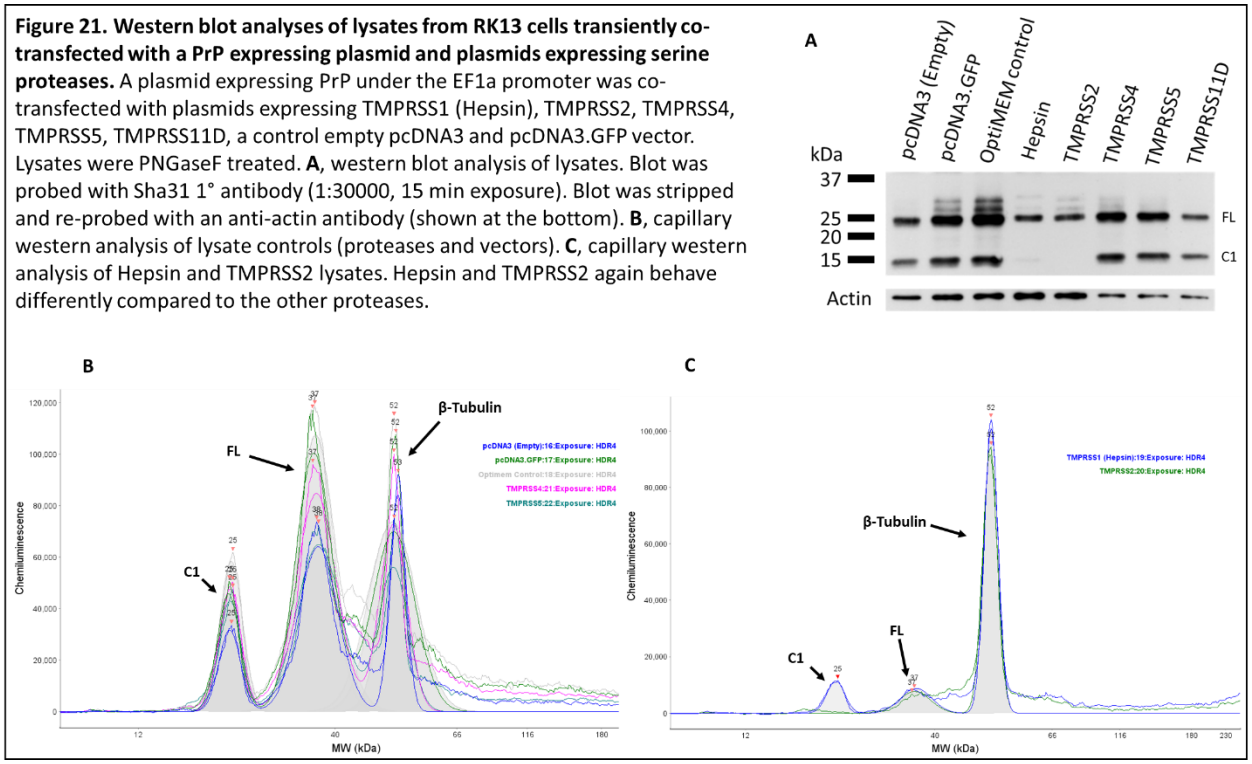

Figure 21. Western blot analyses of lysates from RK13 cells transiently co-transfected with a PrP expressing plasmid and plasmids expressing serine proteases. A plasmid expressing PrP under the EF1a promoter was co-transfected with plasmids expressing TMPRSS1 (Hepsin), TMPRSS2, TMPRSS4, TMPRSS5, TMPRSS11D, a control empty pcDNA3 and pcDNA3.GFP vector. Lysates were PNGaseF treated. **A**, western blot analysis of lysates. Blot was probed with Sha31 1° antibody (1:30000, 15 min exposure). Blot was stripped and re-probed with an anti-actin antibody (shown at the bottom). **B**, capillary western analysis of lysate controls (proteases and vectors). **C**, capillary western analysis of Hepsin and TMPRSS2 lysates. Hepsin and TMPRSS2 again behave differently compared to the other proteases.

Chapter 4: Discussion

Our goal for the projects discussed in this thesis was to modulate the production and/or processing of PrP^{C} to be able to attenuate prion disease. The rationale was that if the PrP substrate for conversion to the pathogenic PrP^{Sc} is either not present or is in a non-convertible form (C1 fragment), then prion disease would be mitigated. We sought to create a gene drive system targeting the expression of the *PRNP* gene in cervids; the drive would inhibit the spread of CWD without gross phenotypic perturbations (as previous research has indicated)[99,100,256,257]. Even though a complete understanding of which proteases are performing α- and β- cleavage of PrP^{C} is lacking, the ability of the C1 fragment to be neuroprotective and the C2 fragment to be converted to PrP^{Sc} gave us the impetus to pursue fragmentation as an intervention for prion disease[95,96].

4.1: Developing CRISPR/Cas9 technology for the elimination of prion disease

4.1.1: Targeting the PRNP gene by CRISPR/Cas9 technologies

In our project of targeting the *PRNP* gene for permanent knockout, as a means of CWD intervention, we found that the development of targeting vectors was the most straightforward. The development of the px330 and px458 Cas9/gRNA expression vectors by the Zhang lab (MIT) allowed for the ligation of designed gRNA-encoding DNAs into the *Bbs*I cleavage site with relative ease. Even though the targeting specificity of Cas9 is strictly regulated by the 20 bp gRNA sequence and presence of the PAM recognition motif, there is still the potential for off-target cleavage to occur in other genomic locations[217,218]. Furthermore, mismatches in the PAM-distal region between the gRNA and target sequence can be tolerated by the Cas9 endonuclease[274]. To improve understanding of the possible off-target loci, we utilised online

tools for the design of our gRNA, crispr.mit.edu (Zhang lab gRNA design tool) and e-crispr.org (recommendation of Zhang lab). However, caveats to our off-target assessment through the online design tools are extremely pertinent; no accessible tools had the mule deer, or for that matter, any cervid genomes for sequence homology interrogation. Moreover, at the time of our studies we did not have access to the mule deer genome for potential uploading and off-target assessment through other online tools. We chose the most phylogenetically related species of pig (for crispr.mit.edu) and cow (e-crisp.org) for gRNA design and off-target assessment, and cross referenced the output of both tools for the most applicable gRNA(s). It must be noted that gRNA online tools are not a guarantee of effectiveness and sequence homology outputs do not completely encapsulate the possibility of off-target sites[275,276]. In addition, the prevalence of off-target effects is under debate; some studies have reported low levels of off-targeting, while others have stated high levels[277,278]. Altogether, we decided upon two CRIPSR/Cas9 editing plasmids, neither of which have off-target binding in coding regions. With a complete mule deer genome now available, further work can be done regarding target design for the elimination of off-target effects.

4.1.2: Utilising a mule deer cell line and exclusion of a deer PRNP pseudogene

In our studies we utilised the MDB cell line to immediately situate editing within the target species. The cell line was developed through transformation of primary brain cultures (derived from hunter-harvested mule deer brain) with the SV40 genome, and found to be immortalised after several passages (unpublished data/personal correspondence)[261]. Subsequently, for editing assessment using the T7E1 mismatch assay, we had to isolate the coding *PRNP* gene from the pseudogene present in mule deer. Through adapting the forward primer of the PCR amplicon to be present within intron 2 of *PRNP*, we were able to amplify

solely our editing target region. Even though the MDB cell line was likely transformed, due to the presence of a viral T-antigen gene, we found that in some respects, it still behaved like primary neuronal cells[279]. The transfection efficiency of the cells was poor (highest achieved was ~21% with a pBud.GFP plasmid comparing GFP expressing cells to DAPI stained cells, data not shown) and perhaps could be improved through transduction with viral particles, which have been found to be typically more efficient with gRNA/Cas9 plasmid delivery into primary cells[275]. Another suggestion for inducing editing in the context of primary cells has been non-simultaneous administration of the gRNA and Cas9 protein[280]. Alternatively, we could use a cell line with different growth properties and lacking a pseudogene (e.g., RK13 cells stably expressing elk PrP) to better ascertain the editing of an expressed cervid PrP ORF. Furthermore, we could employ a preliminary experiment of targeting editing to a control gene with gRNA not expressed from the CRISPR vector, to determine if Cas9 expression is successful.

4.1.3 Assessment of CRISPR/Cas9 mediated editing of mule deer PRNP proved fruitless

We used the T7E1 mismatch assay to assess for NHEJ edits induced through our designed gRNA and Cas9, but were unable to find any indication of successful editing events (Figure 5D). We must consider limitations such as the T7E1 assay is able to detect indels of a larger magnitude (≥2 bp mismatch) with relative sensitivity but can miss smaller indels or single nucleotide changes[265,281]. Surveyor is another gene editing assessment assay that utilises an enzyme able to detect mismatches which provides greater recognition of single nucleotide edits but lacks with larger indels[275,281]. These mismatch cleavage assays are the simplest and most cost effective methods of editing detection which is why we chose to utilise the T7E1 assay; however, perhaps using the gold standard editing assessment of next generation sequencing (NGS) could

have provided us with an indication that editing was occurring in any form, rather than just having detection for indels[275].

Prior to developing a complete mobile genetic element used for a gene drive, the ability of the CRISPR/Cas9 technology to target and edit our region of interest had to be ascertained. We need to have firm conclusions that Cas9 is inducing a double stranded break for the homology arms of the mobile genetic element to be added through homology-directed repair. We were unable to confirm and assess if our CRISPR machinery was able to induce any editing. The lack of detectable editing can be due to a cohort of reasons. Possible explanations include, but are not limited to, the target region of *PRNP* is narrow and so target region optimisation is limited, transfection efficiency of the MDB cell line was too low to present enough targets, and the restricted sensitivity of editing assessment assay. These limitations would need to be overcome to be able to pursue the next steps in development of a gene drive for attenuation of CWD in cervid populations.

4.1.4 Employing a blue light CRISPRa system for inducible PRNP expression does not increase levels of the PrP^C protein

In an attempt to develop a system for inducible PrP to aid in drug studies, we looked at modifying previously published CRISPRa machinery. We adapted a blue light-inducible optogenetic system that saw the dimerization of two fusion proteins (dCas9/CIB1 and CRY2/p65) under blue light conditions able to induce the expression of endogenous genes[241]. We designed five gRNA sequences targeting the human *PRNP* promoter for maximal success in dCas9 binding, and transcriptional activation. However, in our experiments we failed to detect an increase in PrP^C production assessed either through conventional western or capillary western

analyses (Figure 10). Of note, the study describing the original methods did not indicate if protein expression was increased after CRISPRa induction; the researchers used qRT-PCR to detect overall overexpression of endogenous gene mRNA, and such increases in mRNA may not translate to protein overexpression[241]. Another issue possibly interfering with the success of our experiment is that a series of large plasmids essential for blue light induction need to be transfected into cells. Large plasmids needed for CRISPR/Cas9 machinery are known to result in low transfection efficiency and reduce cell viability[282-284]. At the very least, the gRNA expression vector (pgRNA.Humanized, ~8300 bp), and the two fusion protein expressing vectors (NLSx3-CRY2PHY-p65, ~8000 bp, and NLS-dCas9-trCIB1, ~10600 bp) need to be present. In the most optimistic and ideal experimental outcome, there would be a total of seven plasmids transfected into the cell (two fusion proteins and five gRNA targeting sequences), which is too many to maintain any semblance of transfection efficiency or cell viability [282-284].

4.2: A compound library screen for modulators of PrP^C cleavage

4.2.1 Candidate compounds for modulation of PrP^C cleavage

Hoping to find compounds that modulate PrP^C cleavage for possible attenuation of prion disease, an ideal compound would either increase the levels of C1 fragmentation (as the C1 fragment is neuroprotective) or decrease the levels of C2 fragmentation (as the fragment is long enough for possible conversion to PrP^{Sc}, Figure 3). After defining our filtering process for compound addition and running the compounds through said selection gauntlet, we found seven compounds that increased C1 fragmentation and two that lowered C2 fragmentation (Figure 12). However, these did not fit into a single common biochemical pathway to modulate C1/C2 production and are further described below.

C1 modulators

1) **Felbamate** is a N-methyl-D-aspartate (NMDA) antagonist which could be acting similarly to PrP^C, as PrP^C is known to inhibit the activity of NMDA receptors (NDMARs)[285,286]. NMDAR overactivation can result in excitotoxic neuronal death through dysregulation of intracellular calcium homeostasis, and studies have suggested that PrP^C can protect neurons from NMDAR induced excitotoxic death[285]. 2) **Carbamazepine** also interacts with the function of NMDARs; it is an inhibitor of voltage-gated sodium channels (with anti-convulsant activity) and can prevent NMDAR hypofunction[287]. It is unclear exactly how Felbamate and Carbamazepine are boosting C1 production, but it is likely through modulation of NMDAR function, be that through inhibition of overactivation or prevention of hypofunction. 3) **Repaglinide** is an ATP-sensitive potassium channel blocker used in the treatment of type II diabetes[288]. A relationship between type II diabetes and PrP^C function has yet to have been established. However, there has been a suggestion that type II diabetes results in prion-like aggregation of the islet amyloid polypeptide (IAPP), and moreover, IAPP interacts with the amyloidogenic cytotoxic fragment of Tau R3 found in AD[289,290]. 4) **GANT 58** is a GLI1 (glioma-associated) antagonist that inhibits Hedgehog (Hh) signalling[291]. Dysfunction in the Hh signalling pathway is responsible for a range of diseases such as cancers and neurodegenerative disorders[292]. Specifically, in relationship to adult neurodegenerative diseases, it has been found that sufficient activation of the Hh pathway can provide neuroprotective and regenerative activities[293]. 5) **NK 252** is a nuclear factor erythroid 2-related factor 2 (Nrf2) agonist/activator that increases the antioxidant potential of Nrf2[294]. The interaction of Nrf2 and antioxidant response elements (ARE) in gene promoter regions increase the antioxidant capacity of the brain, providing protection against oxidative stress found in neurodegenerative disorders[295]. One of the putative functions of PrP^C is remediation of oxidative

stress where PrP^C modulates antioxidant enzymes that convert ROS into non-toxic products[97,98]. Therefore, it is not unreasonable to suggest that NK 252 is stimulating the production of PrP^C (and α-cleavage) for its antioxidant properties. 6) **C-1** is a protein kinase C (PKC) inhibitor, which lowers the intracellular signalling pathway transduction ability of PKC[296]. PKC is a known regulator of PrP^C α-cleavage and if inhibited, it would be expected to lower the amount of C1 production, in contrast to the experimental results[84]. It must be noted that the α-cleavage regulation by PKC is dependent on the kinase isoform, and it is possible that C-1 inhibits alternative isoforms of PKC, which is why we see an increase in C1 production rather than a decrease[84]. 7) **S 18886** is a thromboxane A_2 antagonist able to inhibit vascular contractions and platelet aggregation, ultimately slowing atherosclerosis development[297]. Thromboxane A_2 is an isoprostane shown to have increased levels in neurological diseases, such as AD, PD, and CJD[298,299]. The exact mechanism by which the seven compounds are increasing C1 production remains to be elucidated; however, in six cases (excluding Repaglinide), the compounds have an association with neurodegenerative disorders or neurological dysfunction. In summary, further clarification on the mechanistic actions of these compounds with PrP^C would be needed to draw conclusions as to why there is an increase in C1 production; just having a neuropathological link does not develop our understanding of α-cleavage.

C2 modulators

The two C2 decreasing compounds, **FG 7142** and **nor-Binaltorphimine dihydrochloride**, work on different pathways, neither directly related to aspects of PrP^C biochemistry. FG 7142 is a benzodiazepine inverse agonist activating an anxiety-related neural network that interacts with neurotransmitter modulatory systems[300]. Nor-Binaltorphimine dihydrochloride is a kappa opioid receptor (KOR) antagonist with a long-lasting duration which

can inhibit behavioral responses to stressors when tested in mice[301,302]. The two compounds that decrease C2 levels could be activating the β-PrPase through systems and pathways not yet elucidated. However, as C2 fragmentation occurs at low amounts *in vivo*, it is possible that the decreases seen in experimentation with FG 7142 and nor-Binaltorphimine dihydrochloride are artifacts from the higher C2 production of the S3 RK13 cell line and are not applicable to complex mammalian systems.

Altogether, the nine compounds identified as possible modulators of PrP^C are involved in neurological pathways which is promising, as PrP^C is predominantly expressed in the CNS and has neurologically related functions[65,303]. However, without further experimentation, the direct interaction/capability of these compounds for PrP^C cleavage, whether by direct interaction or pathway modulation, will remain hidden.

4.2.2 The variability of PrP^C cleavage induced by compounds does not allow for therapeutic development

After identification of the nine potential target compounds, we retested them over a dose response and found considerable variability in the results. In all but one case (30 μM nor-Binaltorphimine dihydrochloride), we saw mixed outcomes, in direct contrast with what our initial screen indicated (Table 5). Probing the serial dilution capabilities of the selected compounds resulted in outcomes not concordant with previous results, which does not provide any indication for therapeutic capabilities. We would be unable to provide any components of target validation such as: site of action exposure, quantification of target occupancy, or proof of a relevant phenotypic perturbation[304]. Furthermore, the initial concentration tested was 20 μM which is higher than would be physiologically possible to attain, possibly inducing significant

off-target effects, a caveat of all *in vivo* based screens[304,305]. Using a cell-based model, we also run into complications that the effects may not be biochemically relevant; the compound effects achieved may not be mimicked in the human system[305]. Some possible reasons for the variation seen in the screen can be due to unavoidable experimental steps. For instance, the transportation of the cells from location to location for compound addition (cells were left with the HCA) can induce small temperature fluctuations resulting in variability of gene expression and the cell cycle[306]. Another example is the time span in which the screen was performed; to avoid a bottleneck of samples prior to western capillary analysis, we performed compound addition of two Tocris plates at a time, rather than the complete library. We attempted to mitigate the effects of increased passage number on gene expression and cell phenotypic variability through limiting the maximum passage number to 20 (from the starting aliquots of passage 5 for the S3 RK13 cells)[307,308]. However, as no study has yet documented the resilience to passage number of S3 RK13 cells, we are uncertain on the possible variability induced. Despite no therapeutically relevant outcomes from the compound library, our positive control of Linagliptin (a DPP-4 inhibitor) was consistently successful in lowering C2 production, providing us with confirmational data for other projects occurring within the Westaway lab (unpublished data).

4.3: A candidate driven approach to elucidate the PrP^C α-cleavage protease has identified TMPRSS1 (Hepsin) and TMPRSS2 as modulators of PrP^C expression

In an alternative avenue of experimentation, we used a candidate driven approach to identify α-PrPase. If the identity of the α-PrPase can be deciphered, then therapeutic interventions for prion disease can be surmised; by increasing α-cleavage, it would be possible to direct the cellular PrP pool to be unconvertable to PrP^{Sc}.

4.3.1: Trypsin-like serine type II membrane protease selection as potential α-PrPases

Preliminary work completed by Dr. Andrew Castle identified the non-specific serine protease inhibitor of Camostat mesylate as a modulator of PrP^C α-cleavage (unpublished data). Camostat mesylate provided a dose range response of α-cleavage with S3-PrP as well as wildtype PrP (unpublished data); furthermore, we know that trypsin-like proteases cleave after Arg/Lys residues and that α-cleavage occurs after residues 110/111 (human numbering) with residue 110 being Lys[80-82]. Moreover, the serine protease inhibitor gene, *SERPINA*3, is upregulated and transcribed in all prion diseases, another factor suggesting that a serine protease is involved in the cleavage of PrP^C [309]. Upon accumulation of this data, we wished to look for trypsin-like, type II membrane serine proteases that are present in the brain and demonstrate inhibition or probable inhibition by Camostat mesylate. To determine tissue expression, we utilised the Human Protein Atlas (proteinatlas.org)[310]. We identified TMPRSS1 (aka Hepsin), TMPRSS2, TMPRSS4, TMPRSS5, TMPRSS11D, and HTRA1 as potential candidates. Hepsin, TMPRSS5, and HTRA1 do not have any literature specifically showing inhibition by Camostat mesylate but instead, were selected based on expression in the brain and substrate specificity (i.e., Arg/Lys at P1)[311-313]. TMPRSS4 and TMPRSS11D have indirect evidence of Camostat mesylate inhibition, demonstrate expression in the brain and appropriate substrate specificity (Trypsin-like, and Arg(P1)>Lys(P1) (respectively))[314-316]. TMPRSS2 has several studies describing its inhibition by Camostat mesylate, especially in reference to treatment of SARS-CoV-2 and other coronaviruses, as TMPRSS2 is used for cleavage and activation of the viral spike protein[317-320]. TMPRSS2 primes the spike protein of SARS-CoV-2 prior to attachment to the angiotensin-converting enzyme 2 (ACE2) receptor, the receptor SARS-CoV-2 uses for viral entry into target cells[321].

4.3.2: Behaviour of Hepsin and TMPRSS2 in a PrP-based assay

Co-transfections of the proteases and PrP (under two different expression promoters) resulted in the discovery that Hepsin and TMPRSS2 are changing the way PrP presents on western blots. We found that PrP expressed under the CMV promoter is only present in the C1 form (very low amounts) when co-transfected with a Hepsin expressing plasmid, and for TMPRSS2 co-transfections, the overall levels of PrP (both FL and C1) are drastically lowered (Figure 16). Using the alternative expression promoter, EF1a, we can see FL PrP is still present in the cell lysates of Hepsin/TMPRSS2 co-transfections (although at low amounts, as confirmed by capillary western analysis) and with little to no C1 fragmentation (Figure 21). We initially hypothesised that Hepsin and TMPRSS2 are inducing shedding of PrP through the activation of ADAM10, as studies have shown that Hepsin is able to induce metalloprotease activation and cause subsequent metalloprotease cascades[273]. However, after probing media from the cell culture (following co-transfection) with a primary antibody specific for shed PrP (sPrPG228), there is no indication of any PrP ending at residue 228 due to the action of ADAM10 (Figure 18B). Furthermore, the total PrP present (as measured by Sha31 1° antibody) is diminished in Hepsin and TMPRSS2 protease conditions, in contrast to the other proteases and controls, and visually resembles PrP that has been chemically deglycosylated with PNGase F (Figure 18A).

The effects produced by Hepsin and TMPRSS2 were apparent when co-transfected into RK13 cells lacking detectable endogenous PrP (Figure 16). To account for shared transcription factor competition with promoters, we performed the co-transfections with a plasmid expressing PrP under the EF1a promoter, rather than the CMV promoter. We see that Hepsin and TMPRSS2 are inducing the same effect regardless of the PrP promoter (Figure 21). On the other hand, when PrP is produced in a stable cell line with high levels of endogenous PrP^C (RK13-WT10 cells), we

do not see any changes in the repertoire of PrP species with immunoblotting (Figure 17). If the action of proteases, such as Hepsin and TMPRSS2, is only applicable to nascent PrP^C, it is possible that this effect is obscured by the presence of metabolically stable, pre-existing PrP species[267,268].

4.3.3: Hepsin and TMPRSS2 interact with GPI-anchored proteins lowering the detection in western analyses

Since we did not detect ADAM10 derived shed PrP and found a lack of change of PrP under stable cell conditions, we hypothesised that Hepsin and TMPRSS2 are acting on the biogenesis of PrP, rather than mature forms. We wished to test the candidate type II proteases upon other GPI-anchored proteins, both within the prion family (Sho and Dpl) and outside (Thy1); GPI-anchoring is a crucial post-translational modification that has a significant impact on cellular function of these proteins[322,323]. Addition of the GPI-anchor occurs following the precursor protein translocating to the ER, and involves several processing steps in the ER and Golgi apparatus[322]. We found that Hepsin and TMPRSS2 induce their effects on GPI-anchored proteins in comparison to the other proteases and controls, as there is significantly reduced or no detectable amounts of the GPI-anchored proteins when co-expressed with these proteases (Figure 19 and 20). We know that the GPI anchor is crucial for PrP^C trafficking through the secretory pathway and GPI-anchorless PrP shows slower transportation to the cell surface and is under-glycosylated[323]. Due to the apparent absence of glycosylation in Figure 18A, we suggest that Hepsin and TMPRSS2 are interacting with the GPI-anchored proteins at an early stage in protein maturation, prior to glycosylation and GPI anchor addition. Other studies looking at Hepsin and its potential cleavage targets have identified Uromodulin, a glycoprotein abundantly found in urine, as another GPI-anchored substrate; Uromodulin levels were significantly lowered when

Hepsin levels were artificially reduced[324,325]. There is no specific literature demonstrating that TMPRSS2 acts upon GPI-anchored proteins, but there are virus-specific differences in GPI anchor biosynthesis across coronaviruses that could potentially occur through the function of TMPRSS2[326].

4.3.4: Hepsin and TMPRSS2 have overlapping functions reported within the literature

Within the literature, Hepsin and TMPRSS2 have been linked to prostate carcinogenesis, based upon their expression profiles[327]. The two proteases are also able to cleave the ACE2 viral receptor for the SARS-CoV spike protein attachment[328]. In terms of neurological function and perturbations induced by Hepsin and TMPRSS2, both proteases can activate protease-activated receptor 2 (PAR2), which has been implicated in neurodegenerative diseases[273,327,329]. Altogether, we can surmise that the substrates Hepsin and TMPRSS2 cleave are closely related. We can see that the action of these proteases affects the production of GPI-anchored proteins (Figure 16 to 21). To our current knowledge, no study has explored Hepsin and TMPRSS2, or the other proteases studied here, in connection with PrP^{C}.

4.3.5: The proteases studied are not candidates for being α-PrPase

In conclusion, neither Hepsin nor TMPRSS2 (or any of the other proteases studied here), are a candidate for being the α-PrPase, as would be verified by an increase of the C1 fragment in western analyses. However, looking at the overall modulation and/or synthesis of GPI-anchored proteins, Hepsin and TMPRSS2 are prime candidates for future experiments.

4.4: Future directions and conclusions

With the identification of Hepsin and TMPRSS2 as modulators of GPI-anchored proteins, we will continue to elucidate by which manner they are affecting biosynthesis. We will initially perform confirmation experiments such as: quantification of protease production through detection with corresponding primary antibodies, protein expression recovery with co-transfections occurring under the presence of Camostat mesylate, and a negative control experiment with the co-transfection and expression of GPI-anchorless PrP. Another experiment we will perform is an extended transfection of the proteases into the stably expressing PrP cell line (RK13 WT-10), in order to control for metabolically stable PrP fragments which can be confounding the western analyses[267,268]. We wish to explore when and where the proteases are exerting their effect on the GPI-anchored proteins; we can perform the protease transfection into an inducible PrP system (Ponasterone A two-plasmid system used previously in the Westaway lab) where following the transfection, we will induce expression so that only nascent PrP molecules are present. We will also perform a pulse-chase experiment to determine the cellular processes occurring over a period of time, and when the proteases are inhibiting typical production of GPI-anchored proteins[330]. As N-linked glycosyl side chains are a feature of many GPI-anchored proteins (added in the Golgi apparatus), we wish to understand if the glycans are changed by the presence of Hepsin and/or TMPRSS2; to explore this we can perform analyses on the cell lysates without PNGase F treatment[322]. We intend to continue with the candidate-based protease selection for elucidation of the α-PrPase, following our initial rationale for candidate selection (i.e., serine proteases that are expressed in the brain and can be inhibited by Camostat mesylate). We will test the action of proteases upon PrP substrates through co-transfections, with analyses completed through conventional and capillary westerns.

Ascertaining the identity of the α-PrPase would be a significant step in the mitigation of prion disease, as a protease antagonist can be subsequently identified. This would ensure that the cellular pool of PrP is solely the C1 fragment, a dominant negative inhibitor of PrP^{Sc} prolonging time to disease onset[90,91].

Thus far, we have been unsuccessful in the exploration of attenuating prion disease through modulation of PrP^{C}. Our foray into CRISPR/Cas9 technologies under the logic of "no PrP^{C}, no PrP^{Sc}" was hindered by the complexity of targeting and editing detection. Our compound library screen looking to increase the neuroprotective C1 fragment and lower the PrP^{Sc}-convertible C2 fragment provided results of high variance, not amenable to the establishment of a potential therapeutic. We achieved results in our candidate-driven approach for the elucidation of α-PrPase, not in terms of identifying said protease, but rather in establishing that Hepsin and TMPRSS2 are modulators of GPI-anchored protein production/synthesis/biogenesis. The concept of modulating the production/proteolysis of PrP^{C} for attenuation of prion disease remains compelling and will continue to be optimistically pursued by the Westaway lab.

Bibliography

1 Collinge, J. Prion diseases of humans and animals: Their causes and molecular basis. *Annual Review of Neuroscience* **24**, 519-550, doi:DOI 10.1146/annurev.neuro.24.1.519 (2001).

2 Prusiner, S. B. Novel proteinaceous infectious particles cause scrapie. *Science* **216**, 136-144, doi:10.1126/science.6801762 (1982).

3 McGowan, J. Scrapie in sheep. *Scott J Agric* **5**, 365-375 (1922).

4 Bolton, D. C., Mckinley, M. P. & Prusiner, S. B. Identification of a Protein That Purifies with the Scrapie Prion. *Science* **218**, 1309-1311, doi:DOI 10.1126/science.6815801 (1982).

5 Prusiner, S. B. *et al.* Further purification and characterization of scrapie prions. *Biochemistry* **21**, 6942-6950, doi:10.1021/bi00269a050 (1982).

6 Mckinley, M. P., Bolton, D. C. & Prusiner, S. B. A Protease-Resistant Protein Is a Structural Component of the Scrapie Prion. *Cell* **35**, 57-62, doi:Doi 10.1016/0092-8674(83)90207-6 (1983).

7 Prusiner, S. B., Groth, D. F., Bolton, D. C., Kent, S. B. & Hood, L. E. Purification and structural studies of a major scrapie prion protein. *Cell* **38**, 127-134, doi:10.1016/0092-8674(84)90533-6 (1984).

8 Borchelt, D. R., Scott, M., Taraboulos, A., Stahl, N. & Prusiner, S. B. Scrapie and cellular prion proteins differ in their kinetics of synthesis and topology in cultured cells. *The Journal of cell biology* **110**, 743-752 (1990).

9 Prusiner, S. B. Molecular biology of prion diseases. *Science* **252**, 1515-1522 (1991).

10 Aguzzi, A., Heikenwalder, M. & Miele, G. Progress and problems in the biology, diagnostics, and therapeutics of prion diseases. *J Clin Invest* **114**, 153-160, doi:10.1172/JCI22438 (2004).

11 Gambetti, P., Kong, Q., Zou, W., Parchi, P. & Chen, S. G. Sporadic and familial CJD: classification and characterisation. *Br Med Bull* **66**, 213-239, doi:10.1093/bmb/66.1.213 (2003).

12 Glatzel, M., Stoeck, K., Seeger, H., Lührs, T. & Aguzzi, A. Human prion diseases: molecular and clinical aspects. *Archives of neurology* **62**, 545-552 (2005).

13 Prusiner, S. B. Prions are novel infectious pathogens causing scrapie and Creutzfeldt-Jakob disease. *Bioessays* **5**, 281-286, doi:10.1002/bies.950050612 (1986).

14 Alpers, M. P. Review. The epidemiology of kuru: monitoring the epidemic from its peak to its end. *Philos Trans R Soc Lond B Biol Sci* **363**, 3707-3713, doi:10.1098/rstb.2008.0071 (2008).

15 Gajdusek, D. C. & Zigas, V. Kuru - Clinical, Pathological and Epidemiological Study of an Acute Progressive Degenerative Disease of the Central Nervous System among Natives of the Eastern Highlands of New-Guinea. *Am J Med* **26**, 442-469, doi:Doi 10.1016/0002-9343(59)90251-7 (1959).

16 Field, E. J., Mathews, J. D. & Raine, C. S. Electron microscopic observations on the cerebellar cortex in kuru. *J Neurol Sci* **8**, 209-224, doi:10.1016/0022-510x(69)90111-7 (1969).

17 Snow, A. D., Kisilevsky, R., Willmer, J., Prusiner, S. B. & DeArmond, S. J. Sulfated glycosaminoglycans in amyloid plaques of prion diseases. *Acta Neuropathol* **77**, 337-342, doi:10.1007/BF00687367 (1989).

18 Collinge, J. *et al.* A clinical study of kuru patients with long incubation periods at the end of the epidemic in Papua New Guinea. *Philos Trans R Soc Lond B Biol Sci* **363**, 3725-3739, doi:10.1098/rstb.2008.0068 (2008).

19 Brown, P. *et al.* Iatrogenic Creutzfeldt-Jakob disease, final assessment. *Emerg Infect Dis* **18**, 901-907, doi:10.3201/eid1806.120116 (2012).

20 Schmitz, M. *et al.* Hereditary Human Prion Diseases: an Update. *Mol Neurobiol* **54**, 4138-4149, doi:10.1007/s12035-016-9918-y (2017).

21 Harder, A. *et al.* Novel twelve-generation kindred of fatal familial insomnia from germany representing the entire spectrum of disease expression. *Am J Med Genet* **87**, 311-316, doi:10.1002/(sici)1096-8628(19991203)87:4<311::aid-ajmg6>3.0.co;2-5 (1999).

22 Windl, O. *et al.* Molecular genetics of human prion diseases in Germany. *Hum Genet* **105**, 244-252, doi:10.1007/s004399900124 (1999).

23 Palmer, M. S., Dryden, A. J., Hughes, J. T. & Collinge, J. Homozygous prion protein genotype predisposes to sporadic Creutzfeldt-Jakob disease. *Nature* **352**, 340-342, doi:10.1038/352340a0 (1991).

24 Detwiler, L. A. & Baylis, M. The epidemiology of scrapie. *Rev Sci Tech* **22**, 121-143, doi:10.20506/rst.22.1.1386 (2003).

25 Migliore, S., Puleio, R. & Loria, G. R. Scrapie Control in EU Goat Population: Has the Last Gap Been Overcome? *Front Vet Sci* **7**, 581969, doi:10.3389/fvets.2020.581969 (2020).

26 Authority, E. F. S. Annual Report of the Scientific Network on BSE-TSE 2019. Report No. 2397-8325, (Wiley Online Library, 2019).

27 Foster, J. D., Parnham, D., Chong, A., Goldmann, W. & Hunter, N. Clinical signs, histopathology and genetics of experimental transmission of BSE and natural scrapie to sheep and goats. *Vet Rec* **148**, 165-171, doi:10.1136/vr.148.6.165 (2001).

28 Laegreid, W. W. *et al.* Scrapie resistance in ARQ sheep. *J Virol* **82**, 10318-10320, doi:10.1128/JVI.00710-08 (2008).

29 Andreoletti, O. *et al.* Atypical/Nor98 scrapie infectivity in sheep peripheral tissues. *PLoS Pathog* **7**, e1001285, doi:10.1371/journal.ppat.1001285 (2011).

30 Wells, G. A. *et al.* A novel progressive spongiform encephalopathy in cattle. *Veterinary Record* **121**, 419-420 (1987).

31 Casalone, C. & Hope, J. Atypical and classic bovine spongiform encephalopathy. *Handb Clin Neurol* **153**, 121-134, doi:10.1016/B978-0-444-63945-5.00007-6 (2018).

32 Donnelly, C. A., Ferguson, N. M., Ghani, A. C. & Anderson, R. M. Implications of BSE infection screening data for the scale of the British BSE epidemic and current European infection levels. *Proc Biol Sci* **269**, 2179-2190, doi:10.1098/rspb.2002.2156 (2002).

33 Anderson, R. M. *et al.* Transmission dynamics and epidemiology of BSE in British cattle. *Nature* **382**, 779-788, doi:10.1038/382779a0 (1996).

34 Wells, G. A. & Wilesmith, J. W. The neuropathology and epidemiology of bovine spongiform encephalopathy. *Brain Pathol* **5**, 91-103, doi:10.1111/j.1750-3639.1995.tb00580.x (1995).

35 Konold, T. *et al.* Clinical findings in 78 suspected cases of bovine spongiform encephalopathy in Great Britain. *Vet Rec* **155**, 659-666, doi:10.1136/vr.155.21.659 (2004).

36 Buschmann, A. *et al.* Atypical BSE in Germany--proof of transmissibility and biochemical characterization. *Vet Microbiol* **117**, 103-116, doi:10.1016/j.vetmic.2006.06.016 (2006).

37 Will, R. G. *et al.* A new variant of Creutzfeldt-Jakob disease in the UK. *Lancet* **347**, 921-925, doi:10.1016/s0140-6736(96)91412-9 (1996).

38 Ironside, J. W. Variant Creutzfeldt-Jakob disease: an update. *Folia Neuropathol* **50**, 50-56 (2012).

39 Ward, H. J. *et al.* Risk factors for variant Creutzfeldt-Jakob disease: a case-control study. *Ann Neurol* **59**, 111-120, doi:10.1002/ana.20708 (2006).

40 Wadsworth, J. D. *et al.* Human prion protein with valine 129 prevents expression of variant CJD phenotype. *Science* **306**, 1793-1796, doi:10.1126/science.1103932 (2004).

41 Boyle, A. *et al.* No Adaptation of the Prion Strain in a Heterozygous Case of Variant Creutzfeldt-Jakob Disease. *Emerg Infect Dis* **26**, 1300-1303, doi:10.3201/eid2606.191116 (2020).

42 Mok, T. *et al.* Variant Creutzfeldt-Jakob disease in a patient with heterozygosity at PRNP codon 129. *The New England journal of medicine* **376**, 292-294 (2017).

43 Wilesmith, J. What can we learn from BSE? *The Bovine Practitioner*, 71-75 (1997).

44 Requena, J. R. *et al.* The Priority position paper: Protecting Europe's food chain from prions. *Prion* **10**, 165-181, doi:10.1080/19336896.2016.1175801 (2016).

45 Gilch, S. *et al.* Chronic wasting disease. *Top Curr Chem* **305**, 51-77, doi:10.1007/128_2011_159 (2011).

46 Williams, E. S. & Young, S. Chronic wasting disease of captive mule deer: a spongiform encephalopathy. *J Wildl Dis* **16**, 89-98, doi:10.7589/0090-3558-16.1.89 (1980).

47 Hannaoui, S., Schatzl, H. M. & Gilch, S. Chronic wasting disease: Emerging prions and their potential risk. *PLoS Pathog* **13**, e1006619, doi:10.1371/journal.ppat.1006619 (2017).

48 Center, U. N. W. H. *Map of Chronic Wasting Disease in North America*, <www.usgs.gov/centers/nwhc/science/chronic-wasting-disease> (2020).

49 Kim, T. Y. *et al.* Additional cases of Chronic Wasting Disease in imported deer in Korea. *J Vet Med Sci* **67**, 753-759, doi:10.1292/jvms.67.753 (2005).

50 Benestad, S. L., Mitchell, G., Simmons, M., Ytrehus, B. & Vikoren, T. First case of chronic wasting disease in Europe in a Norwegian free-ranging reindeer. *Vet Res* **47**, 88, doi:10.1186/s13567-016-0375-4 (2016).

51 Pirisinu, L. *et al.* Novel Type of Chronic Wasting Disease Detected in Moose (Alces alces), Norway. *Emerg Infect Dis* **24**, 2210-2218, doi:10.3201/eid2412.180702 (2018).

52 Williams, E. S. Chronic wasting disease. *Vet Pathol* **42**, 530-549, doi:10.1354/vp.42-5-530 (2005).

53 Williams, E. S. & Young, S. Neuropathology of chronic wasting disease of mule deer (Odocoileus hemionus) and elk (Cervus elaphus nelsoni). *Vet Pathol* **30**, 36-45, doi:10.1177/030098589303000105 (1993).

54 Cervenáková, L., Rohwer, R., Williams, E. S., Brown, P. & Gajdusek, D. C. High sequence homology of the PrP gene in mule deer and Rocky Mountain elk. *The Lancet* **350**, 219-220, doi:10.1016/s0140-6736(05)62387-2 (1997).

55 Bian, J. *et al.* Primary structural differences at residue 226 of deer and elk PrP dictate selection of distinct CWD prion strains in gene-targeted mice. *Proc Natl Acad Sci U S A* **116**, 12478-12487, doi:10.1073/pnas.1903947116 (2019).

56 Davenport, K. A. *et al.* Comparative analysis of prions in nervous and lymphoid tissues of chronic wasting disease-infected cervids. *J Gen Virol* **99**, 753-758, doi:10.1099/jgv.0.001053 (2018).

57 Miller, M. W., Williams, E. S., Hobbs, N. T. & Wolfe, L. L. Environmental sources of prion transmission in mule deer. *Emerg Infect Dis* **10**, 1003-1006, doi:10.3201/eid1006.040010 (2004).

58 Taylor, D. M. Inactivation of transmissible degenerative encephalopathy agents: A review. *Vet J* **159**, 10-17, doi:10.1053/tvjl.1999.0406 (2000).

59 Waddell, L. *et al.* Current evidence on the transmissibility of chronic wasting disease prions to humans-A systematic review. *Transbound Emerg Dis* **65**, 37-49, doi:10.1111/tbed.12612 (2018).

60 Harrison, P. M., Khachane, A. & Kumar, M. Genomic assessment of the evolution of the prion protein gene family in vertebrates. *Genomics* **95**, 268-277, doi:10.1016/j.ygeno.2010.02.008 (2010).

61 Oesch, B. *et al.* A cellular gene encodes scrapie PrP 27-30 protein. *Cell* **40**, 735-746, doi:10.1016/0092-8674(85)90333-2 (1985).

62 Sparkes, R. S. *et al.* Assignment of the human and mouse prion protein genes to homologous chromosomes. *Proc Natl Acad Sci U S A* **83**, 7358-7362, doi:10.1073/pnas.83.19.7358 (1986).

63 Watts, J. C. & Westaway, D. The prion protein family: diversity, rivalry, and dysfunction. *Biochim Biophys Acta* **1772**, 654-672, doi:10.1016/j.bbadis.2007.05.001 (2007).

64 Schmitt-Ulms, G., Ehsani, S., Watts, J. C., Westaway, D. & Wille, H. Evolutionary descent of prion genes from the ZIP family of metal ion transporters. *PLoS One* **4**, e7208, doi:10.1371/journal.pone.0007208 (2009).

65 Castle, A. R. & Gill, A. C. Physiological Functions of the Cellular Prion Protein. *Front Mol Biosci* **4**, 19, doi:10.3389/fmolb.2017.00019 (2017).

66 Weissmann, C. Molecular biology of prion diseases. *Trends Cell Biol* **4**, 10-14, doi:10.1016/0962-8924(94)90032-9 (1994).

67 Riesner, D. Biochemistry and structure of PrPC and PrPSc. *Brit Med Bull* **66**, 21-+, doi:10.1093/bmb/66.1.21 (2003).

68 Stahl, N., Borchelt, D. R., Hsiao, K. & Prusiner, S. B. Scrapie prion protein contains a phosphatidylinositol glycolipid. *Cell* **51**, 229-240, doi:10.1016/0092-8674(87)90150-4 (1987).

69 Bolton, D. C., Meyer, R. K. & Prusiner, S. B. Scrapie Prp 27-30 Is a Sialoglycoprotein. *Journal of Virology* **53**, 596-606, doi:Doi 10.1128/Jvi.53.2.596-606.1985 (1985).

70 Garcia, F. L., Zahn, R., Riek, R. & Wuthrich, K. NMR structure of the bovine prion protein. *P Natl Acad Sci USA* **97**, 8334-8339, doi:DOI 10.1073/pnas.97.15.8334 (2000).

71 Riek, R. *et al.* NMR structure of the mouse prion protein domain PrP(121-231). *Nature* **382**, 180-182, doi:10.1038/382180a0 (1996).

72 Zahn, R. *et al.* NMR solution structure of the human prion protein. *Proc Natl Acad Sci U S A* **97**, 145-150, doi:10.1073/pnas.97.1.145 (2000).

73 Donne, D. G. *et al.* Structure of the recombinant full-length hamster prion protein PrP(29-231): the N terminus is highly flexible. *Proc Natl Acad Sci U S A* **94**, 13452-13457, doi:10.1073/pnas.94.25.13452 (1997).

74 Lau, A. *et al.* Octarepeat region flexibility impacts prion function, endoproteolysis and disease manifestation. *EMBO Mol Med* **7**, 339-356, doi:10.15252/emmm.201404588 (2015).

75 Brown, D. R. *et al.* The cellular prion protein binds copper in vivo. *Nature* **390**, 684-687, doi:10.1038/37783 (1997).

76 Beland, M., Motard, J., Barbarin, A. & Roucou, X. PrP(C) homodimerization stimulates the production of PrPC cleaved fragments PrPN1 and PrPC1. *J Neurosci* **32**, 13255-13263, doi:10.1523/JNEUROSCI.2236-12.2012 (2012).

77 Su, A. I. *et al.* A gene atlas of the mouse and human protein-encoding transcriptomes. *Proc Natl Acad Sci U S A* **101**, 6062-6067, doi:10.1073/pnas.0400782101 (2004).

78 Sales, N. *et al.* Developmental expression of the cellular prion protein in elongating axons. *Eur J Neurosci* **15**, 1163-1177, doi:10.1046/j.1460-9568.2002.01953.x (2002).

79 Adle-Biassette, H. *et al.* Immunohistochemical expression of prion protein (PrPC) in the human forebrain during development. *J Neuropathol Exp Neurol* **65**, 698-706, doi:10.1097/01.jnen.0000228137.10531.72 (2006).

80 Chen, S. G. *et al.* Truncated forms of the human prion protein in normal brain and in prion diseases. *J Biol Chem* **270**, 19173-19180, doi:10.1074/jbc.270.32.19173 (1995).

81 Mange, A. *et al.* Alpha- and beta- cleavages of the amino-terminus of the cellular prion protein. *Biol Cell* **96**, 125-132, doi:10.1016/j.biolcel.2003.11.007 (2004).

82 McDonald, A. J., Dibble, J. P., Evans, E. G. & Millhauser, G. L. A new paradigm for enzymatic control of alpha-cleavage and beta-cleavage of the prion protein. *J Biol Chem* **289**, 803-813, doi:10.1074/jbc.M113.502351 (2014).

83 Vincent, B. *et al.* The disintegrins ADAM10 and TACE contribute to the constitutive and phorbol ester-regulated normal cleavage of the cellular prion protein. *J Biol Chem* **276**, 37743-37746, doi:10.1074/jbc.M105677200 (2001).

84 Alfa Cisse, M. *et al.* Isoform-specific contribution of protein kinase C to prion processing. *Mol Cell Neurosci* **39**, 400-410, doi:10.1016/j.mcn.2008.07.013 (2008).

85 Wik, L., Klingeborn, M., Willander, H. & Linne, T. Separate mechanisms act concurrently to shed and release the prion protein from the cell. *Prion* **6**, 498-509, doi:10.4161/pri.22588 (2012).

86 Altmeppen, H. C. *et al.* Lack of a-disintegrin-and-metalloproteinase ADAM10 leads to intracellular accumulation and loss of shedding of the cellular prion protein in vivo. *Mol Neurodegener* **6**, 36, doi:10.1186/1750-1326-6-36 (2011).

87 Taylor, D. R. *et al.* Role of ADAMs in the ectodomain shedding and conformational conversion of the prion protein. *J Biol Chem* **284**, 22590-22600, doi:10.1074/jbc.M109.032599 (2009).

88 Walmsley, A. R., Watt, N. T., Taylor, D. R., Perera, W. S. & Hooper, N. M. alpha-cleavage of the prion protein occurs in a late compartment of the secretory pathway and is independent of lipid rafts. *Mol Cell Neurosci* **40**, 242-248, doi:10.1016/j.mcn.2008.10.012 (2009).

89 Shyng, S. L., Huber, M. T. & Harris, D. A. A Prion Protein Cycles between the Cell-Surface and an Endocytic Compartment in Cultured Neuroblastoma-Cells. *Journal of Biological Chemistry* **268**, 15922-15928 (1993).

90 Westergard, L., Turnbaugh, J. A. & Harris, D. A. A naturally occurring C-terminal fragment of the prion protein (PrP) delays disease and acts as a dominant-negative

inhibitor of PrPSc formation. *J Biol Chem* **286**, 44234-44242, doi:10.1074/jbc.M111.286195 (2011).

91 Lewis, V. *et al.* Increased proportions of C1 truncated prion protein protect against cellular M1000 prion infection. *J Neuropathol Exp Neurol* **68**, 1125-1135, doi:10.1097/NEN.0b013e3181b96981 (2009).

92 Altmeppen, H. C. *et al.* Proteolytic processing of the prion protein in health and disease. *Am J Neurodegener Dis* **1**, 15-31 (2012).

93 Mattei, V. *et al.* Morphine Withdrawal Modifies Prion Protein Expression in Rat Hippocampus. *PLoS One* **12**, e0169571, doi:10.1371/journal.pone.0169571 (2017).

94 Campbell, L. *et al.* The PrP(C) C1 fragment derived from the ovine A136R154R171PRNP allele is highly abundant in sheep brain and inhibits fibrillisation of full-length PrP(C) protein in vitro. *Biochim Biophys Acta* **1832**, 826-836, doi:10.1016/j.bbadis.2013.02.020 (2013).

95 Owen, J. P. *et al.* Molecular profiling of ovine prion diseases by using thermolysin-resistant PrPSc and endogenous C2 PrP fragments. *J Virol* **81**, 10532-10539, doi:10.1128/JVI.00640-07 (2007).

96 Pan, T. *et al.* Biochemical fingerprints of prion infection: accumulations of aberrant full-length and N-terminally truncated PrP species are common features in mouse prion disease. *J Virol* **79**, 934-943, doi:10.1128/JVI.79.2.934-943.2005 (2005).

97 McMahon, H. E. *et al.* Cleavage of the amino terminus of the prion protein by reactive oxygen species. *J Biol Chem* **276**, 2286-2291, doi:10.1074/jbc.M007243200 (2001).

98 Watt, N. T. *et al.* Reactive oxygen species-mediated beta-cleavage of the prion protein in the cellular response to oxidative stress. *J Biol Chem* **280**, 35914-35921, doi:10.1074/jbc.M507327200 (2005).

99 Bueler, H. *et al.* Normal development and behaviour of mice lacking the neuronal cell-surface PrP protein. *Nature* **356**, 577-582, doi:10.1038/356577a0 (1992).

100 Manson, J. *et al.* 129/Ola mice carrying a null mutation in PrP that abolishes mRNA production are developmentally normal. *Molecular neurobiology* **8**, 121-127 (1994).

101 Sakaguchi, S. *et al.* Loss of cerebellar Purkinje cells in aged mice homozygous for a disrupted PrP gene. *Nature* **380**, 528-531, doi:10.1038/380528a0 (1996).

102 Moore, R. C. *et al.* Ataxia in prion protein (PrP)-deficient mice is associated with upregulation of the novel PrP-like protein Doppel. *Journal of Molecular Biology* **292**, 797-817, doi:DOI 10.1006/jmbi.1999.3108 (1999).

103 Rossi, D. *et al.* Onset of ataxia and Purkinje cell loss in PrP null mice inversely correlated with Dpl level in brain. *EMBO J* **20**, 694-702, doi:10.1093/emboj/20.4.694 (2001).

104 Nuvolone, M. *et al.* SIRPalpha polymorphisms, but not the prion protein, control phagocytosis of apoptotic cells. *J Exp Med* **210**, 2539-2552, doi:10.1084/jem.20131274 (2013).

105 Brown, D. R., Nicholas, R. S. & Canevari, L. Lack of prion protein expression results in a neuronal phenotype sensitive to stress. *J Neurosci Res* **67**, 211-224, doi:10.1002/jnr.10118 (2002).

106 Wong, B. S. *et al.* Increased levels of oxidative stress markers detected in the brains of mice devoid of prion protein. *J Neurochem* **76**, 565-572, doi:10.1046/j.1471-4159.2001.00028.x (2001).

107 Spudich, A. *et al.* Aggravation of ischemic brain injury by prion protein deficiency: role of ERK-1/-2 and STAT-1. *Neurobiol Dis* **20**, 442-449, doi:10.1016/j.nbd.2005.04.002 (2005).

108 Sakurai-Yamashita, Y. *et al.* Female-specific neuroprotection against transient brain ischemia observed in mice devoid of prion protein is abolished by ectopic expression of prion protein-like protein. *Neuroscience* **136**, 281-287, doi:10.1016/j.neuroscience.2005.06.095 (2005).

109 Paterson, A. W., Curtis, J. C. & Macleod, N. K. Complex I specific increase in superoxide formation and respiration rate by PrP-null mouse brain mitochondria. *J Neurochem* **105**, 177-191, doi:10.1111/j.1471-4159.2007.05123.x (2008).

110 Sakudo, A. *et al.* Impairment of superoxide dismutase activation by N-terminally truncated prion protein (PrP) in PrP-deficient neuronal cell line. *Biochemical and Biophysical Research Communications* **308**, 660-667, doi:10.1016/s0006-291x(03)01459-1 (2003).

111 Rachidi, W. *et al.* Expression of prion protein increases cellular copper binding and antioxidant enzyme activities but not copper delivery. *J Biol Chem* **278**, 9064-9072, doi:10.1074/jbc.M211830200 (2003).

112 Miele, G., Jeffrey, M., Turnbull, D., Manson, J. & Clinton, M. Ablation of cellular prion protein expression affects mitochondrial numbers and morphology. *Biochem Biophys Res Commun* **291**, 372-377, doi:10.1006/bbrc.2002.6460 (2002).

113 Hutter, G., Heppner, F. L. & Aguzzi, A. No superoxide dismutase activity of cellular prion protein in vivo. *Biol Chem* **384**, 1279-1285, doi:10.1515/BC.2003.142 (2003).

114 Waggoner, D. J. *et al.* Brain copper content and cuproenzyme activity do not vary with prion protein expression level. *Journal of Biological Chemistry* **275**, 7455-7458 (2000).

115 Walter, E. D., Chattopadhyay, M. & Millhauser, G. L. The affinity of copper binding to the prion protein octarepeat domain: evidence for negative cooperativity. *Biochemistry* **45**, 13083-13092, doi:10.1021/bi060948r (2006).

116 Leclerc, E., Serban, H., Prusiner, S. B., Burton, D. R. & Williamson, R. A. Copper induces conformational changes in the N-terminal part of cell-surface PrPC. *Arch Virol* **151**, 2103-2109, doi:10.1007/s00705-006-0804-1 (2006).

117 Chattopadhyay, M. *et al.* The octarepeat domain of the prion protein binds Cu(II) with three distinct coordination modes at pH 7.4. *J Am Chem Soc* **127**, 12647-12656, doi:10.1021/ja053254z (2005).

118 Pauly, P. C. & Harris, D. A. Copper stimulates endocytosis of the prion protein. *J Biol Chem* **273**, 33107-33110, doi:10.1074/jbc.273.50.33107 (1998).

119 Hooper, N. M., Taylor, D. R. & Watt, N. T. Mechanism of the metal-mediated endocytosis of the prion protein. *Biochem Soc Trans* **36**, 1272-1276, doi:10.1042/BST0361272 (2008).

120 Wu, B. *et al.* The N-terminus of the prion protein is a toxic effector regulated by the C-terminus. *Elife* **6**, doi:10.7554/eLife.23473 (2017).

121 Spevacek, A. R. *et al.* Zinc drives a tertiary fold in the prion protein with familial disease mutation sites at the interface. *Structure* **21**, 236-246, doi:10.1016/j.str.2012.12.002 (2013).

122 Nishida, N. *et al.* A mouse prion protein transgene rescues mice deficient for the prion protein gene from purkinje cell degeneration and demyelination. *Laboratory investigation; a journal of technical methods and pathology* **79**, 689 (1999).

123 Weissmann, C. & Flechsig, E. PrP knock-out and PrP transgenic mice in prion research. *Br Med Bull* **66**, 43-60, doi:10.1093/bmb/66.1.43 (2003).

124 Bremer, J. *et al.* Axonal prion protein is required for peripheral myelin maintenance. *Nat Neurosci* **13**, 310-318, doi:10.1038/nn.2483 (2010).

125 Kuffer, A. *et al.* The prion protein is an agonistic ligand of the G protein-coupled receptor Adgrg6. *Nature* **536**, 464-468, doi:10.1038/nature19312 (2016).

126 Scalabrino, G., Veber, D., De Giuseppe, R. & Roncaroli, F. Low levels of cobalamin, epidermal growth factor, and normal prions in multiple sclerosis spinal cord. *Neuroscience* **298**, 293-301, doi:10.1016/j.neuroscience.2015.04.020 (2015).

127 Barmada, S., Piccardo, P., Yamaguchi, K., Ghetti, B. & Harris, D. A. GFP-tagged prion protein is correctly localized and functionally active in the brains of transgenic mice. *Neurobiol Dis* **16**, 527-537, doi:10.1016/j.nbd.2004.05.005 (2004).

128 Laine, J., Marc, M. E., Sy, M. S. & Axelrad, H. Cellular and subcellular morphological localization of normal prion protein in rodent cerebellum. *Eur J Neurosci* **14**, 47-56, doi:10.1046/j.0953-816x.2001.01621.x (2001).

129 Mironov, A., Jr. *et al.* Cytosolic prion protein in neurons. *J Neurosci* **23**, 7183-7193 (2003).

130 Ford, M. *et al.* A marked disparity between the expression of prion protein and its message by neurones of the CNS. *Neuroscience* **111**, 533-551 (2002).

131 Kanaani, J., Prusiner, S. B., Diacovo, J., Baekkeskov, S. & Legname, G. Recombinant prion protein induces rapid polarization and development of synapses in embryonic rat hippocampal neurons in vitro. *J Neurochem* **95**, 1373-1386, doi:10.1111/j.1471-4159.2005.03469.x (2005).

132 Colling, S. B., Khana, M., Collinge, J. & Jefferys, J. G. R. Mossy fibre reorganization in the hippocampus of prion protein null mice. *Brain Research* **755**, 28-35, doi:10.1016/s0006-8993(97)00087-5 (1997).

133 Kamenetz, F. *et al.* APP processing and synaptic function. *Neuron* **37**, 925-937, doi:10.1016/s0896-6273(03)00124-7 (2003).

134 Lauren, J., Gimbel, D. A., Nygaard, H. B., Gilbert, J. W. & Strittmatter, S. M. Cellular prion protein mediates impairment of synaptic plasticity by amyloid-beta oligomers. *Nature* **457**, 1128-1132, doi:10.1038/nature07761 (2009).

135 De Strooper, B. & Karran, E. The Cellular Phase of Alzheimer's Disease. *Cell* **164**, 603-615, doi:10.1016/j.cell.2015.12.056 (2016).

136 Parkin, E. T. *et al.* Cellular prion protein regulates beta-secretase cleavage of the Alzheimer's amyloid precursor protein. *Proc Natl Acad Sci U S A* **104**, 11062-11067, doi:10.1073/pnas.0609621104 (2007).

137 Whitehouse, I. J. *et al.* Prion protein is decreased in Alzheimer's brain and inversely correlates with BACE1 activity, amyloid-beta levels and Braak stage. *PLoS One* **8**, e59554, doi:10.1371/journal.pone.0059554 (2013).

138 Whitehouse, I. J. *et al.* Ablation of Prion Protein in Wild Type Human Amyloid Precursor Protein (APP) Transgenic Mice Does Not Alter The Proteolysis of APP, Levels

of Amyloid-beta or Pathologic Phenotype. *PLoS One* **11**, e0159119, doi:10.1371/journal.pone.0159119 (2016).

139 Gimbel, D. A. *et al.* Memory impairment in transgenic Alzheimer mice requires cellular prion protein. *J Neurosci* **30**, 6367-6374, doi:10.1523/JNEUROSCI.0395-10.2010 (2010).

140 Larson, M. *et al.* The complex PrP(c)-Fyn couples human oligomeric Abeta with pathological tau changes in Alzheimer's disease. *J Neurosci* **32**, 16857-16871a, doi:10.1523/JNEUROSCI.1858-12.2012 (2012).

141 Corbett, G. T. *et al.* PrP is a central player in toxicity mediated by soluble aggregates of neurodegeneration-causing proteins. *Acta Neuropathol* **139**, 503-526, doi:10.1007/s00401-019-02114-9 (2020).

142 Alper, T., Cramp, W., Haig, D. A. & Clarke, M. C. Does the agent of scrapie replicate without nucleic acid? *Nature* **214**, 764-766 (1967).

143 Prusiner, S. B. Prions. *Proc Natl Acad Sci U S A* **95**, 13363-13383, doi:10.1073/pnas.95.23.13363 (1998).

144 Crick, F. Central dogma of molecular biology. *Nature* **227**, 561-563, doi:10.1038/227561a0 (1970).

145 Wille, H. & Requena, J. R. The Structure of PrP(Sc) Prions. *Pathogens* **7**, doi:10.3390/pathogens7010020 (2018).

146 Wille, H. *et al.* Structural studies of the scrapie prion protein by electron crystallography. *Proc Natl Acad Sci U S A* **99**, 3563-3568, doi:10.1073/pnas.052703499 (2002).

147 Govaerts, C., Wille, H., Prusiner, S. B. & Cohen, F. E. Evidence for assembly of prions with left-handed β-helices into trimers. *Proceedings of the National Academy of Sciences* **101**, 8342-8347 (2004).

148 Vazquez-Fernandez, E. *et al.* The Structural Architecture of an Infectious Mammalian Prion Using Electron Cryomicroscopy. *PLoS Pathog* **12**, e1005835, doi:10.1371/journal.ppat.1005835 (2016).

149 Vazquez-Fernandez, E. *et al.* Structural organization of mammalian prions as probed by limited proteolysis. *PLoS One* **7**, e50111, doi:10.1371/journal.pone.0050111 (2012).

150 Wille, H. *et al.* Natural and synthetic prion structure from X-ray fiber diffraction. *Proc Natl Acad Sci U S A* **106**, 16990-16995, doi:10.1073/pnas.0909006106 (2009).

151 Smirnovas, V. *et al.* Structural organization of brain-derived mammalian prions examined by hydrogen-deuterium exchange. *Nat Struct Mol Biol* **18**, 504-506, doi:10.1038/nsmb.2035 (2011).

152 Caughey, B., Raymond, G. J. & Bessen, R. A. Strain-dependent differences in beta-sheet conformations of abnormal prion protein. *J Biol Chem* **273**, 32230-32235, doi:10.1074/jbc.273.48.32230 (1998).

153 Caughey, B. W. *et al.* Secondary structure analysis of the scrapie-associated protein PrP 27-30 in water by infrared spectroscopy. *Biochemistry* **30**, 7672-7680, doi:10.1021/bi00245a003 (1991).

154 Pan, K. M. *et al.* Conversion of Alpha-Helices into Beta-Sheets Features in the Formation of the Scrapie Prion Proteins. *P Natl Acad Sci USA* **90**, 10962-10966, doi:DOI 10.1073/pnas.90.23.10962 (1993).

155 Safar, J., Roller, P. P., Gajdusek, D. C. & Gibbs, C. J., Jr. Conformational transitions, dissociation, and unfolding of scrapie amyloid (prion) protein. *J Biol Chem* **268**, 20276-20284 (1993).

156 Groveman, B. R. *et al.* Parallel in-register intermolecular beta-sheet architectures for prion-seeded prion protein (PrP) amyloids. *J Biol Chem* **289**, 24129-24142, doi:10.1074/jbc.M114.578344 (2014).

157 Baskakov, I. V. & Katorcha, E. Multifaceted Role of Sialylation in Prion Diseases. *Front Neurosci* **10**, 358, doi:10.3389/fnins.2016.00358 (2016).

158 Artikis, E., Roy, A., Verli, H., Cordeiro, Y. & Caughey, B. Accommodation of In-Register N-Linked Glycans on Prion Protein Amyloid Cores. *ACS Chem Neurosci* **11**, 4092-4097, doi:10.1021/acschemneuro.0c00635 (2020).

159 Spagnolli, G. *et al.* Modeling PrP(Sc) Generation Through Deformed Templating. *Front Bioeng Biotechnol* **8**, 590501, doi:10.3389/fbioe.2020.590501 (2020).

160 Wang, L. Q. *et al.* Cryo-EM structure of an amyloid fibril formed by full-length human prion protein. *Nat Struct Mol Biol* **27**, 598-602, doi:10.1038/s41594-020-0441-5 (2020).

161 Kraus, A. *et al.* Structure of an infectious mammalian prion. *bioRxiv* (2021).

162 Tuttle, M. D. *et al.* Solid-state NMR structure of a pathogenic fibril of full-length human alpha-synuclein. *Nat Struct Mol Biol* **23**, 409-415, doi:10.1038/nsmb.3194 (2016).

163 Spagnolli, G. *et al.* Full atomistic model of prion structure and conversion. *PLoS Pathog* **15**, e1007864, doi:10.1371/journal.ppat.1007864 (2019).

164 Chen, S. G. & Gambetti, P. A journey through the species barrier. *Neuron* **34**, 854-856, doi:Doi 10.1016/S0896-6273(02)00736-5 (2002).

165 Pattison, I. H. The relative susceptibility of sheep, goats and mice to two types of the goat scrapie agent. *Res Vet Sci* **7**, 207-212 (1966).

166 Prusiner, S. B. *et al.* Transgenetic studies implicate interactions between homologous PrP isoforms in scrapie prion replication. *Cell* **63**, 673-686 (1990).

167 Gibbs, C. J., Jr. & Gajdusek, D. C. Experimental subacute spongiform virus encephalopathies in primates and other laboratory animals. *Science* **182**, 67-68, doi:10.1126/science.182.4107.67 (1973).

168 Vorberg, I., Groschup, M. H., Pfaff, E. & Priola, S. A. Multiple amino acid residues within the rabbit prion protein inhibit formation of its abnormal isoform. *J Virol* **77**, 2003-2009, doi:10.1128/jvi.77.3.2003-2009.2003 (2003).

169 Nonno, R. *et al.* Efficient transmission and characterization of Creutzfeldt-Jakob disease strains in bank voles. *PLoS Pathog* **2**, e12, doi:10.1371/journal.ppat.0020012 (2006).

170 Safar, J. G. *et al.* Measuring prions causing bovine spongiform encephalopathy or chronic wasting disease by immunoassays and transgenic mice. *Nat Biotechnol* **20**, 1147-1150, doi:10.1038/nbt748 (2002).

171 Korth, C. *et al.* Prion (PrPSc)-specific epitope defined by a monoclonal antibody. *Nature* **390**, 74-77, doi:10.1038/36337 (1997).

172 Hsiao, K. K. *et al.* Serial transmission in rodents of neurodegeneration from transgenic mice expressing mutant prion protein. *Proc Natl Acad Sci U S A* **91**, 9126-9130, doi:10.1073/pnas.91.19.9126 (1994).

173 Lasmezas, C. I. *et al.* Transmission of the BSE agent to mice in the absence of detectable abnormal prion protein. *Science* **275**, 402-405, doi:10.1126/science.275.5298.402 (1997).

174 Green, A. J. E. & Zanusso, G. Prion protein amplification techniques. *Handb Clin Neurol* **153**, 357-370, doi:10.1016/B978-0-444-63945-5.00019-2 (2018).

175 Saborio, G. P., Permanne, B. & Soto, C. Sensitive detection of pathological prion protein by cyclic amplification of protein misfolding. *Nature* **411**, 810-813, doi:10.1038/35081095 (2001).

176 Atarashi, R. *et al.* Simplified ultrasensitive prion detection by recombinant PrP conversion with shaking. *Nat Methods* **5**, 211-212, doi:10.1038/nmeth0308-211 (2008).

177 Schmitz, M. *et al.* The real-time quaking-induced conversion assay for detection of human prion disease and study of other protein misfolding diseases. *Nat Protoc* **11**, 2233-2242, doi:10.1038/nprot.2016.120 (2016).

178 Haley, N. J. & Richt, J. A. Evolution of Diagnostic Tests for Chronic Wasting Disease, a Naturally Occurring Prion Disease of Cervids. *Pathogens* **6**, doi:10.3390/pathogens6030035 (2017).

179 Ferreira, N. C. *et al.* Detection of chronic wasting disease in mule and white-tailed deer by RT-QuIC analysis of outer ear. *Sci Rep* **11**, 7702, doi:10.1038/s41598-021-87295-8 (2021).

180 Giles, K., Olson, S. H. & Prusiner, S. B. Developing Therapeutics for PrP Prion Diseases. *Cold Spring Harb Perspect Med* **7**, doi:10.1101/cshperspect.a023747 (2017).

181 Gabizon, R., Meiner, Z., Halimi, M. & Bensasson, S. A. Heparin-Like Molecules Bind Differentially to Prion-Proteins and Change Their Intracellular Metabolic-Fate. *J Cell Physiol* **157**, 319-325, doi:DOI 10.1002/jcp.1041570215 (1993).

182 Ingrosso, L., Ladogana, A. & Pocchiari, M. Congo red prolongs the incubation period in scrapie-infected hamsters. *J Virol* **69**, 506-508, doi:10.1128/JVI.69.1.506-508.1995 (1995).

183 Caughey, B. & Race, R. E. Potent inhibition of scrapie-associated PrP accumulation by congo red. *J Neurochem* **59**, 768-771, doi:10.1111/j.1471-4159.1992.tb09437.x (1992).

184 Rudyk, H. *et al.* Screening Congo Red and its analogues for their ability to prevent the formation of PrP-res in scrapie-infected cells. *Journal of General Virology* **81**, 1155-1164, doi:Doi 10.1099/0022-1317-81-4-1155 (2000).

185 Korth, C., May, B. C. H., Cohen, F. E. & Prusiner, S. B. Acridine and phenothiazine derivatives as pharmacotherapeutics for prion disease. *P Natl Acad Sci USA* **98**, 9836-9841, doi:DOI 10.1073/pnas.161274798 (2001).

186 Collinge, J. *et al.* Safety and efficacy of quinacrine in human prion disease (PRION-1 study): a patient-preference trial. *The Lancet Neurology* **8**, 334-344, doi:10.1016/s1474-4422(09)70049-3 (2009).

187 Haik, S. *et al.* Compassionate use of quinacrine in Creutzfeldt-Jakob disease fails to show significant effects. *Neurology* **63**, 2413-2415, doi:Doi 10.1212/01.Wnl.0000148596.15681.4d (2004).

188 Geschwind, M. D. *et al.* Quinacrine treatment trial for sporadic Creutzfeldt-Jakob disease. *Neurology* **81**, 2015-2023, doi:10.1212/WNL.0b013e3182a9f3b4 (2013).

189 Haïk, S. *et al.* Doxycycline in Creutzfeldt-Jakob disease: a phase 2, randomised, double-blind, placebo-controlled trial. *The Lancet Neurology* **13**, 150-158, doi:10.1016/s1474-4422(13)70307-7 (2014).

190 Forloni, G. *et al.* Tetracyclines affect prion infectivity. *Proc Natl Acad Sci U S A* **99**, 10849-10854, doi:10.1073/pnas.162195499 (2002).

191 Aguzzi, A., Lakkaraju, A. K. K. & Frontzek, K. Toward Therapy of Human Prion Diseases. *Annu Rev Pharmacol Toxicol* **58**, 331-351, doi:10.1146/annurev-pharmtox-010617-052745 (2018).

192 Brody, D. L. & Holtzman, D. M. Active and passive immunotherapy for neurodegenerative disorders. *Annu Rev Neurosci* **31**, 175-193, doi:10.1146/annurev.neuro.31.060407.125529 (2008).

193 Roettger, Y. *et al.* Immunotherapy in prion disease. *Nat Rev Neurol* **9**, 98-105, doi:10.1038/nrneurol.2012.258 (2013).

194 Gabizon, R., McKinley, M. P., Groth, D. & Prusiner, S. B. Immunoaffinity purification and neutralization of scrapie prion infectivity. *Proc Natl Acad Sci U S A* **85**, 6617-6621, doi:10.1073/pnas.85.18.6617 (1988).

195 Enari, M., Flechsig, E. & Weissmann, C. Scrapie prion protein accumulation by scrapie-infected neuroblastoma cells abrogated by exposure to a prion protein antibody. *Proc Natl Acad Sci U S A* **98**, 9295-9299, doi:10.1073/pnas.151242598 (2001).

196 Peretz, D. *et al.* Antibodies inhibit prion propagation and clear cell cultures of prion infectivity. *Nature* **412**, 739-743, doi:10.1038/35089090 (2001).

197 Kim, C. L. *et al.* Cell-surface retention of PrPC by anti-PrP antibody prevents protease-resistant PrP formation. *J Gen Virol* **85**, 3473-3482, doi:10.1099/vir.0.80113-0 (2004).

198 Antonyuk, S. V. *et al.* Crystal structure of human prion protein bound to a therapeutic antibody. *Proc Natl Acad Sci U S A* **106**, 2554-2558, doi:10.1073/pnas.0809170106 (2009).

199 Goni, F. *et al.* Mucosal immunization with an attenuated Salmonella vaccine partially protects white-tailed deer from chronic wasting disease. *Vaccine* **33**, 726-733, doi:10.1016/j.vaccine.2014.11.035 (2015).

200 Schwarz, A. *et al.* Immunisation with a synthetic prion protein-derived peptide prolongs survival times of mice orally exposed to the scrapie agent. *Neuroscience Letters* **350**, 187-189, doi:10.1016/s0304-3940(03)00907-8 (2003).

201 Sigurdsson, E. M. *et al.* Immunization Delays the Onset of Prion Disease in Mice. *The American Journal of Pathology* **161**, 13-17, doi:10.1016/s0002-9440(10)64151-x (2002).

202 Wood, M. E. *et al.* Accelerated onset of chronic wasting disease in elk (Cervus canadensis) vaccinated with a PrP(Sc)-specific vaccine and housed in a prion contaminated environment. *Vaccine* **36**, 7737-7743, doi:10.1016/j.vaccine.2018.10.057 (2018).

203 Forloni, G., Roiter, I. & Tagliavini, F. Clinical trials of prion disease therapeutics. *Curr Opin Pharmacol* **44**, 53-60, doi:10.1016/j.coph.2019.04.019 (2019).

204 Solforosi, L. *et al.* Cross-linking cellular prion protein triggers neuronal apoptosis in vivo. *Science* **303**, 1514-1516, doi:10.1126/science.1094273 (2004).

205 Potapov, A., Merrill, E., Pybus, M. & Lewis, M. A. Chronic Wasting Disease: Transmission Mechanisms and the Possibility of Harvest Management. *PLoS One* **11**, e0151039, doi:10.1371/journal.pone.0151039 (2016).

206 Jennelle, C. S. *et al.* Transmission of chronic wasting disease in Wisconsin white-tailed deer: implications for disease spread and management. *PLoS One* **9**, e91043, doi:10.1371/journal.pone.0091043 (2014).

207 Barrangou, R. *et al.* CRISPR provides acquired resistance against viruses in prokaryotes. *Science* **315**, 1709-1712, doi:10.1126/science.1138140 (2007).

208 Bhaya, D., Davison, M. & Barrangou, R. CRISPR-Cas systems in bacteria and archaea: versatile small RNAs for adaptive defense and regulation. *Annu Rev Genet* **45**, 273-297, doi:10.1146/annurev-genet-110410-132430 (2011).

209 Karginov, F. V. & Hannon, G. J. The CRISPR system: small RNA-guided defense in bacteria and archaea. *Mol Cell* **37**, 7-19, doi:10.1016/j.molcel.2009.12.033 (2010).

210 Swarts, D. C., Mosterd, C., van Passel, M. W. & Brouns, S. J. CRISPR interference directs strand specific spacer acquisition. *PLoS One* **7**, e35888, doi:10.1371/journal.pone.0035888 (2012).

211 Brouns, S. J. *et al.* Small CRISPR RNAs guide antiviral defense in prokaryotes. *Science* **321**, 960-964, doi:10.1126/science.1159689 (2008).

212 Makarova, K. S. *et al.* An updated evolutionary classification of CRISPR-Cas systems. *Nat Rev Microbiol* **13**, 722-736, doi:10.1038/nrmicro3569 (2015).

213 Garneau, J. E. *et al.* The CRISPR/Cas bacterial immune system cleaves bacteriophage and plasmid DNA. *Nature* **468**, 67-71, doi:10.1038/nature09523 (2010).

214 Sapranauskas, R. *et al.* The Streptococcus thermophilus CRISPR/Cas system provides immunity in Escherichia coli. *Nucleic Acids Res* **39**, 9275-9282, doi:10.1093/nar/gkr606 (2011).

215 Deltcheva, E. *et al.* CRISPR RNA maturation by trans-encoded small RNA and host factor RNase III. *Nature* **471**, 602-607, doi:10.1038/nature09886 (2011).

216 Jinek, M. *et al.* A programmable dual-RNA-guided DNA endonuclease in adaptive bacterial immunity. *Science* **337**, 816-821, doi:10.1126/science.1225829 (2012).

217 Cong, L. *et al.* Multiplex Genome Engineering Using CRISPR/Cas Systems. *Science* **339**, 819-823, doi:10.1126/science.1231143 (2013).

218 Ran, F. A. *et al.* Genome engineering using the CRISPR-Cas9 system. *Nat Protoc* **8**, 2281-2308, doi:10.1038/nprot.2013.143 (2013).

219 Saleh-Gohari, N. & Helleday, T. Conservative homologous recombination preferentially repairs DNA double-strand breaks in the S phase of the cell cycle in human cells. *Nucleic Acids Res* **32**, 3683-3688, doi:10.1093/nar/gkh703 (2004).

220 van Gent, D. C., Hoeijmakers, J. H. & Kanaar, R. Chromosomal stability and the DNA double-stranded break connection. *Nat Rev Genet* **2**, 196-206, doi:10.1038/35056049 (2001).

221 Ran, F. A. *et al.* Double nicking by RNA-guided CRISPR Cas9 for enhanced genome editing specificity. *Cell* **154**, 1380-1389, doi:10.1016/j.cell.2013.08.021 (2013).

222 Gaj, T., Gersbach, C. A. & Barbas, C. F., 3rd. ZFN, TALEN, and CRISPR/Cas-based methods for genome engineering. *Trends Biotechnol* **31**, 397-405, doi:10.1016/j.tibtech.2013.04.004 (2013).

223 Chen, F. *et al.* High-frequency genome editing using ssDNA oligonucleotides with zinc-finger nucleases. *Nat Methods* **8**, 753-755, doi:10.1038/nmeth.1653 (2011).

224 Perez, E. E. *et al.* Establishment of HIV-1 resistance in CD4+ T cells by genome editing using zinc-finger nucleases. *Nat Biotechnol* **26**, 808-816, doi:10.1038/nbt1410 (2008).

225 Miller, J. C. *et al.* An improved zinc-finger nuclease architecture for highly specific genome editing. *Nat Biotechnol* **25**, 778-785, doi:10.1038/nbt1319 (2007).

226 Sanjana, N. E. *et al.* A transcription activator-like effector toolbox for genome engineering. *Nat Protoc* **7**, 171-192, doi:10.1038/nprot.2011.431 (2012).

227 Wood, A. J. *et al.* Targeted Genome Editing Across Species Using ZFNs and TALENs. *Science* **333**, 307-307, doi:10.1126/science.1207773 (2011).

228 Qi, L. S. *et al.* Repurposing CRISPR as an RNA-guided platform for sequence-specific control of gene expression. *Cell* **152**, 1173-1183, doi:10.1016/j.cell.2013.02.022 (2013).

229 Dominguez, A. A., Lim, W. A. & Qi, L. S. Beyond editing: repurposing CRISPR-Cas9 for precision genome regulation and interrogation. *Nat Rev Mol Cell Biol* **17**, 5-15, doi:10.1038/nrm.2015.2 (2016).

230 Bikard, D. *et al.* Programmable repression and activation of bacterial gene expression using an engineered CRISPR-Cas system. *Nucleic Acids Res* **41**, 7429-7437, doi:10.1093/nar/gkt520 (2013).

231 Larson, M. H. *et al.* CRISPR interference (CRISPRi) for sequence-specific control of gene expression. *Nat Protoc* **8**, 2180-2196, doi:10.1038/nprot.2013.132 (2013).

232 Gilbert, L. A. *et al.* Genome-Scale CRISPR-Mediated Control of Gene Repression and Activation. *Cell* **159**, 647-661, doi:10.1016/j.cell.2014.09.029 (2014).

233 Xu, X. & Qi, L. S. A CRISPR-dCas Toolbox for Genetic Engineering and Synthetic Biology. *J Mol Biol* **431**, 34-47, doi:10.1016/j.jmb.2018.06.037 (2019).

234 Chavez, A. *et al.* Highly efficient Cas9-mediated transcriptional programming. *Nat Methods* **12**, 326-328, doi:10.1038/nmeth.3312 (2015).

235 Maeder, M. L. *et al.* CRISPR RNA-guided activation of endogenous human genes. *Nat Methods* **10**, 977-979, doi:10.1038/nmeth.2598 (2013).

236 Perez-Pinera, P. *et al.* RNA-guided gene activation by CRISPR-Cas9-based transcription factors. *Nat Methods* **10**, 973-976, doi:10.1038/nmeth.2600 (2013).

237 Tanenbaum, M. E., Gilbert, L. A., Qi, L. S., Weissman, J. S. & Vale, R. D. A protein-tagging system for signal amplification in gene expression and fluorescence imaging. *Cell* **159**, 635-646, doi:10.1016/j.cell.2014.09.039 (2014).

238 Konermann, S. *et al.* Genome-scale transcriptional activation by an engineered CRISPR-Cas9 complex. *Nature* **517**, 583-588, doi:10.1038/nature14136 (2015).

239 Wang, T., Chen, C., Larcher, L. M., Barrero, R. A. & Veedu, R. N. Three decades of nucleic acid aptamer technologies: Lessons learned, progress and opportunities on aptamer development. *Biotechnol Adv* **37**, 28-50, doi:10.1016/j.biotechadv.2018.11.001 (2019).

240 Zetsche, B., Volz, S. E. & Zhang, F. A split-Cas9 architecture for inducible genome editing and transcription modulation. *Nat Biotechnol* **33**, 139-142, doi:10.1038/nbt.3149 (2015).

241 Nihongaki, Y., Yamamoto, S., Kawano, F., Suzuki, H. & Sato, M. CRISPR-Cas9-based photoactivatable transcription system. *Chem Biol* **22**, 169-174, doi:10.1016/j.chembiol.2014.12.011 (2015).

242 Levskaya, A., Weiner, O. D., Lim, W. A. & Voigt, C. A. Spatiotemporal control of cell signalling using a light-switchable protein interaction. *Nature* **461**, 997-1001, doi:10.1038/nature08446 (2009).

243 Champer, J., Buchman, A. & Akbari, O. S. Cheating evolution: engineering gene drives to manipulate the fate of wild populations. *Nat Rev Genet* **17**, 146-159, doi:10.1038/nrg.2015.34 (2016).

244 Gantz, V. M. & Bier, E. Genome editing. The mutagenic chain reaction: a method for converting heterozygous to homozygous mutations. *Science* **348**, 442-444, doi:10.1126/science.aaa5945 (2015).

245 DiCarlo, J. E., Chavez, A., Dietz, S. L., Esvelt, K. M. & Church, G. M. Safeguarding CRISPR-Cas9 gene drives in yeast. *Nat Biotechnol* **33**, 1250-1255, doi:10.1038/nbt.3412 (2015).

246 Gantz, V. M. *et al.* Highly efficient Cas9-mediated gene drive for population modification of the malaria vector mosquito Anopheles stephensi. *Proc Natl Acad Sci U S A* **112**, E6736-6743, doi:10.1073/pnas.1521077112 (2015).

247 Hammond, A. *et al.* A CRISPR-Cas9 gene drive system targeting female reproduction in the malaria mosquito vector Anopheles gambiae. *Nat Biotechnol* **34**, 78-83, doi:10.1038/nbt.3439 (2016).

248 Champer, J. *et al.* Novel CRISPR/Cas9 gene drive constructs reveal insights into mechanisms of resistance allele formation and drive efficiency in genetically diverse populations. *PLoS Genet* **13**, e1006796, doi:10.1371/journal.pgen.1006796 (2017).

249 Grunwald, H. A. *et al.* Super-Mendelian inheritance mediated by CRISPR-Cas9 in the female mouse germline. *Nature* **566**, 105-109, doi:10.1038/s41586-019-0875-2 (2019).

250 Pfitzner, C. *et al.* Development of zygotic and germline gene drives in mice. *bioRxiv* (2020).

251 Akbari, O. S. *et al.* BIOSAFETY. Safeguarding gene drive experiments in the laboratory. *Science* **349**, 927-929, doi:10.1126/science.aac7932 (2015).

252 Esvelt, K. M. & Gemmell, N. J. Conservation demands safe gene drive. *PLoS Biol* **15**, e2003850, doi:10.1371/journal.pbio.2003850 (2017).

253 Kyrou, K. *et al.* A CRISPR-Cas9 gene drive targeting doublesex causes complete population suppression in caged Anopheles gambiae mosquitoes. *Nat Biotechnol* **36**, 1062-1066, doi:10.1038/nbt.4245 (2018).

254 Raban, R. R., Marshall, J. M. & Akbari, O. S. Progress towards engineering gene drives for population control. *J Exp Biol* **223**, doi:10.1242/jeb.208181 (2020).

255 Belsare, A. V. *et al.* Getting in Front of Chronic Wasting Disease: Model-Informed Proactive Approach for Managing an Emerging Wildlife Disease. *Front Vet Sci* **7**, 608235, doi:10.3389/fvets.2020.608235 (2020).

256 Benestad, S. L., Austbo, L., Tranulis, M. A., Espenes, A. & Olsaker, I. Healthy goats naturally devoid of prion protein. *Vet Res* **43**, 87, doi:10.1186/1297-9716-43-87 (2012).

257 Richt, J. A. *et al.* Production of cattle lacking prion protein. *Nat Biotechnol* **25**, 132-138, doi:10.1038/nbt1271 (2007).

258 Castle, A. R., Daude, N., Gilch, S. & Westaway, D. Application of high-throughput, capillary-based Western analysis to modulated cleavage of the cellular prion protein. *J Biol Chem* **294**, 2642-2650, doi:10.1074/jbc.RA118.006367 (2019).

259 Schagger, H. Tricine-SDS-PAGE. *Nat Protoc* **1**, 16-22, doi:10.1038/nprot.2006.4 (2006).

260 Lee, P. Y., Costumbrado, J., Hsu, C. Y. & Kim, Y. H. Agarose gel electrophoresis for the separation of DNA fragments. *J Vis Exp*, doi:10.3791/3923 (2012).

261 Raymond, G. J. *et al.* Inhibition of protease-resistant prion protein formation in a transformed deer cell line infected with chronic wasting disease. *J Virol* **80**, 596-604, doi:10.1128/JVI.80.2.596-604.2006 (2006).

262 Ghetti, B. *et al.* Vascular variant of prion protein cerebral amyloidosis with tau-positive neurofibrillary tangles: the phenotype of the stop codon 145 mutation in PRNP. *Proc Natl Acad Sci U S A* **93**, 744-748, doi:10.1073/pnas.93.2.744 (1996).

263 Jayadev, S. *et al.* Familial prion disease with Alzheimer disease-like tau pathology and clinical phenotype. *Ann Neurol* **69**, 712-720, doi:10.1002/ana.22264 (2011).

264 Mead, S. *et al.* A novel prion disease associated with diarrhea and autonomic neuropathy. *N Engl J Med* **369**, 1904-1914, doi:10.1056/NEJMoa1214747 (2013).

265 Zischewski, J., Fischer, R. & Bortesi, L. Detection of on-target and off-target mutations generated by CRISPR/Cas9 and other sequence-specific nucleases. *Biotechnol Adv* **35**, 95-104, doi:10.1016/j.biotechadv.2016.12.003 (2017).

266 Brayton, K. A., O'Rourke, K. I., Lyda, A. K., Miller, M. W. & Knowles, D. P. A processed pseudogene contributes to apparent mule deer prion gene heterogeneity. *Gene* **326**, 167-173, doi:10.1016/j.gene.2003.10.022 (2004).

267 Safar, J. G. *et al.* Prion clearance in bigenic mice. *J Gen Virol* **86**, 2913-2923, doi:10.1099/vir.0.80947-0 (2005).

268 Price, J. C., Guan, S., Burlingame, A., Prusiner, S. B. & Ghaemmaghami, S. Analysis of proteome dynamics in the mouse brain. *Proc Natl Acad Sci U S A* **107**, 14508-14513, doi:10.1073/pnas.1006551107 (2010).

269 Janzen, W. P. Screening technologies for small molecule discovery: the state of the art. *Chem Biol* **21**, 1162-1170, doi:10.1016/j.chembiol.2014.07.015 (2014).

270 Sunyach, C., Cisse, M. A., da Costa, C. A., Vincent, B. & Checler, F. The C-terminal products of cellular prion protein processing, C1 and C2, exert distinct influence on p53-

dependent staurosporine-induced caspase-3 activation. *J Biol Chem* **282**, 1956-1963, doi:10.1074/jbc.M609663200 (2007).

271 Dandapani, S., Rosse, G., Southall, N., Salvino, J. M. & Thomas, C. J. Selecting, Acquiring, and Using Small Molecule Libraries for High-Throughput Screening. *Curr Protoc Chem Biol* **4**, 177-191, doi:10.1002/9780470559277.ch110252 (2012).

272 Luduena, R. F. A hypothesis on the origin and evolution of tubulin. *Int Rev Cell Mol Biol* **302**, 41-185, doi:10.1016/B978-0-12-407699-0.00002-9 (2013).

273 Wilkinson, D. J. *et al.* The serine proteinase hepsin is an activator of pro-matrix metalloproteinases: molecular mechanisms and implications for extracellular matrix turnover. *Sci Rep* **7**, 16693, doi:10.1038/s41598-017-17028-3 (2017).

274 Hsu, P. D. *et al.* DNA targeting specificity of RNA-guided Cas9 nucleases. *Nat Biotechnol* **31**, 827-832, doi:10.1038/nbt.2647 (2013).

275 Campenhout, C. V. *et al.* Guidelines for optimized gene knockout using CRISPR/Cas9. *BioTechniques* **66**, 295-302 (2019).

276 Haeussler, M. *et al.* Evaluation of off-target and on-target scoring algorithms and integration into the guide RNA selection tool CRISPOR. *Genome Biol* **17**, 148, doi:10.1186/s13059-016-1012-2 (2016).

277 Kim, D. *et al.* Digenome-seq: genome-wide profiling of CRISPR-Cas9 off-target effects in human cells. *Nat Methods* **12**, 237-243, 231 p following 243, doi:10.1038/nmeth.3284 (2015).

278 Tsai, S. Q. *et al.* GUIDE-seq enables genome-wide profiling of off-target cleavage by CRISPR-Cas nucleases. *Nat Biotechnol* **33**, 187-197, doi:10.1038/nbt.3117 (2015).

279 Zeitelhofer, M. *et al.* High-efficiency transfection of mammalian neurons via nucleofection. *Nat Protoc* **2**, 1692-1704, doi:10.1038/nprot.2007.226 (2007).

280 Shifrut, E. *et al.* Genome-wide CRISPR Screens in Primary Human T Cells Reveal Key Regulators of Immune Function. *Cell* **175**, 1958-1971 e1915, doi:10.1016/j.cell.2018.10.024 (2018).

281 Vouillot, L., Thelie, A. & Pollet, N. Comparison of T7E1 and surveyor mismatch cleavage assays to detect mutations triggered by engineered nucleases. *G3 (Bethesda)* **5**, 407-415, doi:10.1534/g3.114.015834 (2015).

282 Sondergaard, J. N. *et al.* Successful delivery of large-size CRISPR/Cas9 vectors in hard-to-transfect human cells using small plasmids. *Commun Biol* **3**, 319, doi:10.1038/s42003-020-1045-7 (2020).

283 Lesueur, L. L., Mir, L. M. & Andre, F. M. Overcoming the Specific Toxicity of Large Plasmids Electrotransfer in Primary Cells In Vitro. *Mol Ther Nucleic Acids* **5**, e291, doi:10.1038/mtna.2016.4 (2016).

284 Roth, T. L. *et al.* Reprogramming human T cell function and specificity with non-viral genome targeting. *Nature* **559**, 405-409, doi:10.1038/s41586-018-0326-5 (2018).

285 Khosravani, H. *et al.* Prion protein attenuates excitotoxicity by inhibiting NMDA receptors. *J Cell Biol* **181**, 551-565, doi:10.1083/jcb.200711002 (2008).

286 Dobrek, Ł. & Thor, P. Glutamate NMDA receptors in pathophysiology and pharmacotherapy of selected nervous system diseases. *Postępy Higieny i Medycyny Doświadczalnej* **65** (2011).

287 Farber, N. B., Jiang, X. P., Heinkel, C. & Nemmers, B. Antiepileptic drugs and agents that inhibit voltage-gated sodium channels prevent NMDA antagonist neurotoxicity. *Mol Psychiatry* **7**, 726-733, doi:10.1038/sj.mp.4001087 (2002).

288 Hansen, A. M., Hansen, J. B., Carr, R. D., Ashcroft, F. M. & Wahl, P. Kir6.2-dependent high-affinity repaglinide binding to beta-cell K(ATP) channels. *Br J Pharmacol* **144**, 551-557, doi:10.1038/sj.bjp.0706082 (2005).

289 Mukherjee, A. & Soto, C. Prion-Like Protein Aggregates and Type 2 Diabetes. *Cold Spring Harb Perspect Med* **7**, doi:10.1101/cshperspect.a024315 (2017).

290 Arya, S., Claud, S. L., Cantrell, K. L. & Bowers, M. T. Catalytic Prion-Like Cross-Talk between a Key Alzheimer's Disease Tau-Fragment R3 and the Type 2 Diabetes Peptide IAPP. *ACS Chem Neurosci* **10**, 4757-4765, doi:10.1021/acschemneuro.9b00516 (2019).

291 Zhang, F. *et al.* Canonical hedgehog signalling regulates hepatic stellate cell-mediated angiogenesis in liver fibrosis. *Br J Pharmacol* **174**, 409-423, doi:10.1111/bph.13701 (2017).

292 Gulino, A., Di Marcotullio, L., Ferretti, E., De Smaele, E. & Screpanti, I. Hedgehog signaling pathway in neural development and disease. *Psychoneuroendocrinology* **32 Suppl 1**, S52-56, doi:10.1016/j.psyneuen.2007.03.017 (2007).

293 Dellovade, T., Romer, J. T., Curran, T. & Rubin, L. L. The hedgehog pathway and neurological disorders. *Annu Rev Neurosci* **29**, 539-563, doi:10.1146/annurev.neuro.29.051605.112858 (2006).

294 Guo, S. Q. *et al.* Tim-3 deteriorates neuroinflammatory and neurocyte apoptosis after subarachnoid hemorrhage through the Nrf2/HMGB1 signaling pathway in rats. *Aging-Us* **12**, 21161-21185 (2020).

295 Joshi, G. & Johnson, J. A. The Nrf2-ARE pathway: a valuable therapeutic target for the treatment of neurodegenerative diseases. *Recent Pat CNS Drug Discov* **7**, 218-229, doi:10.2174/157488912803252023 (2012).

296 Mellor, H. & Parker, P. J. The extended protein kinase C superfamily. *Biochem J* **332 (Pt 2)**, 281-292, doi:10.1042/bj3320281 (1998).

297 Cayatte, A. J. *et al.* The thromboxane receptor antagonist S18886 but not aspirin inhibits atherogenesis in apo E-deficient mice: evidence that eicosanoids other than thromboxane contribute to atherosclerosis. *Arterioscler Thromb Vasc Biol* **20**, 1724-1728, doi:10.1161/01.atv.20.7.1724 (2000).

298 Greco, A., Minghetti, L. & Levi, G. Isoprostanes, novel markers of oxidative injury, help understanding the pathogenesis of neurodegenerative diseases. *Neurochem Res* **25**, 1357-1364, doi:10.1023/a:1007608615682 (2000).

299 Wisniewski, K. *et al.* Isoprostanes as potential cerebral vasospasm biomarkers. *Neurol Neurochir Pol* **52**, 643-651, doi:10.1016/j.pjnns.2018.09.009 (2018).

300 Evans, A. K. & Lowry, C. A. Pharmacology of the β-Carboline FG-7142, a Partial Inverse Agonist at the Benzodiazepine Allosteric Site of the GABAA Receptor: Neurochemical, Neurophysiological, and Behavioral Effects. *CNS drug reviews* **13**, 475-501 (2007).

301 Kishioka, S. *et al.* Pharmacokinetic evidence for the long-lasting effect of nor-binaltorphimine, a potent kappa opioid receptor antagonist, in mice. *Neurosci Lett* **552**, 98-102, doi:10.1016/j.neulet.2013.07.040 (2013).

302 Jackson, K. J., McLaughlin, J. P., Carroll, F. I. & Damaj, M. I. Effects of the kappa opioid receptor antagonist, norbinaltorphimine, on stress and drug-induced reinstatement

of nicotine-conditioned place preference in mice. *Psychopharmacology (Berl)* **226**, 763-768, doi:10.1007/s00213-012-2716-y (2013).

303 Bendheim, P. *et al.* Nearly ubiquitous tissue distribution of the scrapie agent precursor protein. *Neurology* **42**, 149-149 (1992).

304 Jones, L. H. & Bunnage, M. E. Applications of chemogenomic library screening in drug discovery. *Nat Rev Drug Discov* **16**, 285-296, doi:10.1038/nrd.2016.244 (2017).

305 Mishra, K. P., Ganju, L., Sairam, M., Banerjee, P. K. & Sawhney, R. C. A review of high throughput technology for the screening of natural products. *Biomed Pharmacother* **62**, 94-98, doi:10.1016/j.biopha.2007.06.012 (2008).

306 Nordin Henriksson, K. & Trewavas, A. The effect of short-term low-temperature treatments on gene expression in Arabidopsis correlates with changes in intracellular Ca2+ levels. *Plant, Cell & Environment* **26**, 485-496 (2003).

307 Kato, S. *et al.* Characterization and phenotypic variation with passage number of cultured human endometrial adenocarcinoma cells. *Tissue Cell* **40**, 95-102, doi:10.1016/j.tice.2007.09.007 (2008).

308 Chang-Liu, C. M. & Woloschak, G. E. Effect of passage number on cellular response to DNA-damaging agents: cell survival and gene expression. *Cancer Lett* **113**, 77-86, doi:10.1016/s0304-3835(97)04599-0 (1997).

309 Vanni, S. *et al.* Differential overexpression of SERPINA3 in human prion diseases. *Sci Rep* **7**, 15637, doi:10.1038/s41598-017-15778-8 (2017).

310 Ponten, F., Jirstrom, K. & Uhlen, M. The Human Protein Atlas--a tool for pathology. *J Pathol* **216**, 387-393, doi:10.1002/path.2440 (2008).

311 Yamaguchi, N., Okui, A., Yamada, T., Nakazato, H. & Mitsui, S. Spinesin/TMPRSS5, a novel transmembrane serine protease, cloned from human spinal cord. *J Biol Chem* **277**, 6806-6812, doi:10.1074/jbc.M103645200 (2002).

312 Wu, Q. & Peng, J. in *Handbook of Proteolytic Enzymes* 2985-2989 (Elsevier, 2013).

313 Eigenbrot, C. *et al.* Structural and functional analysis of HtrA1 and its subdomains. *Structure* **20**, 1040-1050, doi:10.1016/j.str.2012.03.021 (2012).

314 Jung, H. *et al.* TMPRSS4 promotes invasion, migration and metastasis of human tumor cells by facilitating an epithelial-mesenchymal transition. *Oncogene* **27**, 2635-2647, doi:10.1038/sj.onc.1210914 (2008).

315 Wysocka, M. *et al.* Substrate specificity and inhibitory study of human airway trypsin-like protease. *Bioorg Med Chem* **18**, 5504-5509, doi:10.1016/j.bmc.2010.06.059 (2010).

316 Yamaya, M. *et al.* The serine protease inhibitor camostat inhibits influenza virus replication and cytokine production in primary cultures of human tracheal epithelial cells. *Pulm Pharmacol Ther* **33**, 66-74, doi:10.1016/j.pupt.2015.07.001 (2015).

317 Breining, P. *et al.* Camostat mesylate against SARS-CoV-2 and COVID-19-Rationale, dosing and safety. *Basic Clin Pharmacol Toxicol* **128**, 204-212, doi:10.1111/bcpt.13533 (2021).

318 Hoffmann, M. *et al.* Camostat mesylate inhibits SARS-CoV-2 activation by TMPRSS2-related proteases and its metabolite GBPA exerts antiviral activity. *bioRxiv*, doi:10.1101/2020.08.05.237651 (2020).

319 Shirato, K., Kawase, M. & Matsuyama, S. Middle East respiratory syndrome coronavirus infection mediated by the transmembrane serine protease TMPRSS2. *J Virol* **87**, 12552-12561, doi:10.1128/JVI.01890-13 (2013).

320 Kawase, M., Shirato, K., van der Hoek, L., Taguchi, F. & Matsuyama, S. Simultaneous treatment of human bronchial epithelial cells with serine and cysteine protease inhibitors prevents severe acute respiratory syndrome coronavirus entry. *J Virol* **86**, 6537-6545, doi:10.1128/JVI.00094-12 (2012).

321 Hoffmann, M. *et al.* SARS-CoV-2 Cell Entry Depends on ACE2 and TMPRSS2 and Is Blocked by a Clinically Proven Protease Inhibitor. *Cell* **181**, 271-280 e278, doi:10.1016/j.cell.2020.02.052 (2020).

322 Kinoshita, T. Biosynthesis and biology of mammalian GPI-anchored proteins. *Open Biol* **10**, 190290, doi:10.1098/rsob.190290 (2020).

323 Walmsley, A. R., Zeng, F. & Hooper, N. M. Membrane topology influences N-glycosylation of the prion protein. *EMBO J* **20**, 703-712, doi:10.1093/emboj/20.4.703 (2001).

324 Brunati, M. *et al.* The serine protease hepsin mediates urinary secretion and polymerisation of Zona Pellucida domain protein uromodulin. *Elife* **4**, e08887, doi:10.7554/eLife.08887 (2015).

325 Olinger, E. *et al.* Hepsin-mediated Processing of Uromodulin is Crucial for Salt-sensitivity and Thick Ascending Limb Homeostasis. *Sci Rep* **9**, 12287, doi:10.1038/s41598-019-48300-3 (2019).

326 Hoffmann, H. H. *et al.* Functional interrogation of a SARS-CoV-2 host protein interactome identifies unique and shared coronavirus host factors. *Cell Host Microbe* **29**, 267-280 e265, doi:10.1016/j.chom.2020.12.009 (2021).

327 Lucas, J. M. *et al.* The androgen-regulated type II serine protease TMPRSS2 is differentially expressed and mislocalized in prostate adenocarcinoma. *J Pathol* **215**, 118-125, doi:10.1002/path.2330 (2008).

328 Heurich, A. *et al.* TMPRSS2 and ADAM17 cleave ACE2 differentially and only proteolysis by TMPRSS2 augments entry driven by the severe acute respiratory syndrome coronavirus spike protein. *J Virol* **88**, 1293-1307, doi:10.1128/JVI.02202-13 (2014).

329 Luo, W., Wang, Y. & Reiser, G. Protease-activated receptors in the brain: receptor expression, activation, and functions in neurodegeneration and neuroprotection. *Brain Res Rev* **56**, 331-345, doi:10.1016/j.brainresrev.2007.08.002 (2007).

330 Takahashi, M. & Ono, Y. Pulse-chase analysis of protein kinase C. *Methods Mol Biol* **233**, 163-170, doi:10.1385/1-59259-397-6:163 (2003).